ENHANCED CVD-GROWN GRAPHENE TRANSFER FOR SOLAR CELL APPLICATION

BY

AHMED FOUAD ABDELBADIE ABDELAAL

A Thesis Presented to the
DEANSHIP OF GRADUATE STUDIES

KING FAHD UNIVERSITY OF PETROLEUM & MINERALS

DHAHRAN, SAUDI ARABIA

In Partial Fulfillment of the
Requirements for the Degree of

MASTER OF SCIENCE

In

MECHANICAL ENGINEERING

May, 2018

KING FAHD UNIVERSITY OF PETROLEUM & MINERALS

DHAHRAN- 31261, SAUDI ARABIA

DEANSHIP OF GRADUATE STUDIES

This thesis, written by **Ahmed Fouad Abdelbadie Abdelaal** under the direction his thesis advisor and approved by his thesis committee, has been presented and accepted by the Dean of Graduate Studies, in partial fulfillment of the requirements for the degree of **MASTER OF SCIENCE IN MECHANICAL ENGINEERING.**

Dr. Tahar Laoui
(Advisor)

Dr. Jafar Albinmousa
Department Chairman

Dr. Abdul Samad Mohammad
(Member)

Dr. Salam A. Zummo
Dean of Graduate Studies

Dr. Billel Salhi
(Member)

2/8/2014

Date

I dedicate this thesis to my loving family

ACKNOWLEDGMENTS

I would like to express my sincere gratitude to my advisor, Prof. Tahar Laoui, for his continuous support, guidance, patience, motivation and supervision during my research work and completing this thesis. Special thanks goes to Dr. Billel for his support towards the completion of this work. I would also like to thank my committee member Dr. Abdul Samad for his help.

My sincere thanks also goes to Dr. Ahmed Ibrahim for his insightful comments and encouragement and supporting me throughout the entire work allowing to widen my research from various perspectives. Many thanks to my family for their endless support, prayers and encouragements. Without their continuous support, it was impossible to achieve this goal.

Ahmed Abdelaal

TABLE OF CONTENT

LIST OF TABLES

LIST OF FIGURES

LIST OF ABBREVIATIONS

AA	Alfa Asear copper foil
AFM	Atomic force microscopy
ANOVA	Analysis of variance
APCVD	Atmospheric pressure chemical vapor deposition
APS	Ammonium persulfate
Cu	Copper
CVD	Chemical vapor deposition
DI	Deionized
DOE	Design of experiments
$FeCl_3$	Ferric chloride
$Fe(NO_3)_3$	Iron (III) nitrate
G	Graphene
HCl	Hydrochloric acid
HF	Hydrofluoric acid
HNO_3	Nitric acid
LPCVD	Low pressure chemical vapor deposition

IPA	Iso-propanol alcohol
OM	Optical microscopy
PCE	Power conversion energy
PET	Polyethylene terephthalate
PMMA	Poly-Methyl Methacrylate
SEM	Scanning electron microscopy
SiO_2	Silicon dioxide
SiC	Silicon carbide
SNR	Signal-to-noise ratio
TRT	Thermal release tape
UV-vis	Ultraviolet–visible spectroscopy
WCA	Water contact angle
XPS	X-ray photoelectron spectroscopy
ZnO	Zinc Oxide

ABSTRACT

Full Name : Ahmed Fouad Abdelbadie Abdelaal

Thesis Title : Enhanced CVD-grown graphene transfer for solar cell application

Major Field : [Manufacturing and Materials]

Date of Degree : May, 2018

Graphene has become one of the most widely studied 2D materials since its separation by Geim-Novoselov in 2004. It has been used in a wide range of applications due to its incredible carrier mobility, mechanical strength and thermal conductivity. The applications of graphene are ranging from electronics to energy storage and conversion. Chemical vapor deposition (CVD) is a common method for growing graphene on a metal surface as a catalyst, since it promotes growth of large area and high uniform graphene film. This requires an additional step to transfer graphene onto other target substrates toward fabrication of graphene-based devices. Graphene transfer process comprises many challenges such as presence of polymeric/metal residuals, generation of several extrinsic defects (tears, cracks and wrinkles) and weak adhesion between graphene and underlying target substrate. All these kinds of imperfections degrade graphene properties and hence affect the performance of the fabricated graphene-based devices.

In this work, graphene is grown on copper (Cu) foil using CVD technique. Afterwards, it is transferred to SiO_2/Si substrate using polymethylmethacrylate (PMMA) standard transfer method. Deposition of PMMA along with Cu etching process are optimized to ensure minimum polymeric/metallic contamination (residues) on transferred graphene

film. In addition, the target substrate (SiO_2/Si) surface is cleaned using several surface pre-treatments (e.g. Plasma treatment, Hydrofluoric acid and Ammonia solution) to enhance its adhesion to the transferred graphene and hence reduce the formation of wrinkles, tears and cracks. Using free transfer method, graphene layer is also transferred onto the surface of zinc oxide film deposited on a glass to study its potential for solar cell application. Different characterization techniques have been used including scanning electron microscopy (SEM), atomic force microscopy (AFM), and Raman spectroscopy to analyze the quality of graphene before and after transfer. Then, the electrical and optical properties (sheet resistance and ultraviolet-visible light absorption) are measured to evaluate the impact of transfer process on the properties of transferred graphene layer.

ملخص الرسالة

الاسم الكامل: احمد فؤاد عبدالبديع عبدالعال

عنوان الرسالة: تحسين عملية نقل الجرافين المحضر بطريقة الترسيب بالتبخير الكيميائي لاستخدمه فى تطبيقات الخلايا الشمسية

التخصص: الهندسة الميكانيكية -المواد والتصنيع

تاريخ الدرجة العلمية: مايو ٢٠١٨

الجرافين اصبح أحد أكثر المواد ثنائية الأبعاد التي تمت دراستها على نطاق واسع منذ فصلها عن طريق جيم - نوفوسيلوف في عام ٢٠٠٤. وقد تم استخدامه في مجموعة واسعة من التطبيقات بسبب السرعة المذهلة فى نقل الالكترونات والقوة الميكانيكية والتوصيل الحراري. تتراوح تطبيقات الجرافين من الإلكترونيات إلى تخزين و تحويل الطاقة. يعد الترسب بالتبخير الكيميائي طريقة شائعة لنمو الجرافين على سطح معدني كمحفز ، حيث إنه يعزز نمو منطقة كبيرة ومنتظمة من جرافين. هذا يتطلب خطوة إضافية لنقل الجرافين إلى الركائز المختلفة لتصنيع الأجهزة القائمة على الجرافين. تشتمل عملية نقل الجرافين على العديد من التحديات مثل وجود بقايا بوليمرية / معدنية ، وتوليد العديد من العيوب الخارجية (التمزقات ، والشقوق والتجاعيد) ، والالتصاق الضعيف بين الجرافين والركيزة المستهدفة . كل هذه الأنواع من العيوب تقلل خصائص الجرافين وبالتالي تؤثر على أداء الأجهزة المصنعة من الجرافين.

في هذا العمل ، ينمو الجرافين على رقائق النحاس باستخدام تقنية الترسيب بالتبخير الكيميائى .بعد ذلك ، يتم نقله إلى رقاقة من السيليكون عليها طبقة من ثانى اكسيد السيليكون(SiO_2 / Si) باستخدم طبقة من بوليمرالبولى ميثيل ميتاكريلات. يتم تحسين علمية ترسب بوليمرالبولى ميثيل ميتاكريلات وعملية اذابة طبقة النحاس لضمان الحد الأدنى من وجود بقايا بوليمرية / معدنية على سطح الجرافين. بالإضافة إلى ذلك ، يتم تنظيف سطح الركيزة المستهدفة من السيليكون ذات طبقة ثانى اكسيد السليكون (SiO_2 / Si) باستخدام عدة معالجات مسبقة للسطح (على سبيل المثال معالجة البلازما وحمض الهيدروفلوريك ومحلول الأمونيا) لتعزيز الالتصاق بالجرافين المحول ومن ثم تقليل تكوين التجاعيد واتمزقات والشقوق . باستخدام أسلوب النقل الحر ، يتم نقل طبقة الجرافين أيضًا على سطح طبقة من أكسيد الزنك الموجودة على ركيزة من الزجاج لدراسة قدرتها و اماكنية استخدامها فى تطبيقات الخلايا الشمسية.
وقد تم استخدام تقنيات توصيف مختلفة بما في ذلك المسح المجهري الإلكتروني ، والمجهر الذري ، والطيفي لتحليل جودة الجرافين قبل وبعد النقل. بعد ذلك ، يتم قياس الخواص الكهربائية والضوئية (مقاومة الكهربائية وامتصاص الضوء المرئي فوق البنفسجي) لتقييم أثر عملية النقل على خصائص طبقة الجرافين.

CHAPTER 1
INTRODUCTION

Graphene is the new wonder material. Its unique feature is that it integrates extraordinary electrical, optical and mechanical properties into one material [1]–[3]. For example, there are materials that are as conductive or as transparent as graphene, but it is rare to find materials that are electrically conductive, optically transparent and mechanically flexible all at the same time. The transparency for graphene also covers a wide range of the optical spectrum, from infrared all the way to ultraviolet. Graphene has a high potential in both fundamental research and applications. It provides a good foundation for fundamental studies in quantum mechanics, such as room temperature quantum Hall effect, and relativity effects, such as massless Dirac Fermions [4]. At the same time, downstream graphene products are already on the market, after merely ten years since graphene was first isolated [5]. Graphene is a form of carbon, which is the 4th most abundant element in the universe. This means it is abundant, cheap, ecofriendly and sustainable. Fortunately, graphene is 2-dimensional and therefore its planar structure is compatible with traditional semiconductor processing and can be relatively easily integrated into the existing mainstream technology. There are certainly some challenges when it comes to graphene use/application in technology. Graphene is much stronger than steel, if steel is normalized to the atomic scale. Graphene is rather sensitive to its environment. This is generally a drawback when making devices except for sensors. Up until now, no effective passivation method has been developed to protect graphene electronic devices against moisture, temperature, or oxidation from the environment. At the same time, using too many

protective layers also affects the device properties. Fortunately, cost and sensitivity issues are not intrinsic in graphene. Considering the fact that graphene technology has only been around for ten years, these issues are expected to be resolved in the near future. There are many challenges to graphene technology. First, production of high quality thin graphene film is still lacking in reproducibility, and the yield is not high so far. Second, for graphene produced by chemical vapor deposition, the transfer of graphene from its original metal catalyst foil (such as copper) to an insulating substrate is still irreproducible; holes, wrinkles and other damages can happen. Third, it is not easy to obtain uniformly bilayer or tri-layer graphene in large areas; the controllability of the graphene thickness is still low. Finally, even though graphene is the most conductive material at the monolayer scale, it has to compete with other materials that are tens or even hundreds of nm thick, in which case the resistance of graphene sheet is often not satisfactory [6]. Once this is achieved, it will have a great impact in future life. These challenges, however, have to be objectively addressed. Fortunately, most challenges are not intrinsic, and are expected to be resolved as graphene continues to be developed [7].

1.1 Graphene properties

This part presents a brief overview of the important properties of graphene and explores their potential for solar cell application and how graphene can potentially bring forth significant impact in the future. Graphene has already demonstrated its high potential in applications at this early stage. This is because it is 2-D, which is easier to process compared to 1- and 0-D nanomaterials. Since graphene is made of carbon, the cost could also be relatively low [3].

First, let us look at the electrical properties of graphene, as they are the most fascinating. Graphene is a semi-metal, which means it is not a metal but behaves more or less like one, therefore it is a conductor. In the graphene lattice, it is found that electrons can travel with only little scattering. That is, electrons can easily be accelerated to high speeds. The mobility is the drift velocity (v) of electrons divided by the external electric field (E). It is theoretically estimated that graphene should have a room temperature mobility of about ($2.5 \times 10^5 cm^2$/Vs). Interestingly, this has also been shown, although under very stringent experimental conditions. As shown in **Table 1**, carrier mobility of graphene exceeds that of other common materials [6].

Table 1. Electron mobility of different electronic materials [6].

Materials	μ (cm^2/(Vs))
Si	1000-2000
GaAs	9000
InP	5000-7000
InAs	33000
InSb	78000

The conductivity is determined by mobility and carrier density: $\sigma = ne\mu$, where n, e and μ are carrier density, elementary charge, and mobility, respectively. Comparing graphene with copper, which is one of the best conductors, graphene conductivity is about 35% higher than that of copper. Since metals usually have a high electron density, graphene can beat copper mainly because of its super high mobility [8].

Second, most conductors such as metals are optically opaque. This is because the free electrons in the conductors have a screening effect, preventing the photons from passing

through. However, graphene is an exception. It is one of the few transparent conductors known. It is only one atom thick and each layer only absorbs 2.3% of the incident light. This number is calculated theoretically based on the electrodynamics of graphene's electronic structure [9].

As shown in **Figure 1** , the samples are the same type of quartz substrates with monolayer graphene deposited on their surface at different times. The samples are placed on a piece of paper with a text on it. The text is clearly seen through the samples due to the high transparency of the graphene layer [10].

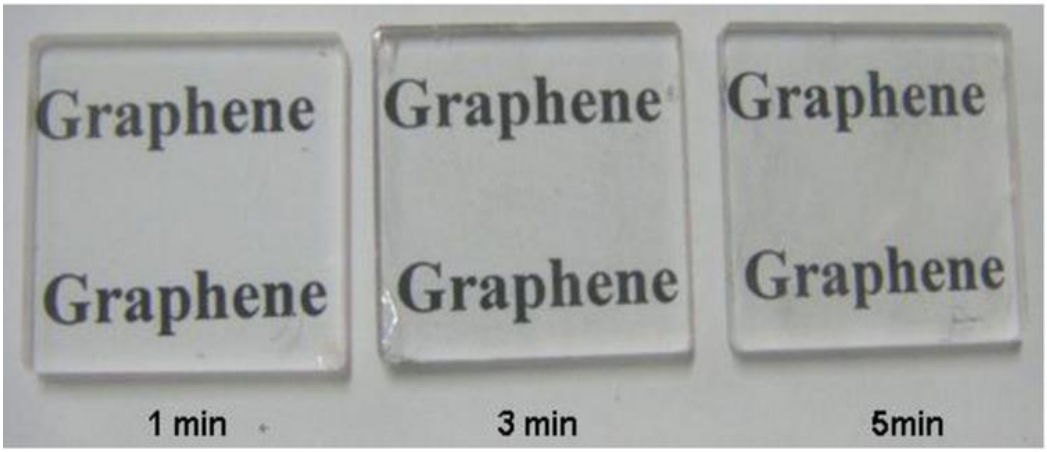

Figure 1. Sample pictures of graphene films on quartz substrates under different times [10]**.**

Quantitative measurements show that after the addition of graphene, the transmittance of the quartz sample is reduced by 2-3%, which is in agreement with the theory. Another amazing optical property is that its transparency is independent to some extent of the wavelength of the light. It is transparent from infrared all the way to the ultraviolet regime [10].

This can be clearly seen in **Figure 2**, where the transmittance of graphene is almost independent of the wavelength of the light. Many other transparent materials, glass for example, are not transparent to UV light [9].

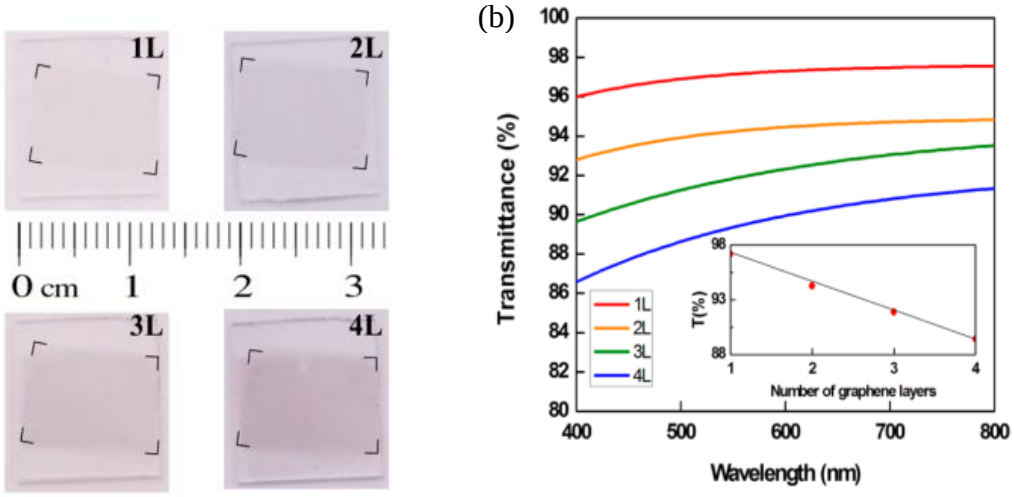

Figure 2. Light transmission rate of the graphene samples with different layers (1L: one layer) [11]

Graphene is an excellent thermal conductor. Its intrinsic thermal conductivity is the highest among all materials, even higher than diamond. It has been shown that the thermal conductivity is isotropic within the basal plane, which means that it is the same in every direction [12].

Graphene is only 0.34 nm thick. Amazingly, it has distinct mechanical properties. For example, the breaking strength of graphene is as high as 130 GPa, which is about 100 times greater than steel [13]. So, it has to be normalized to the cross-sectional area of the material. Therefore, graphene is the strongest material in the world [12]. Graphene is very flexible, because of its atomic thickness. A piece of graphene can be elongated to up to 20% of its initial length. Chemically, graphene is rather stable; the sp2 bonds in graphene are one of

the strongest in nature. Its bond energy is 607 kJ/mole; even higher than that of diamond which is 347 kJ/mole. It is not easily affected by acids and bases, although very strong acids and bases do modify graphene's properties to some extent. At room temperature, it is also rather stable with oxygen, but at high temperatures of around 700^{o}C, graphene is completely burnt into CO_2 [12].

The surface of graphene is relatively easy to modify with oxygen and nitrogen containing functional groups, which means that graphene's chemical properties can be tailored. It has been employed as a substrate to be interfaced with various biomolecules and cells.

Some research indicates that graphene is largely biocompatible, but this is debatable and is still under investigation [12]. However, to use the graphene layer, it has to be transferred from the growth substrate to another substrate. Section 1.4 discusses the transfer methods.

1.2 Potential applications of graphene

Graphene's unique properties could have a great impact and a role in the industrial revolution. Therefore, graphene has many applications which can be categorized according to the possible applications as follows: transparent conductors in optoelectronics [14], integrated circuits [15], energy applications [16] , sensors and actuators [17], water filtration [18], composite materials [19], and biological applications [20], to name a few. This does not include all possible applications because the list is large and may possibly cover almost every field of technology.

1.3 Graphene synthesis

There are many graphene synthesis techniques that are used to produce graphene, such as liquid-phase exfoliation [21], mechanical exfoliation [5] and chemical vapor deposition

(CVD). Synthesis of graphene by CVD is one of the most promising routes for producing large-area and good quality graphene film [22]. This synthesis method is particularly valued for its ability to produce high-quality materials. Compared to other synthesis methods, the resulting materials in CVD usually possess greater purity, hardness, and resistance to agitation or damage. An additional advantage to this method is the wide range of materials that can be deposited, one of which is graphene. [23],[24].

1.4 Graphene transfer techniques

The process of transferring graphene to the target substrate affects its properties and performance. The transfer process can be performed using two main methods; wet or dry; such as polymer assisted [25], electrostatic [26], roll to roll [27], thermal release tape [26] etc. The most commonly used transfer technique is wet transfer, in which Poly-Methyl Methacrylate (PMMA) polymer is used as a supporting layer for graphene during the transfer process. The PMMA/graphene stack has to be transferred to the target substrate. This transfer, as the name suggests, is carried out in a liquid medium (usually water). Due to the hydrophobic nature of the target substrate, the transfer process generally leads to the formation of wrinkles, cracks and tears on the graphene layer, thereby negatively affecting its properties and also reducing its adhesion to the substrate surface [28]–[30].

The details of the transfer method (e.g. graphene on SiO_2/Si) are as follows: graphene is grown on copper (Cu) foil using CVD. Small squares are cut from the CVD grown graphene such that they could fit the 1x 1 cm SiO_2/Si substrate. These squares are then coated in PMMA using the spin-coating technique. This PMMA/Graphene/Copper stack is then placed in Cu etchant solution to etch Cu. The PMMA/Graphene stack is scooped out and placed in DI water. The stack is then transferred to the SiO_2/Si substrate. The

PMMA layer is removed from the substrate by immersing it in an acetone bath as shown in **Figure 3**

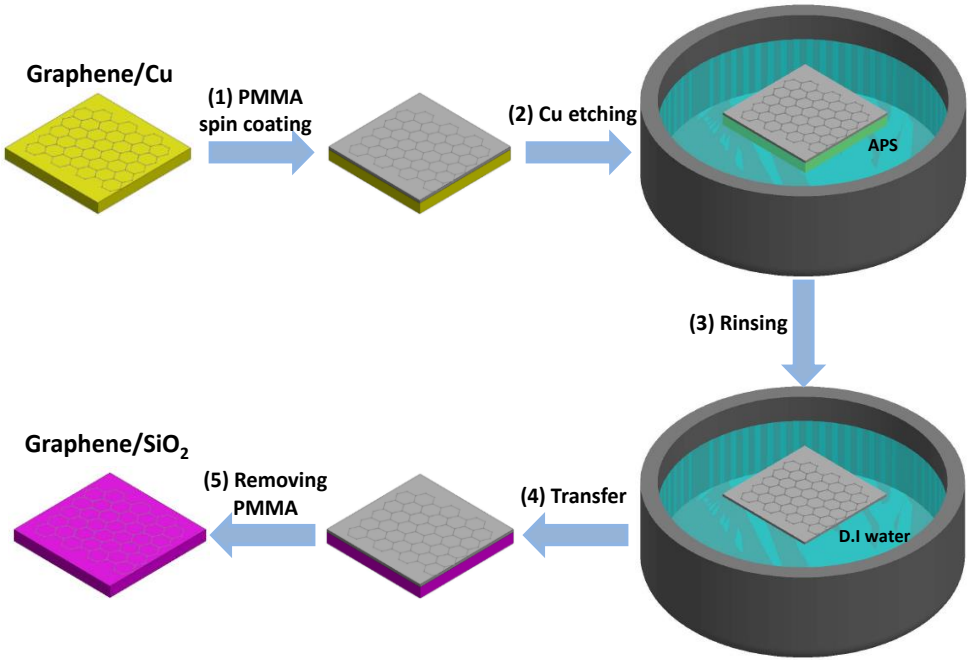

Figure 3. Graphene transfer steps [31].

During the transfer process, many factors can affect the quality of the graphene layer:

- Copper residuals
- PMMA residuals
- Wettability of SiO_2/Si substrate

All these parameters have an effect on the graphene layer and degrade the properties of graphene. Chapter 2 features a literature review on graphene transfer parameters.

1.5 Problem statement

Graphene grown by CVD has been extensively studied for its utility in industrial applications across a range of fields. The drawback in using CVD graphene grown on a

metal catalyst is that during transfer onto a target substrate, a significant number of defects may be generated in the graphene, which deteriorate both the uniformity and the quality of the graphene film/layer.

Present-day graphene transfer using PMMA is complex and, hence, gives rise to defects on the graphene layer. The transfer of CVD-grown graphene onto a target substrate without the formation of cracks and/or wrinkles remains a significant challenge in graphene research. Residues, from Cu and PMMA, left behind also deteriorate graphene properties. For instance, PMMA residues affect the quality of graphene layer and its electrical and optical properties. Moreover, the PMMA/graphene stack does not fully adhere to the SiO_2/Si substrate. Water is usually trapped between the stack and the substrate, causing wrinkles, tears and cracks on the graphene layer. Two of the main parameters which affect contact between the PMMA/graphene stack and the SiO_2/Si substrate are the hydrophilicity of the substrate and the surface tension of the liquid used during the transfer process.

1.6 Thesis overview

This thesis includes five chapters:

Chapter 1 gives a brief introduction to graphene, its importance, transfer methods and the problem statement.

Chapter 2 provides literature on the latest research on graphene synthesis, transfer and characterization techniques. This chapter starts with an introduction of graphene, covers the methods used for synthesizing and transformation and concludes with the proposed aim and objectives for this work.

Chapter 3 outlines the methodology used in this work regarding the synthesizing, characterization, and transferring of graphene.

Chapter 4 presents the results and discussion of the characteristics and performance of graphene.

Chapter 5 concludes the thesis along with recommendations for future work.

CHAPTER 2
LITERATURE REVIEW

One of the most challenging aspects of dealing with graphene is transferring it from the growth substrate to the target substrate. As it is the thinnest material—only one carbon atom thick—the graphene layer is quite fragile and prone to wrinkling and tearing. Graphene can be synthesized by many techniques such as liquid-phase[21] and mechanical exfoliation,[5] however, synthesis of graphene by chemical vapor deposition (CVD) process is one of the most promising ways for producing large area, uniform, low-defect graphene films on suitable substrate [32]. Research groups that are working on graphene have invented different methods to transfer it onto the target substrate. The most common method to transfer a graphene layer from the growth substrate onto the target substrate is using a polymer supported layer using PMMA. Every research group uses a slightly different procedure, and papers have been published claiming that one method is simply better than the other [33]. Each step in the transferring process has an effect on the quality and defects of graphene layer, as mentioned before about the challenges of graphene transfer using PMMA as a supporting layer. The following section provides a literature review of the different transfer methods, how to control the polymeric and metallic contamination and how to reduce the presence of wrinkles, cracks and tears by enhancing the adhesion between graphene layer and the SiO_2/Si substrate.

2.1 Graphene synthesis by CVD technique

In CVD process, there are many parameters which greatly influence the quality and characteristics of grown graphene. The first category of parameters is related to the CVD

system, such as precursor gases (hydrogen (H_2), argon (Ar) and methane (CH_4)), pressure, growth temperature, growth time and cooling rate. The second category of parameters is concerned with the substrate/catalyst, such as its carbon solubility, surface morphology, crystallographic orientation, degree of purity, and cleanliness of substrate surface [32]. Understanding the interaction among these synthesis parameters and their influence on the deposited graphene film is crucial in controlling and optimizing the quality and characteristics of fabricated graphene.

In 2005, E. Rollings et al. have produced graphene layers on silicon carbide (SiC) substrates by thermal decomposition [34]. The graphene films were produced on (001) face of an n-type 6H-SiC single crystalline wafer. Ultrasonic bath has been used to clean the SiC samples. Samples were then inserted into a 10-10 Torr chamber (ultra-high vacuum) and annealed at 850^{o}C in Si flux from a heated Si ingot for 25 minutes to remove native oxides. Subsequent annealing at 1000-1250^{o}C was performed for 5-20 minutes in the absence of Si flux and it resulted to the formation of SLG and FLG, which extended to cover the whole sample area. **Figure 4** shows the progress of the SiC decomposition and graphene formation during growth. However, SLG uniformity has not been realized and the cost of SiC wafers compared to Si wafer is at least 10-15 times. Based on prices of Entegris, Inc, USA, an 8" Si wafer costs $26 whereas an 8'' SiC wafer costs $350 [35].

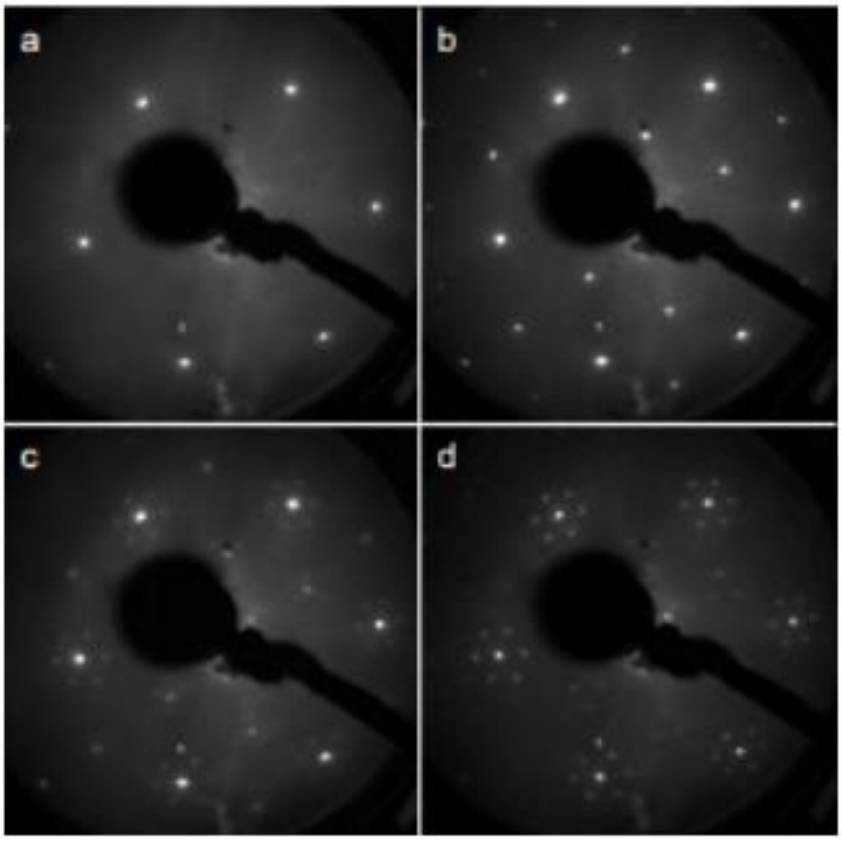

Figure 4. Low Energy Electron Microscopy (LEED) image: a) Bright spots of SiC after 5 minutes annealing at 1000 Celsius, b) Reconstruction of hexagonal Graphene after 5 minutes at 1100 Celsius, c) after 10 minutes at 1200 Celsius, and d) after 4 minutes at 1250 Celsius [34]

In 2006, the first report on graphene synthesis using CVD was reported by Prakash R. Somani et al, Chubu University [36]. Their experiment was mainly a proof of concept. Somani et al evaporated Camphor at 180^{o}C then the gas was passed and subjected pyrolysis (decomposed by heat) at 700-850^{o}C over $2 \times 2\ cm^{2}$ Ni sheets. After the sample was cooled, surface analysis showed that planar FLG can be synthesized using the cost-effective CVD. Recently, a lot of studies have been carried on synthesizing graphene on copper foil. Because Cu exhibits very low carbon solubility (<0.001 atomic %), graphene growth mechanism is limited to the interaction to the catalyst surface only, as depicted in **Figure 5**. First, the carbon species (e.g. methane) diffuses through the stagnant boundary layer (formed by steady state gases flow close to the catalyst surface). The carbonaceous species

is then adsorbed on the substrate surface, and the copper disassociates the carbonaceous gas into carbon and hydrogen atoms. Finally, the carbon atoms are attracted by the substrate surface, forming graphene nucleation sites. The growth begins by diffusion of more carbon atoms onto the copper catalyst surface, forming graphene lattice planes and hence forming graphene domains. The other inactive hydrogen species escapes and is removed by the bulk gas flow through the boundary layer. This is the reason why this mechanism can provide a uniform mono-layer of graphene on the surface compared to the non-uniform graphene layer obtained by segregation process. The domains keep growing till they join with other domains, thus forming a large graphene sheet.

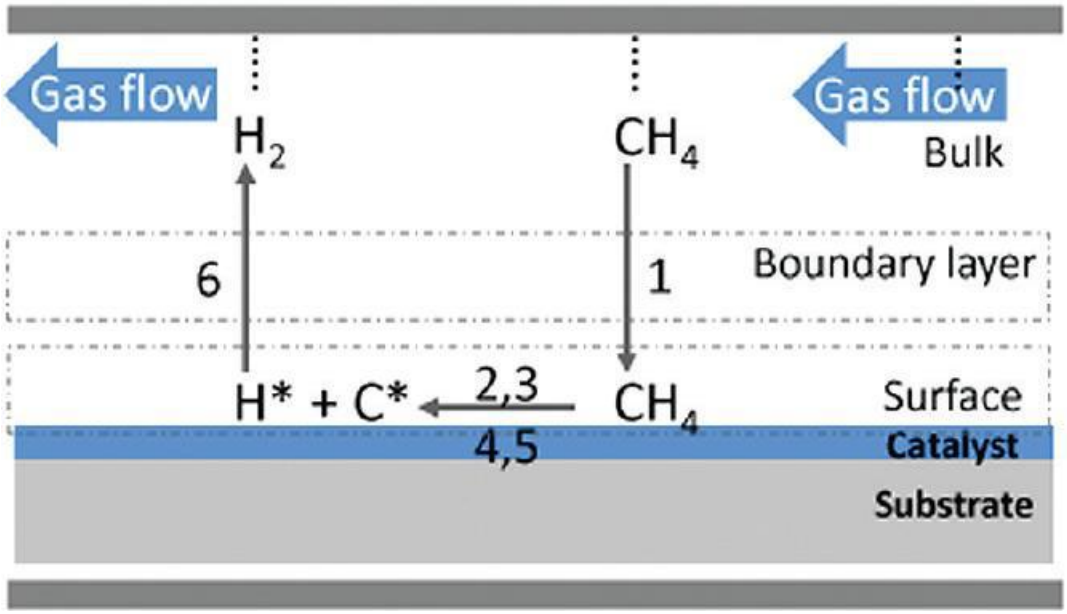

Figure 5. Schematic representation of graphene growth mechanism [37].

Graphene synthesis on Cu substrates can be implemented using either low pressure (LPCVD) or ambient pressure (APCVD) approaches. Many sources reported that, generally, LPCVD was likely to give uniform, monolayer, large area graphene domains. In LPCVD, less concentration of active carbon species results in a smaller boundary layer and

diffuse easier throughout. This type of CVD is found to yield uniform thickness; monolayer graphene, provided that constant temperature is maintained during the synthesis process. As a result, growth automatically stops after a single graphene layer forms, and hence arbitrarily large graphene films can be created.[32]

However, in APCVD graphene quality is controlled by many factors such as; amount of flow gases, surface geometry, position of the substrate and the amount of active species. L. A. David et al. reported [32] that, high flow rate of different precursor gases causes a thick, non-uniform boundary layer to attach to the catalyst surface. Usually this layer significantly reduces carbon species diffusion rate. Therefore, adequate amount of precursor gases is needed to efficiently diffuse through such a large boundary layer, in order to reach the Cu substrate surface. Adversely, this high gas flow rate may lead to more gaseous reactions, causing some particulates to deposit on the catalyst surface during graphene synthesis. This can result in higher defect densities, and hence more nucleation sites. After enough synthesis time, multilayer, non-uniform graphene layers can be obtained. Thus, it is believed that active species (methane and hydrogen) effectively control the quality and thickness of grown graphene in APCVD.

Robertson and Warner [38] declared that, the use of APCVD synthesized graphene yielded few-layer hexagonal-shaped single-crystal domains. The number of layers ranged from 5 to10 in the central region and thinned out toward the domains' edges as shown in **Figure 6**. These findings conflict with previously observed self-limiting graphene growth mechanism which gave monolayer graphene domains.

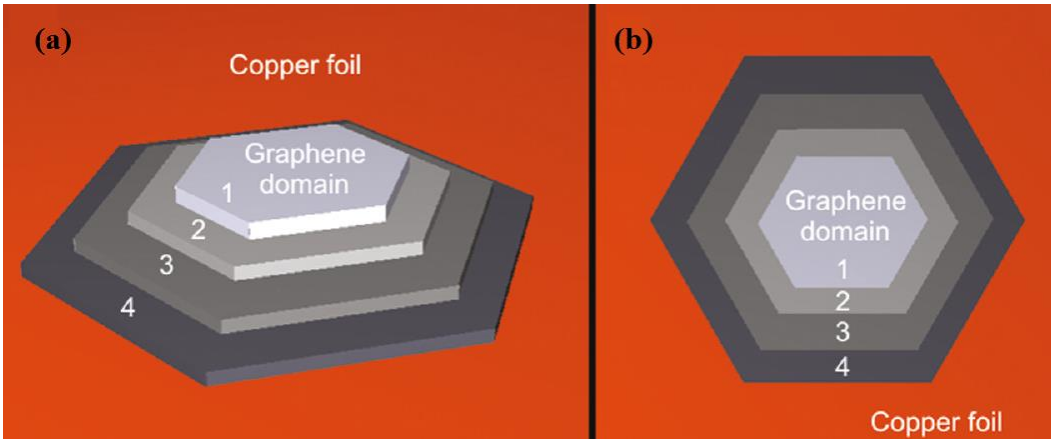

Figure 6. A schematic representation of few layer graphene domains on copper foil [38].

Li, et al. [22] successfully grew large-area graphene films using CVD technique, using specific growth parameters (methane with 35 sccm at 500 mTorr, hydrogen with 2 sccm, growth temperature of 1000 ^{o}C, and growth time of 30 minutes). The grown graphene was continuous across the copper surface steps and grain boundaries. Results revealed the presence of monolayer graphene occupying more than 95% of investigated area, in addition to a small fraction of bilayer and few-layers (<5%).

Li et al. [39] demonstrated that, under certain conditions (growth temperature of 1035 ^{o}C, methane flow rate of 7 sccm, partial pressure 160 mTorr and growth time of 2.5 min), graphene growth terminated before achieving full surface coverage, even if the entire copper surface was exposed to methane. As a result, they needed to introduce a second step process to get full graphene surface coverage by increasing partial pressure to 2000 mTorr for 1-minute growth time. The average domain area was 142 μm^2. The graphene growth in this work is proposed to be a surface adsorption process combined with an epitaxial growth: hydrocarbon precursor (CH_4) is decomposed into free carbon species on the copper foil at high temperatures. The graphene grains start to nucleate and grow at step edges, folds, or other imperfections on the copper foil via a self-limited surface adsorption process.

Subsequent layers can be formed on the underlying layer via an epitaxial growth under a high concentration of carbon species [40].

Ibrahim et al.[41] investigated the effect of H_2 concentration during annealing on evolution of Cu surface morphology, and on deposited graphene characteristics. They concluded that H_2 had an effect on the roughness of the Cu substrate surface and had a smoothing effect on Cu surface. Graphene morphology and its quality were affected by the content of H_2. A low H_2 concentration (0% and 2.5%) during annealing promoted uniform and good quality bilayer graphene. In contrast, a high concentration of H_2 (20% and 50%) resulted in non-uniform, defective, multilayer graphene as shown in **Figure 7** and **Figure 8**. Interestingly, the annealed Cu surface morphology differed considerably from that obtained after deposition of graphene, indicating that graphene deposition had its own impact on Cu surface.

Since, as mentioned before, the surface roughness of Cu surface has an effect on graphene quality so, the Cu substrate pre-cleaning process influences the quality of graphene. Ibrahim et al. [42] investigated the effect of different etchants on the graphene quality. They used ammonium persulfate (APS), ferric chloride ($FeCl_3$) and nitric acid (HNO_3) for short and long times (30s and 5min) to study their effect on graphene quality. They concluded that increasing the etching time produced a rough Cu surface, which, in turn, produced low graphene quality. Therefore, 30s-etching yielded a smoother Cu surface compared to 5min. Besides, using APS for 30s to etch the Cu surface produced the most continuous, uniform, predominantly monolayer graphene film with low density of bi/few layered domains, as shown in **Figure 9** .

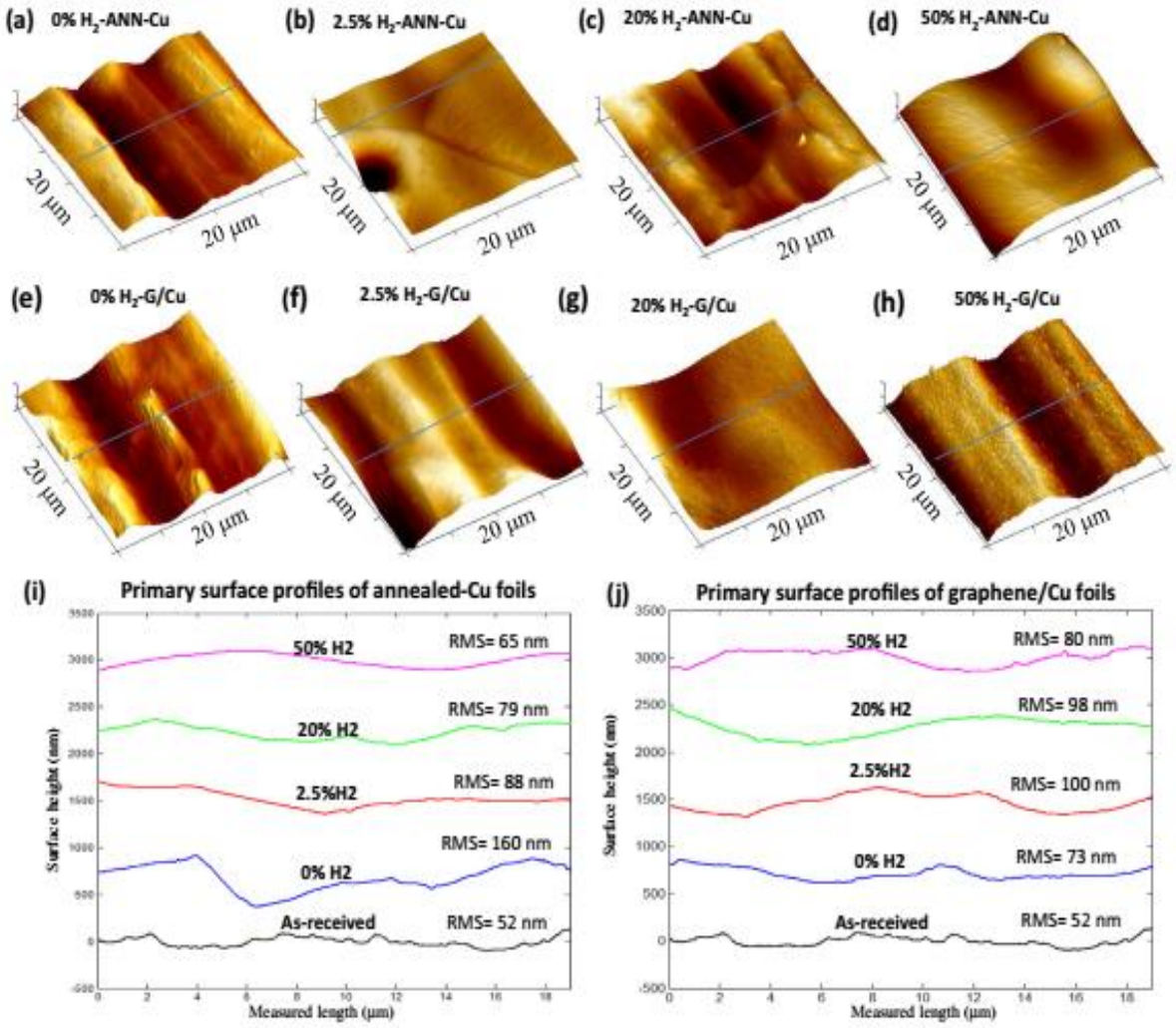

Figure 7. Cu surface morphology before and after graphene deposition and corresponding cross-sectional primary surface profiles. (a–d) 3D-AFM images of annealed Cu foils, (e–h) after graphene growth, (i) primary surface profiles of annealed Cu and (j) of graphene/Cu along with as-received Cu for comparison. The scan area was 20 * 20 µm^2 in each case [41].

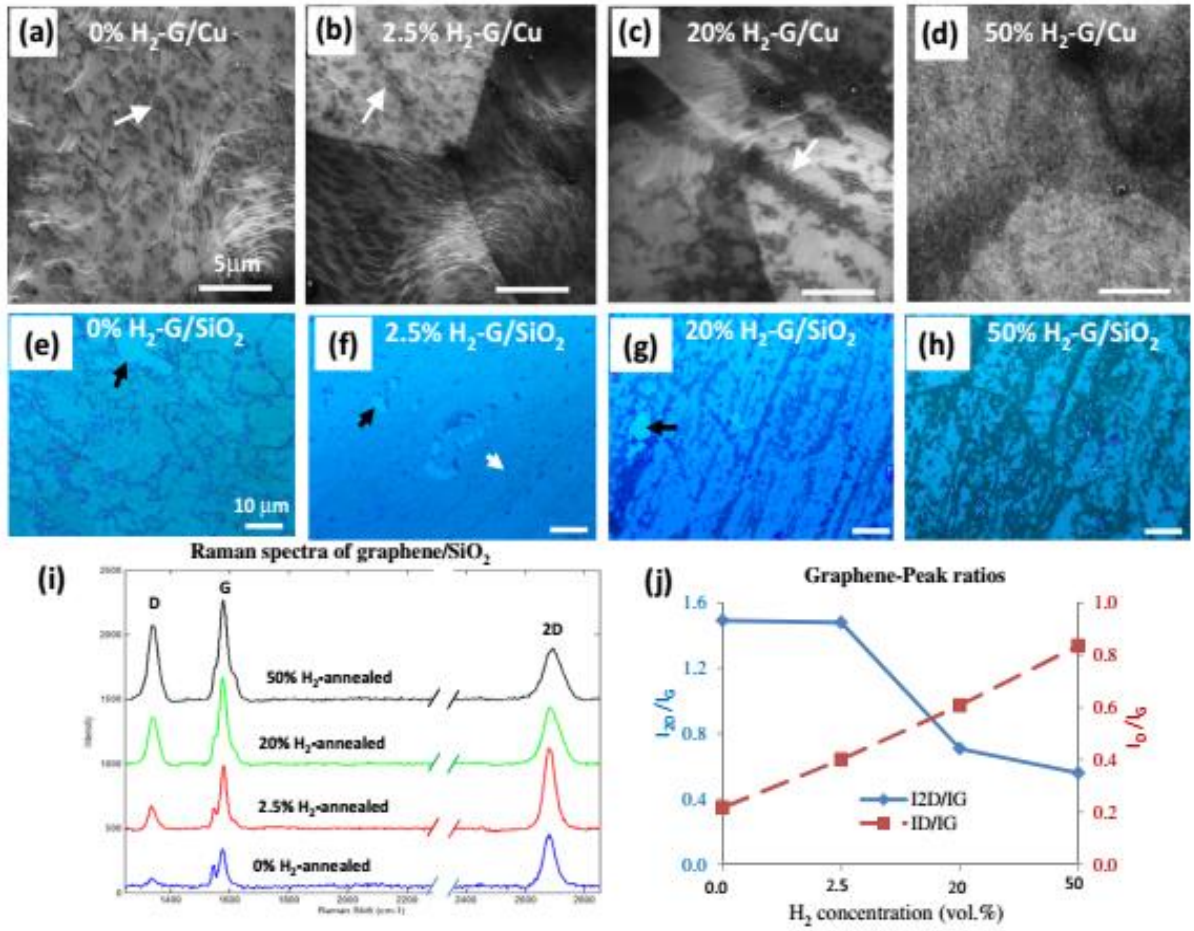

Figure 8. (a–d) SEM micrographs of graphene/Cu samples annealed at 0%, 2.5%, 20% and 50% H2, respectively. Graphene domains are highlighted by white arrows in a–c, (e–h) OM images of transferred graphene onto SiO2/Si, some tears are marked with black arrows. (i) Raman spectra of transferred graphene and (j) plot of I2D/IG and ID/IG ratios measured from Raman spectra shown in panel (i). The scale bars of (a–d) are 5 μm and (e–h) are 10 μm[41].

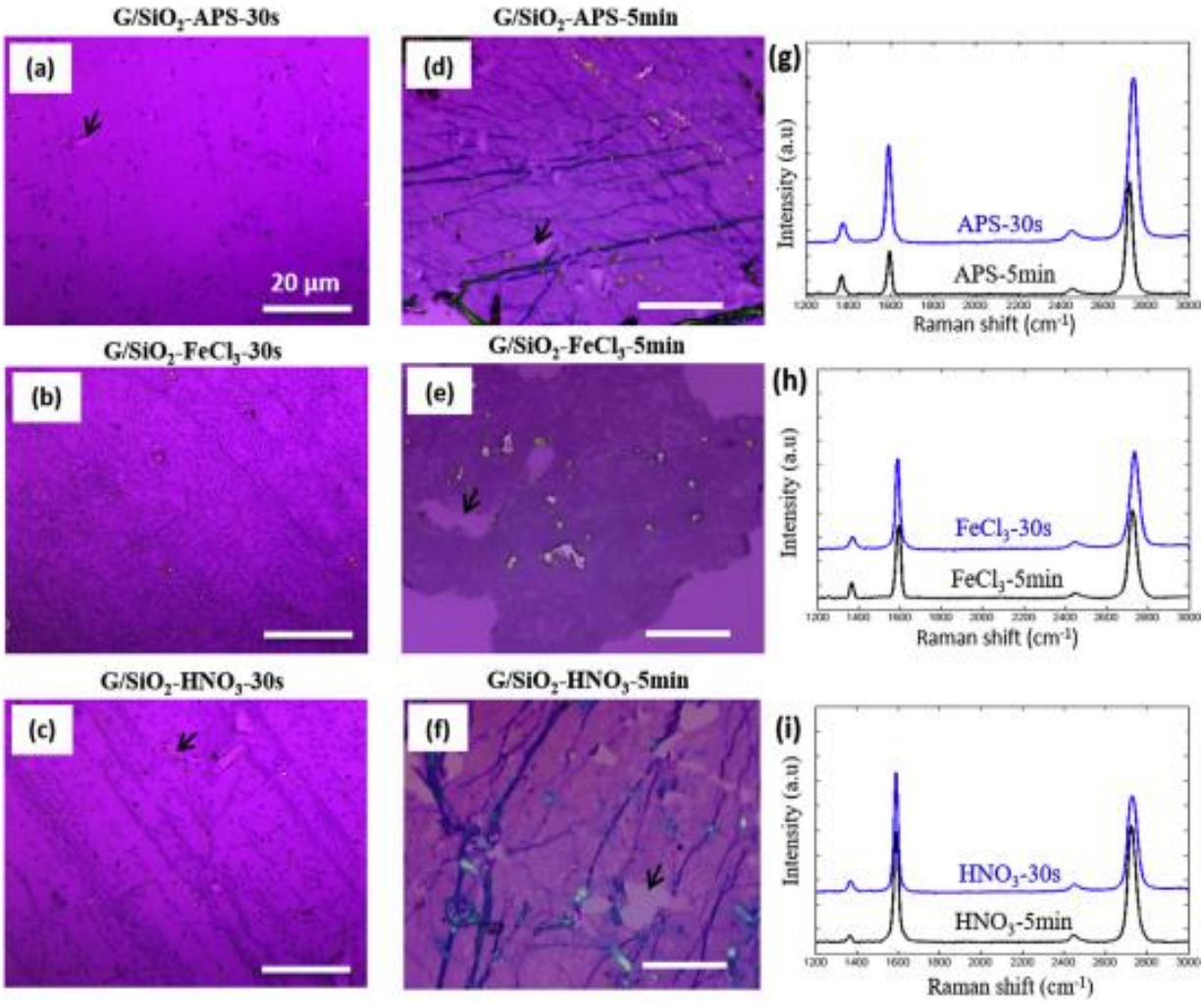

Figure 9. Optical images and Raman spectra of transferred graphene films onto 300 nm SiO2/Si substrates from growth Cu foils that pre-etched for 30s and 5min using (a,d,g) APS, (b,e,h) FeCl3 and (c,f,i) HNO3. It is seen that transferred graphene layers from 30s-etched Cu are more continuous than 5min samples, which contained visible wrinkles, tears and cracks [42].

2.2 Graphene transfer methods.

For the outstanding properties of graphene to be fully utilized, graphene must be able to be transferred to different substrates. There are several techniques to transfer graphene such as roll to roll method, using thermal released tape and using polymer assisted layer. Basically, the transfer process can be divided into two main categories: wet and dry.

Most wet transfer methods are conceptually the same. They involve etching the metal substrate to free the graphene and then scooping the graphene layer using the target substrate.

Reina et al. used the CVD graphene synthesized on Ni evaporated on SiO_2/Si substrates as shown in **Figure 10**. First, they spun Poly-Methyl Methacrylate (PMMA) on the graphene on top of the sample. Then, using a solution of hydrochloric acid (HCl) diluted in DI water (3% by volume), they etched the Ni layer. Now that the graphene/PMMA layer was detached it could be transferred to any target substrate. Once transfer was complete, acetone was used to dissolve the PMMA [43].

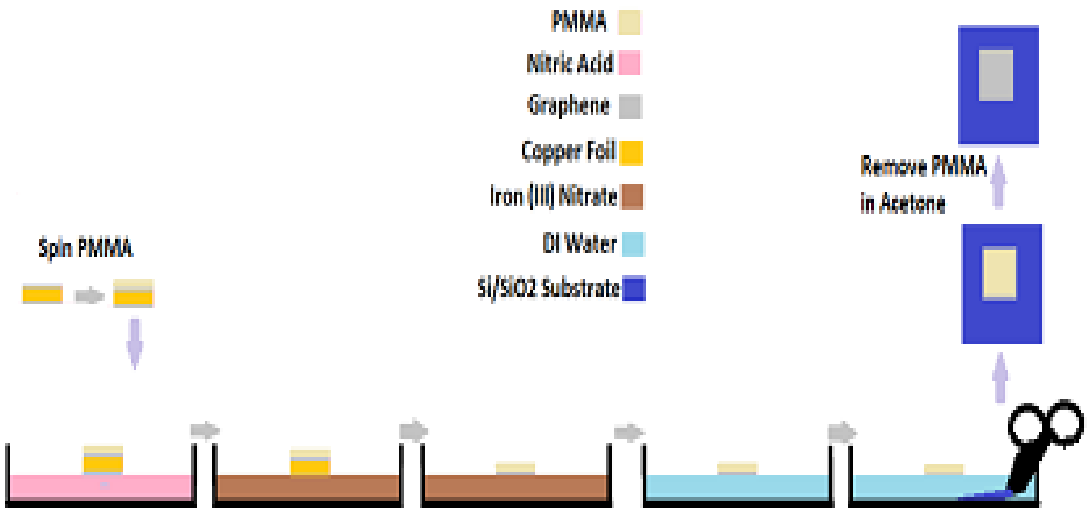

Figure 10. PMMA transfer method [44].

In addition to using PMMA as supportive layer during graphene transfer, another kind of polymer was used in graphene transfer. Lin et al. used Poly (bisphenol A carbonate) PC instead of PMMA to transfer graphene. The benefit of using a PC layer is that it can be easily removed using a chloroform [45].

Li et al. improved the transfer technique by using a double layer of PMMA. The second layer of PMMA was added after copper was etched away. Then both PMMA layers were removed using acetone. Optical images in **Figure 11** show how using double PMMA layers yielded a much improved graphene layer with less cracks [46].

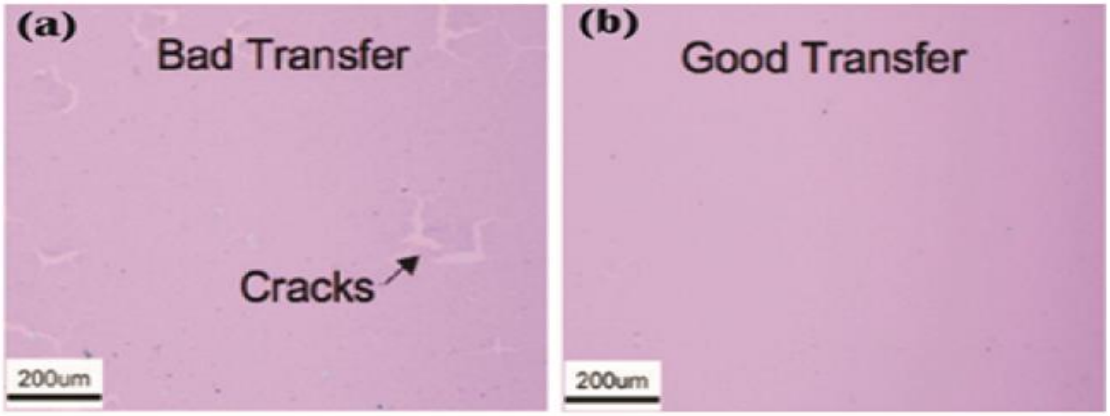

Figure 11. Optical images of graphene transferred by a) single PMMA layer b) Double PMMA layers method [46].

Lin et al. transferred graphene to substrate without using any type of polymer by using graphite holder as shown in **Figure 12**. The purpose of graphite holder was to be a confinement area for graphene. First, copper was etched, and then graphene was transferred to target substrate. This method showed advanced electrical mobility. The size of the transferred graphene was limited by the size of graphite holder[47].

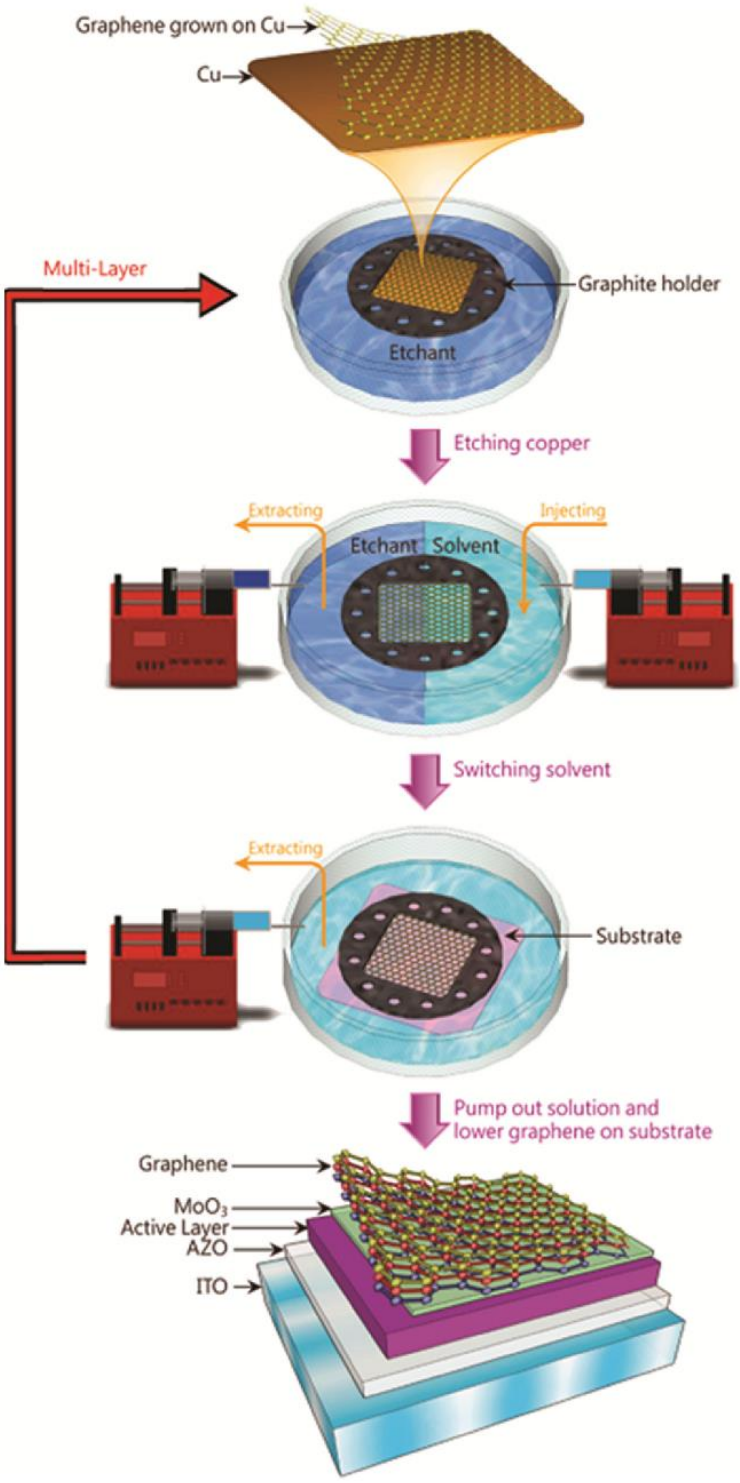

Figure 12. Graphene transferred using graphite holder [47]**.**

Wang et al. demonstrated direct transfer by negatively charging the target substrate and bringing it in contact with CVD grown graphene on Cu as shown in **Figure 13** [28]. This allowed the Graphene to adhere to the substrate after the whole stack was placed in a Cu etchant. However, our target substrate isn't polymeric or flexible as the one used in the paper and that introduce a major problem. Since SiO_2 and Cu are two rigid solid surfaces, some gaps are formed when the two are attached after charging. This causes the graphene to transfer in an uneven and discontinuous form. Moreover, due to the presence of these gaps, the two surfaces aren't even bonded strongly enough to keep them together.

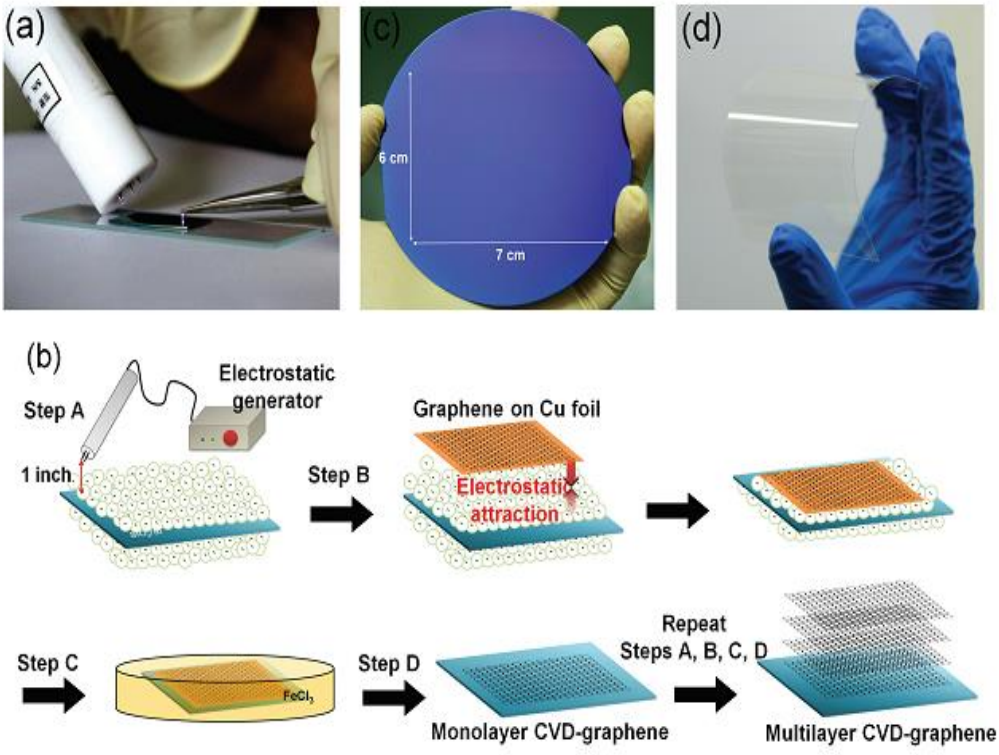

Figure 13. Steps of electrostatic transfer method [28].

Want et al. used the electromechanical delamination method to remove the metal substrate instead of etching it. One of the advantages of this method is that the metal substrate can be reused [48]. **Figure 14** showed how the electrochemical delamination method works. A

layer of PMMA is deposited using the spin coating method. The whole stack is then inserted in an aqueous solution, acting as the cathode electrode. Voltage is applied to form hydrogen bubbles between the interface of graphene and metal substrate. Finally, graphene is delaminated and transferred to the target substrate.

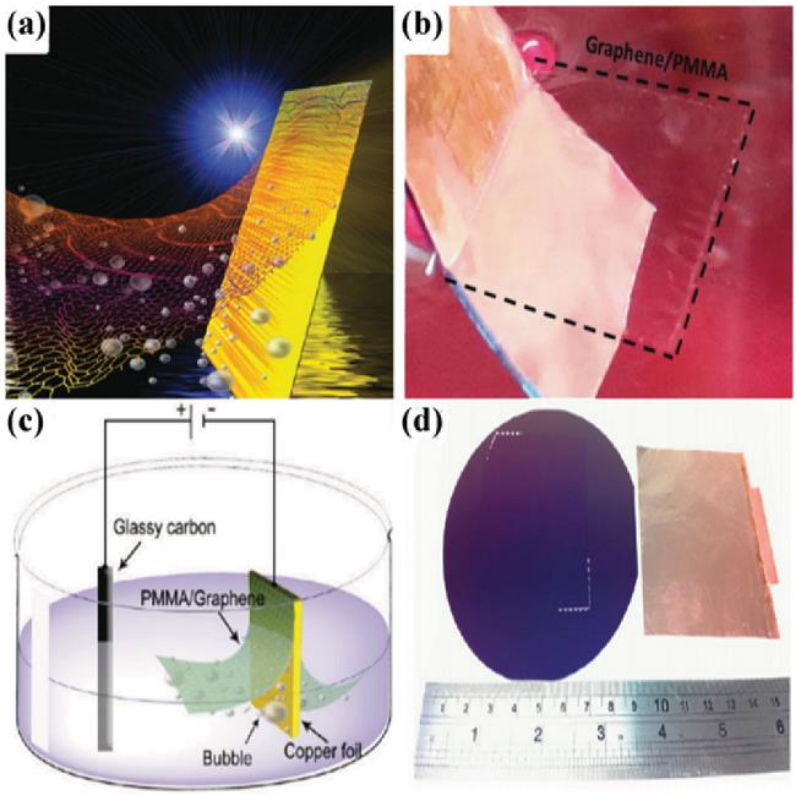

Figure 14. steps of the electromechanical delamination method [48].

The second category of graphene transfer methods, the dry method, does not involve the use of any solutions. One of these methods is roll to roll graphene transfer. Ryu et al. used the roll to roll transfer method, as shown in **Figure 15**. They transferred graphene to the Polyethylene terephthalate (PET) substrate[49]. This transfer method is suitable for transferring graphene, so it can be used as electrode in the capacitive multi touch devices.

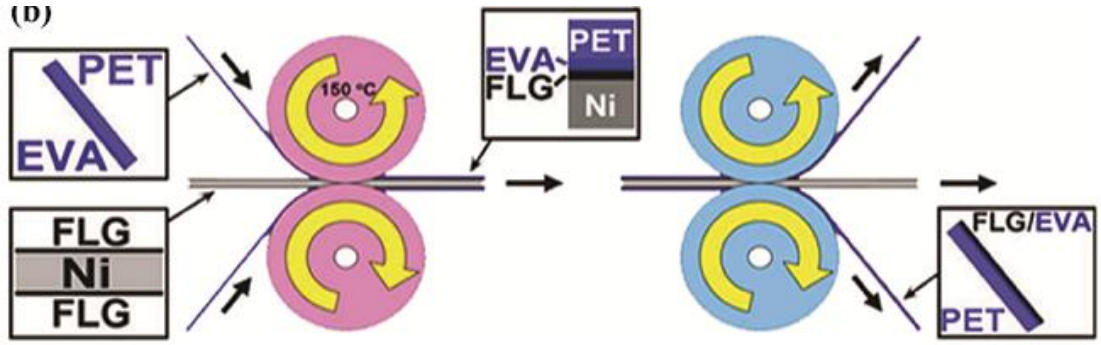

Figure 15. Roll to Roll graphene transfer [49].

2.3 Controlling polymeric and metallic contamination

Graphene is grown on all sides, as the quartz boat is concave, and the Cu foil is usually not perfectly touching the bottom side. This enables the gasses during the growth phase to form a graphene layer on the bottom as well during the growth phase. Hence, since the Cu foil has to be etched away, a good enchant profile for the etchant to Cu has to be provided. It was reported in many studies that using different copper etchants to etch the copper from graphene during the transfer methods affects the quality of graphene and adhesion. The most common used etchants are ammonium persulfate (APS), iron (III) nitrate and ferric chloride ($FeCl_3$).

X. Liang et al. were able to remove the copper residues using the two-step cleaning process, which they call “the modified RCA (Radio Corporation of America) clean method”. They used Iron Nitrate, and then used the two-step cleaning process to remove Copper residues. Step 1 (SC-2) involves the use of 20:1:1 $H_2O/H_2O_2/HCl$ (this removes ionic and metal components). Step 2 (SC-1) involves the use of 20:1:1 $H_2O/H_2O_2/NH_4OH$ to remove insoluble organic contaminants [50].

Copper residuals were observed on SEM images after the etching process, as shown in **Figure 16**. They reported that the graphene/target-substrate interface resulting from this clean transfer process greatly improved, as the copper residuals decreased.

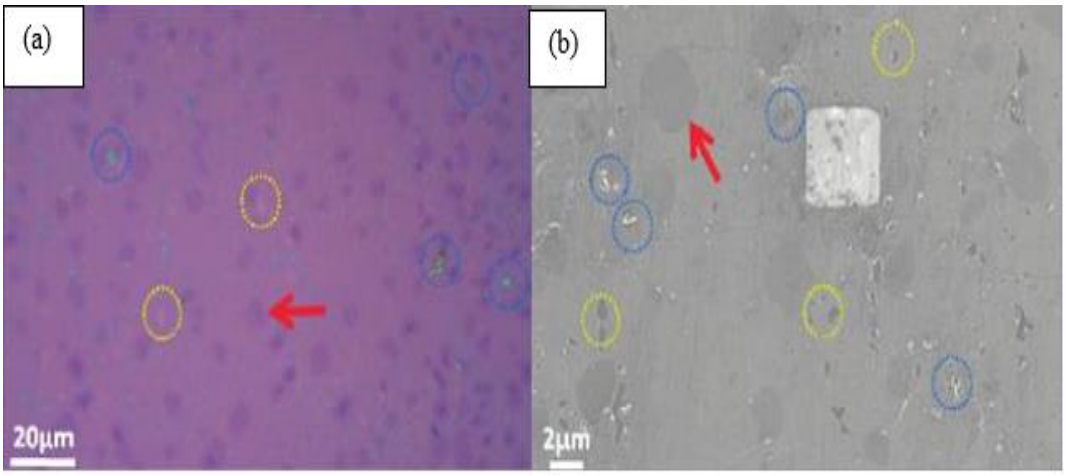

Figure 16. (a) Optical Image (b) SEM image of graphene shown, many residual metal particles (for example, blue circles) and small holes (for example, yellow circles) [50]**.**

X. Li et al. transferred a large area of graphene and investigated its performance as transport conductive electrodes. They used iron nitrate (0.05 g/mL) over a period of ~12 h to etch 1 × 1 cm^2 × 25 µm thick Cu substrate, but did not optimize the time and show the effect of copper residuals on the performance [51].

J. W. Suk et al. transferred graphene onto three different classes of substrates: substrates covered with shallow depressions, perforated substrates, and flat substrates using wet and dry transfer methods. They used iron nitrate with concentration of 0.05 g/mL for 12 hours to etch copper substrate [52].

D. Y. Wang et al. used electrostatic force to attach graphene layer grown on copper directly to substrate and then etched the copper using iron nitrate 0.4 g/ml. to avoid the development of PMMA residuals. They then compared the result using PMMA and using electrostatic

force [28]. As shown in **Figure 17.a** There are still PMMA residuals on the transferred graphene layer

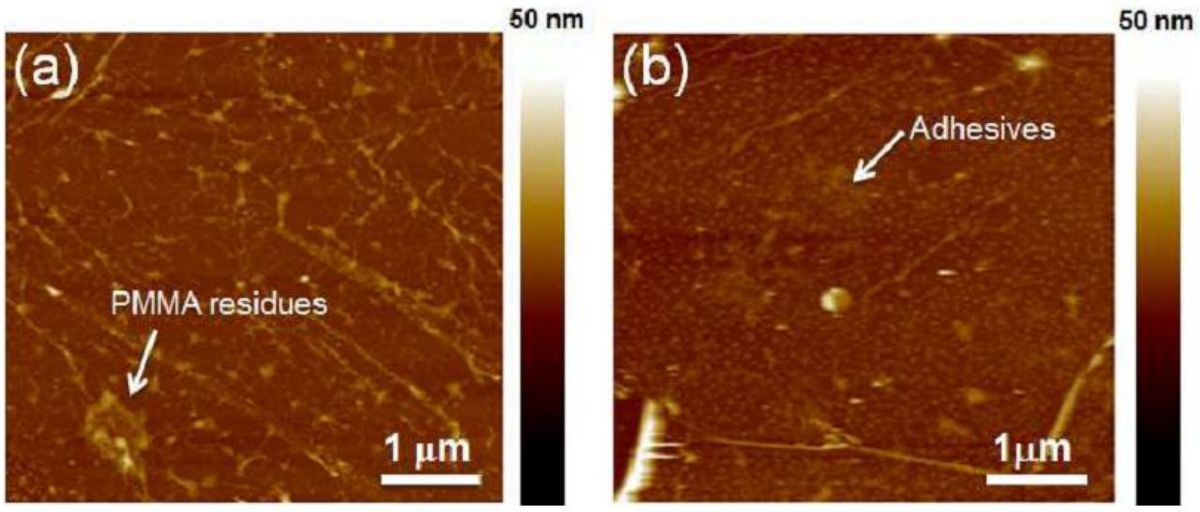

Figure 17. AFM image (a) Using PMM (b) using electrostatic force [28]**.**

W. Regan et al. reported a polymer-free method for transferring the graphene layer directly to the target substrate, in order to avoid the use of a wet chemical removing of the polymer layer. They transferred the graphene directly from copper growth substrate to holey carbon transmission electron microscope grids. **Figure 18** shows the steps of direct transfer, in which they used aqueous ferric chloride (FeCl3) with concentration of 0.1 g/ml for 2 hours to etch the copper [53].

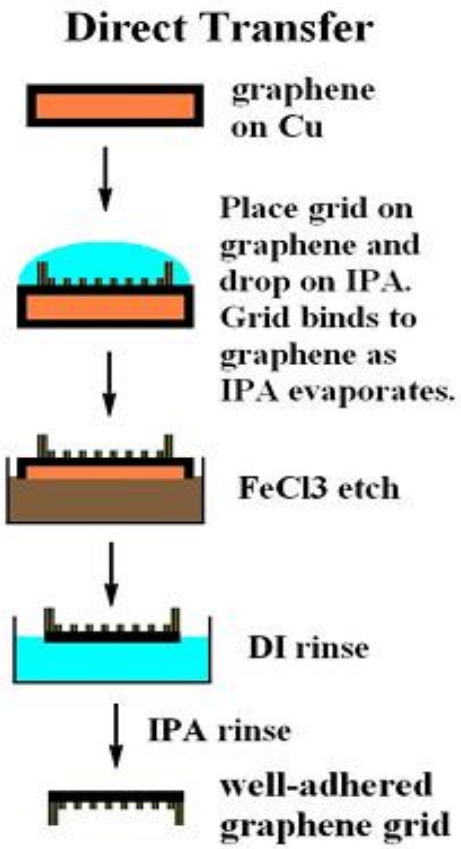

Figure 18. Steps of Direct transfer to TEM grids [53].

X.-D. Chen et al. used a two-layer structure consisting of polyethylene terephthalate (PET) and silicone to transfer graphene growth by chemical vapor deposition onto various rigid and flexible substrates through dispersive adhesion. As shown in **Figure 19** shows the steps of transfer [54]. They used ferric chloride (FeCl3) solution (1 M) for 1 hour to etch copper and concluded that, because of its efficiency and the high-quality sample it yielded, the PET/silicone transfer method would be particularly useful for electronic applications. They made a comparison between different transfer methods using PMMA, PET and thermal release tape (TRT) regarding cracks and wrinkles. As shown in **Figure 20**. There are many copper residuals.

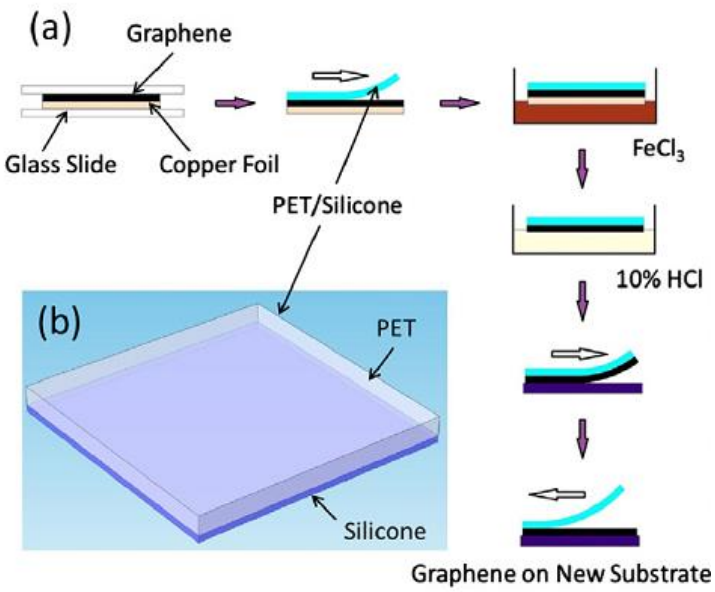

Figure 19 Steps of graphene transfer using PET/Silicon [54]**.**

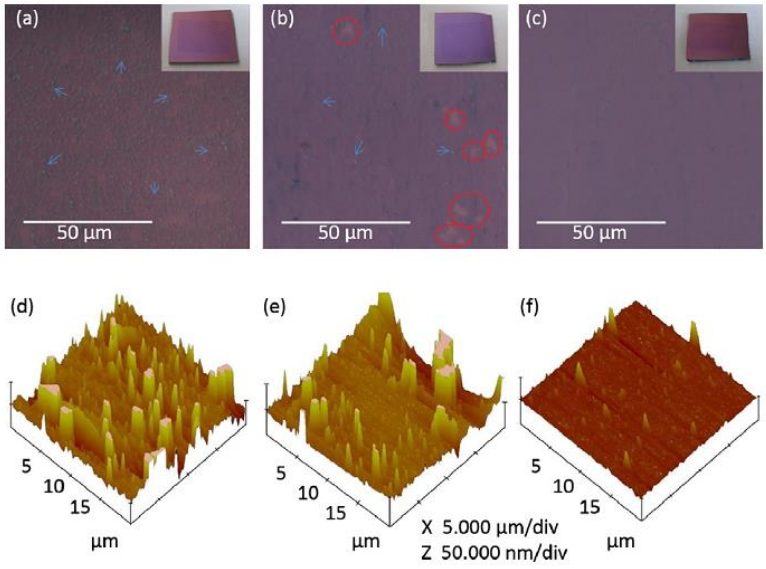

Figure 20. Optical and 3D AFM images of different transfer methods (a-d) TRT, (b-e) PMMA and(c-f) PET/silicone, respectively [54]**.**

K. R. Williams used ferric chloride ($FeCl_{3)}$ mixture (30% FeCl3 + 3-4% HCl + H2O) at room temperature to etch copper. Copper metal is oxidized to Cu^{2+}. HCl assists in the

dissolution of the ferric chloride, and also etches copper itself. They recommended rinsing the sample after etching copper in a 5–10% HCl solution before a final water rinse [55].

H. H. Kim et al. studied the effect of each parameter in transfer method to investigate what causes the cracks and wrinkles. They used APS with concentration of 0.1 M solution in copper etching stage and claimed that the copper etching method would reduce particles residue.

G. Lupina et al, investigated the effect of copper residuals on the electronic and electrochemical properties of graphene. They used Ammonium persulfate (20-50mg/mL in water), iron(III)-chloride (80-120mg/mL in water), and 2:1:1 solution of H_2O:H_2SO_4:H_2O_2 to etch copper [56]. **Figure 21** shows a comparison between different etchants and the concentration of copper residual.

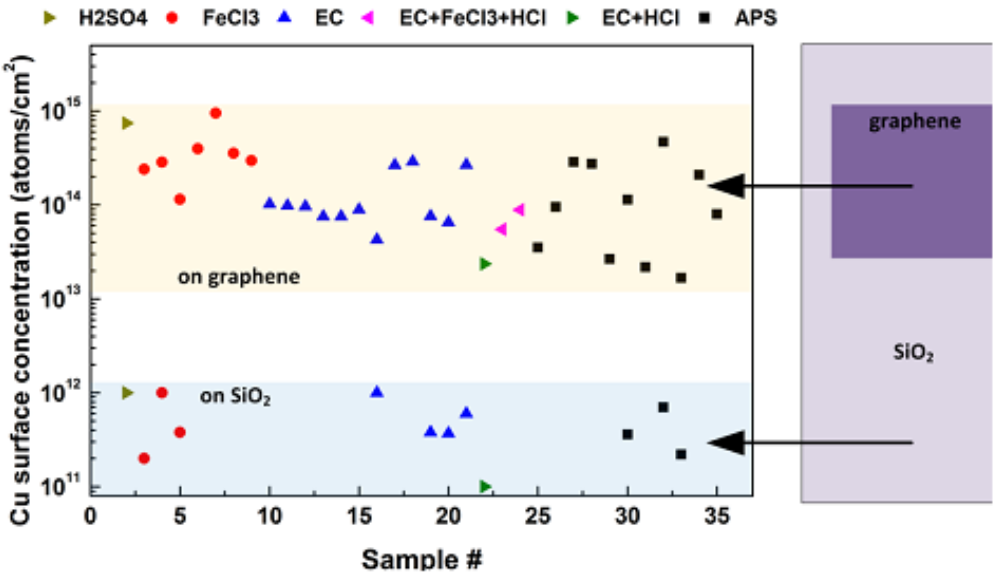

Figure 21. Comparison of concentration of copper for different etchant [56].

As shown in **Figure 21**, APS gave a low copper concentration on the surface of the graphene. G. Lupina et al. found that reducing the copper residuals could be obtained by using thermal treatment. **Figure 22** shows the relation between the annealing effects on the copper residuals using Time-of-Flight Secondary Ion Mass Spectrometry (ToF-SIMS) for reference samples without graphene.

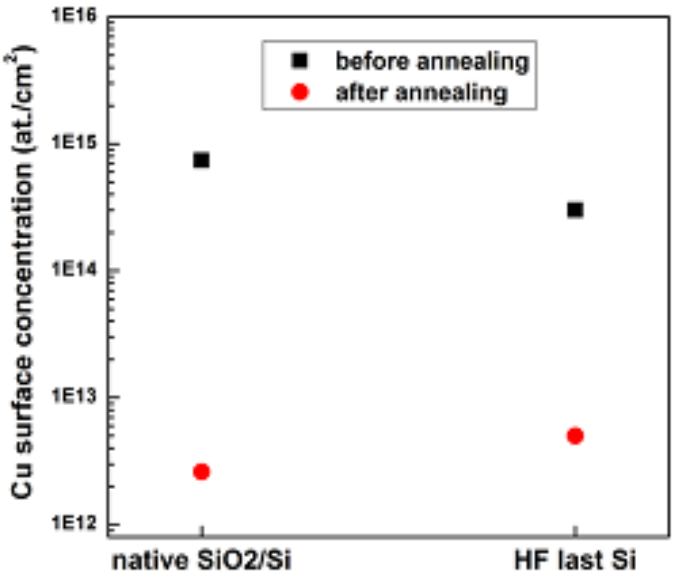

Figure 22. Effect of annealing on Copper concentration [56].

Gabriela et al. used a normal transfer procedure using PMMA to investigate the effect of the transfer method and PMMA residuals on electrical conductivity. For copper etching, they used Trancene CE100 for 15 minutes. **Figure 23** shows that the copper residues were reduced when Trancene CE100 was used [57].

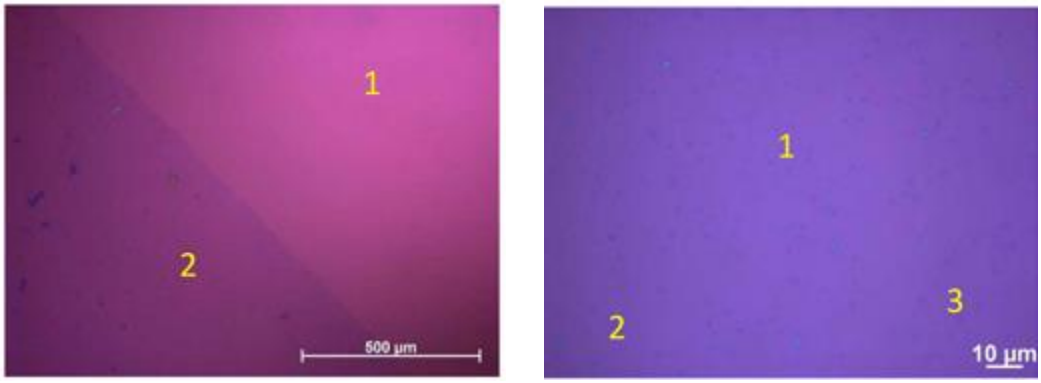

Figure 23. Optical image of graphene showing copper residues [57]**.**

Polymethylmethacrylate (PMMA) is commonly used as a supporting layer to transfer graphene into other substrates.[43] After transfer, the PMMA layer must be removed to in order to obtain a clean graphene layer. The problem is that this layer cannot be completely removed, and the residuals of PMMA degrades the properties of the graphene layer .[58]–[61] Many methods have been suggested to reduce the PMMA residuals, such as annealing [62]–[65], use of chemicals [63], current induction [66] and atomic force microscope (AFM) cleaning [67]–[69]. PMMA residuals have an effect on the electrical and optical properties of the graphene layer; it was reported that less PMMA residuals on the top surface of graphene the layer would result in lower sheet resistance and better electrical and optical properties [64].

The application of acetone and isopropanol at different times and temperatures in order to reduce residuals while removing PMMA was reported in different papers. The following section presents a review of the different times and methods used to remove the PMMA layer.

A. Reina et al. used CVD graphene synthesized on Ni evaporated on SiO_2/Si substrates. First, they spun Poly-Methyl Methacrylate (PMMA) on the Graphene on top of the sample.

Then, using a solution of hydrochloric acid (HCl) diluted in DI water (3% by volume), they etched the Ni layer. Now that the Graphene/PMMA layer was detached, they were able be transfer it to any target substrate. Once transfer was complete, Acetone was used to dissolve the PMMA [43]. **Figure 24** shows the resulting graphene layer transferred to SiO2/Si . This technique is fairly simple and can be easily adapted to Cu foils with no major modifications.

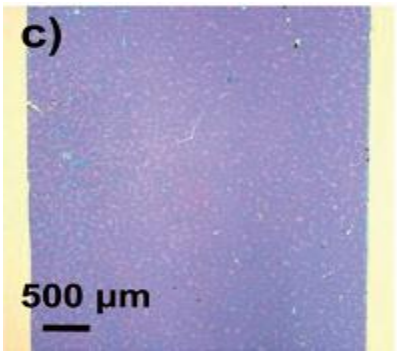

Figure 24. Optical of graphene grown by CVD transferred to a SiO2/Si substrate [43].

2.4 Enhancing the adhesion between the graphene layer and SiO_2/Si substrate

The wettability of SiO_2/Si substrate is one of the main parameters which affects the graphene transfer process and the quality of graphene. This paper will present the effect of altering the SiO_2/Si hydrophilicity and its relation to the quality of graphene [30][26][70].

The PMMA/graphene stack does not fully adhere to the SiO_2 /Si substrate. Furthermore, water is usually trapped between the stack and the substrate which causes wrinkles, tears, and cracks on the graphene film. This is related to the hydrophilicity of the substrate being

used and also the surface tension of the liquid used during transfer. **Figure 25** shows how surface hydrophilicity causes the formation of cracks and wrinkles [56].

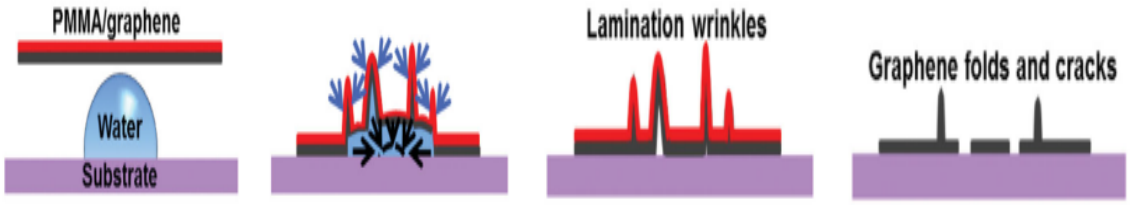

Figure 25. The effect of hydrophilicity of the surface on the crack and wrinkles formation [56].

The transfer of PMMA/graphene stack on hydrophobic substrates is more challenging because water spontaneously de-wets these surfaces as shown in **Figure 26**.

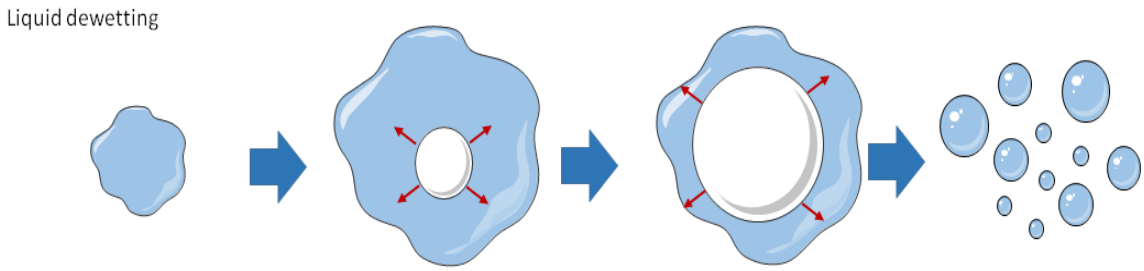

Figure 26. Effect of surface tension on water droplets [71].

To resolve this issue, Martins et al. suggested adding a small amount of isopropanol to the rinsing bath of distilled water, which lowered the solution surface tension enough to induce complete wetting on the hydrophobic surfaces. [72]

A hydrophilic substrate ensures even distribution of water on its surface and will improve the smoothness of the PMMA/graphene stack. Lower contact angle between the substrate and water will make the PMMA/graphene stack adhere to it with minimum folds and cracks. Thus, controlling the wettability of the substrate and decreasing the water contact

angle will have a great effect on the adhesion and will reduce the cracks and wrinkles on the graphene layer.

X. Liang et al. used hydrofluoric acid (HF) to control the hydrophilicity of the surface by dipping the SiO_2/Si substrate in the HF at different times. Water contact angle (WCA) was measured for each sample in order to investigate the effect of decreasing WCA on the graphene layer, as shown in **Figure 27** [50].

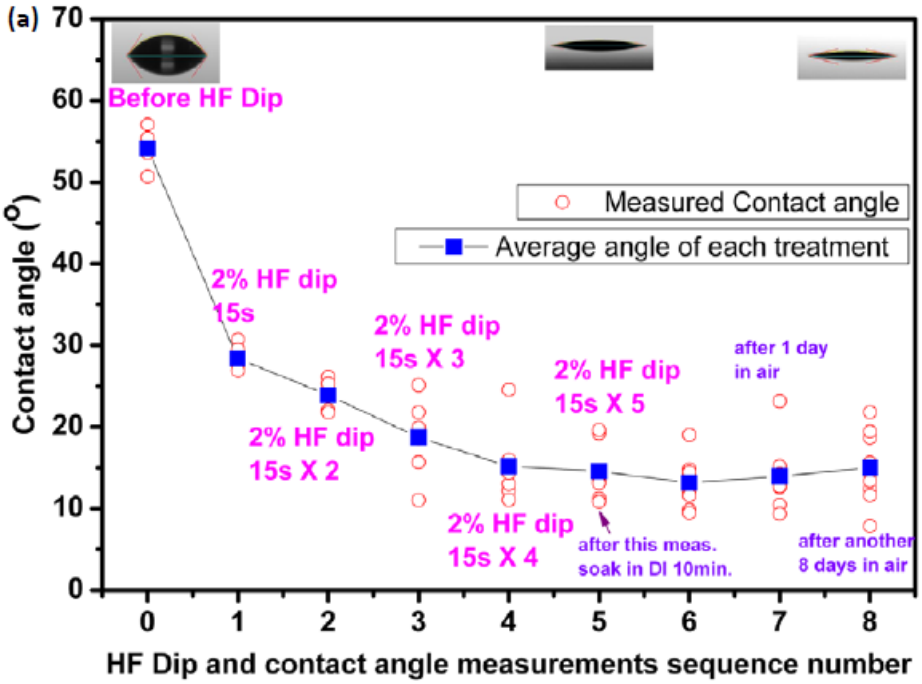

Figure 27. Effect of HF treatment on the WCA [50].

An optical image of a PMMA/graphene stack on a HF treated SiO_2/Si substrate showed improvement in adhesion between stack and substrate due to improvement in the hydrophilicity of the substrate. As shown in **Figure 28 ,** no large folds were formed.

Figure 28. Optical image of PMMA/graphene stack for HF treated SiO_2/Si substrate [50]**.**

H. H. Kim et al. presented another approach to improve the adhesion between the PMMA/graphene stack and SiO_2/Si substrate. They tried to control the surface tension (contact angle) of the liquid used during the transfer process. They used a low surface tension organic volatile liquid (Heptane). This reduced the contact angle even on super-hydrophobic surfaces and formed a uniform layer under the SiO_2/Si substrate during the scooping stage [56]. **Figure 29** shows the effect of uniform water layer between substrate and PMMA/graphene stack.

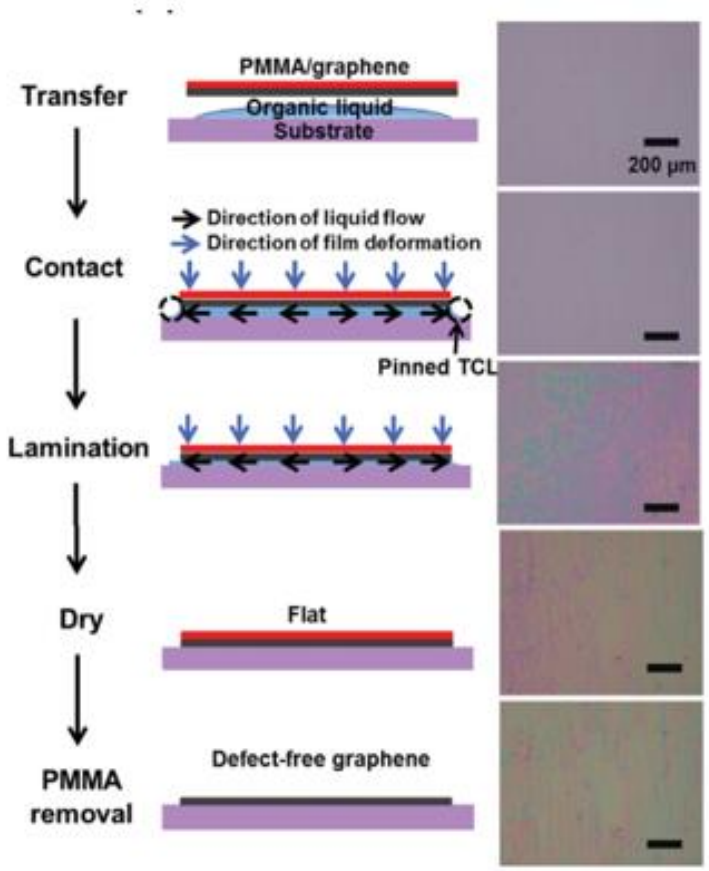

Figure 29. The effect of uniform water layer between substrate and PMMA/graphene stack [56].

Y. Zhao et al. discussed the effect of micro-scale holes array substrate and its effect on wettability. They transferred graphene directly to the target substrate without using any polymer assisted layer. They studied the effect of surface roughness using two models, Wenzel and Cassie equations. Both equations are used in most cases to exclude the effect of the surface roughness on the water contact angle of a water droplet on a target substrate.

Wenzel model $\cos\theta_w = r\ \cos\theta$ (2.1)

Cassie model $\cos\theta_r = rf_1 \cos\theta - f_2$ (2.2)

Where r is the surface roughness, f_1 and f_2 are the fractional interface areas of graphene surface and air in the holes, respectively, the effect of graphene's surface morphology to wettability of graphene will be greatly increased by the regulation effect of a micron-scale hole array (MSHA), as shown in **Figure 30**. Changing from hydrophobic to hydrophilic will provide a relation to control and design surfaces with controllable wettability [70].

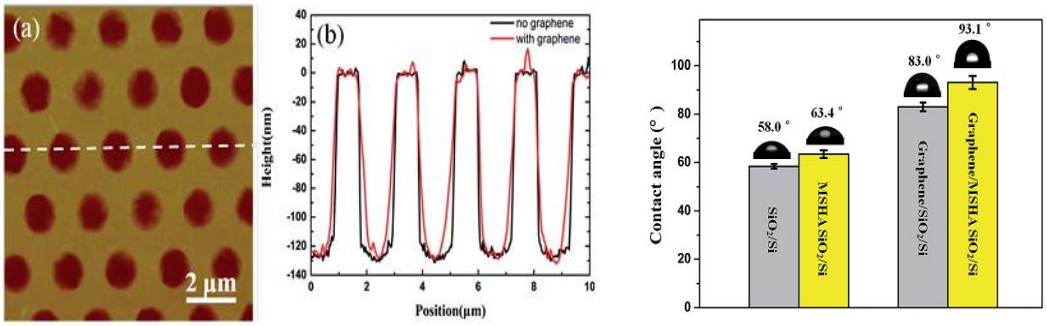

Figure 30 The roughness of the surface and effect on water contact angle [70].

Q. H. Wang et al. reported a stark difference in the rate of electron-transfer reactions with organic diazonium salts for monolayer graphene supported on a variety of substrates. The use of different substrates with different treatment methods and different water contact angles would have an effect on electron transfer reaction. They used oxygen plasma and Piranha solution (3:1 solution of 98 % sulfuric acid and 30% hydrogen peroxide). The intensity ratio between I_G/I_D represents the quality of graphene and the presence of structural defects, as shown in **Figure 31**. It can be observed that as-received substrates have relatively lower defects when the I_D/I_G ratio is considered. It can also be inferred that the defects occurring in the graphene were affected by cleaning/surface treatment of SiO_2/Si substrate, as both substrates have the same ratio between G and D bands which was higher than the as-received sample [73].

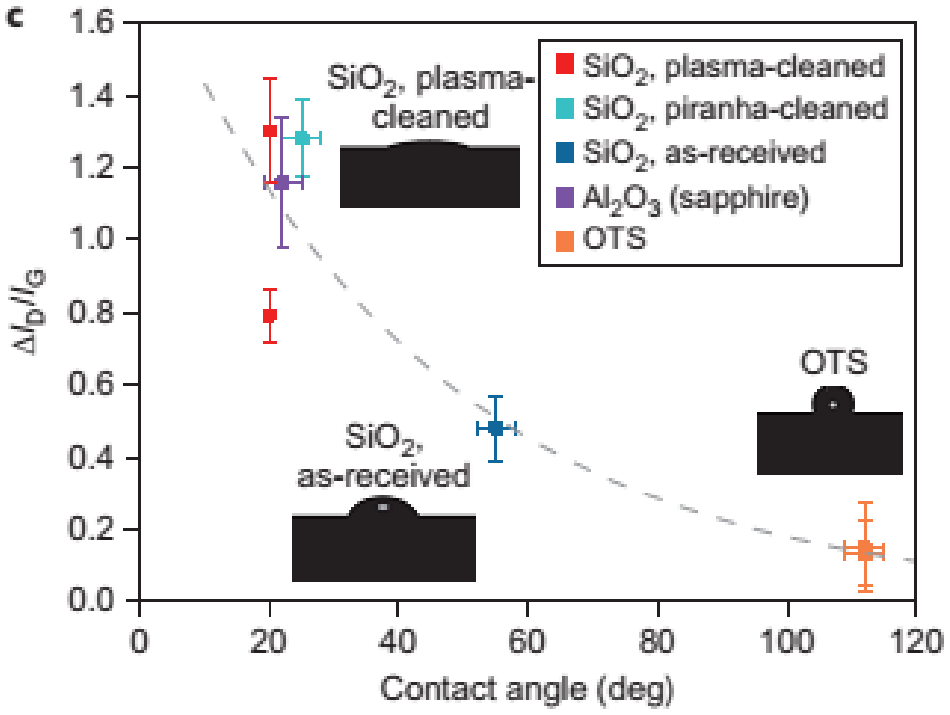

Figure 31. The effect of reducing water contact angle on the I(G)/I(D) ratio [73].

K. Nagashio et al. discussed the effects of surface treatment of the SiO_2/Si substrate using Plasma on graphene electrical mobility. They conclude that, due to strong adhesion between graphene and SiO_2/Si, the mobility was degraded. However, they suggested using annealing to remove the water from the graphene/SiO2 stack, as reducing interaction between the stacks would enhance the mobility [74].

2.5 Usage of graphene for solar cell applications

The unique properties of graphene have been extensively investigated in the field of solar cell. There are some promising results that will enable the usage graphene for solar cell application, such as:

Conductive electrodes:

- Transparent anodes
- Nontransparent anodes

- Transparent cathodes
- Nontransparent cathodes

Active layer:

- Light harvesting material
- Electron transport layer
- Hole transport layer

2.5.1 Graphene as a transparent conductive anode layer

Graphene was used as a transparent conductive layer as an anode for flexible photovoltaic cell. The obtained graphene film showed its sheet resistance down to 230 Ω/sq with transparency of 72%. The power conversion energy (PCE) was improved (η) to 1.8 % Comparing with 1.27 % whiteout graphene as shown in **Figure 32** [6].

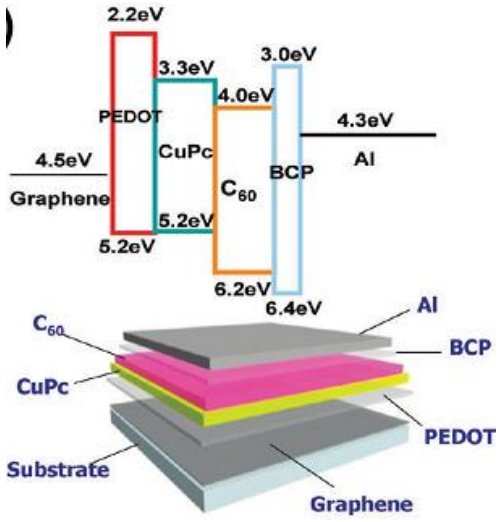

Figure 32. Configuration of flexible solar cell photovoltaic [6].

Chemical reduction method was used to obtain graphene oxide (rGO), used as transparent conductive anode. This achieved a transport efficiency above 65% and a transparency of rGO below 65% [75]. Iijima and his team obtained 97.4% optical transmittance with very low resistance, 125 Ω/sq, when they used four layers of graphene, the resistance and

transparency decreased to 30 Ω/sq and 90 % respectively. They used the roll to roll method to transfer graphene [76].

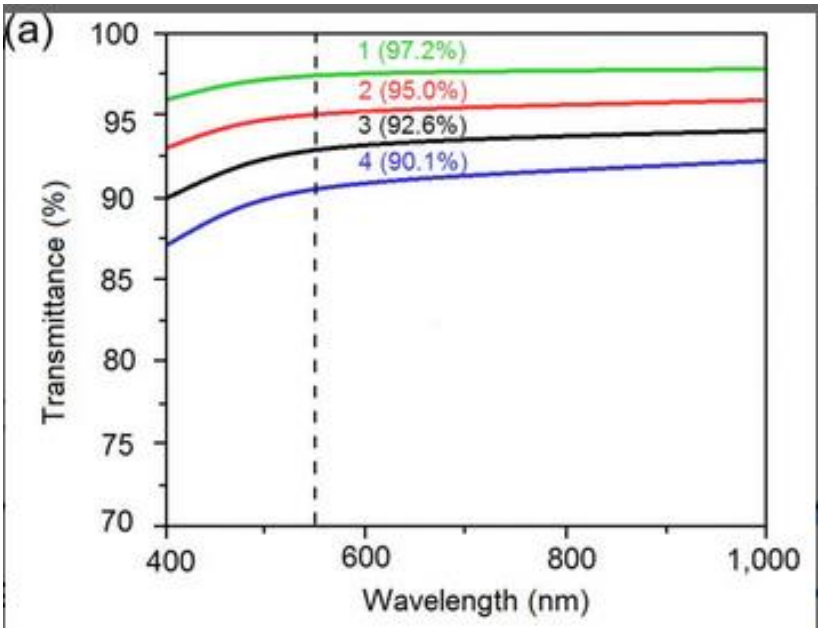

Figure 33. Transmittance spectra of the graphene films for the corresponding layers 1, 2, 3, and 4, respectively [76]**.**

2.5.2 Graphene as transport conductive cathode layer

Using of rGO as a conductive cathode, this layer exhibited a sheet resistance of 420 Ω/sq with 61% transmittance, and yielded a power conversion energy (PCE) of 0.31% [77].

Figure 34 shows the stack of the layers for solar cell.

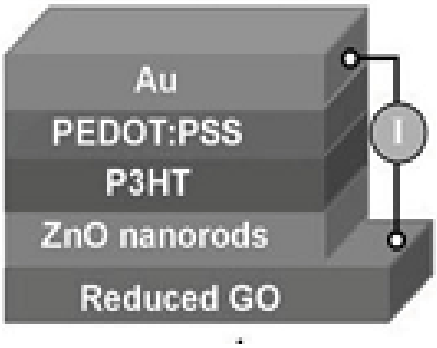

Figure 34. Schematic of photovoltaic solar cell [77]**.**

Jiang and his team demonstrated the CdTe thin film solar cell using CVD-graphene as the front transparent electrode. As shown in **Figure 35**, the resistance of the obtained graphene film was 220Ω /sq, with a transparency of 84% and PCE of 4.17% [78].

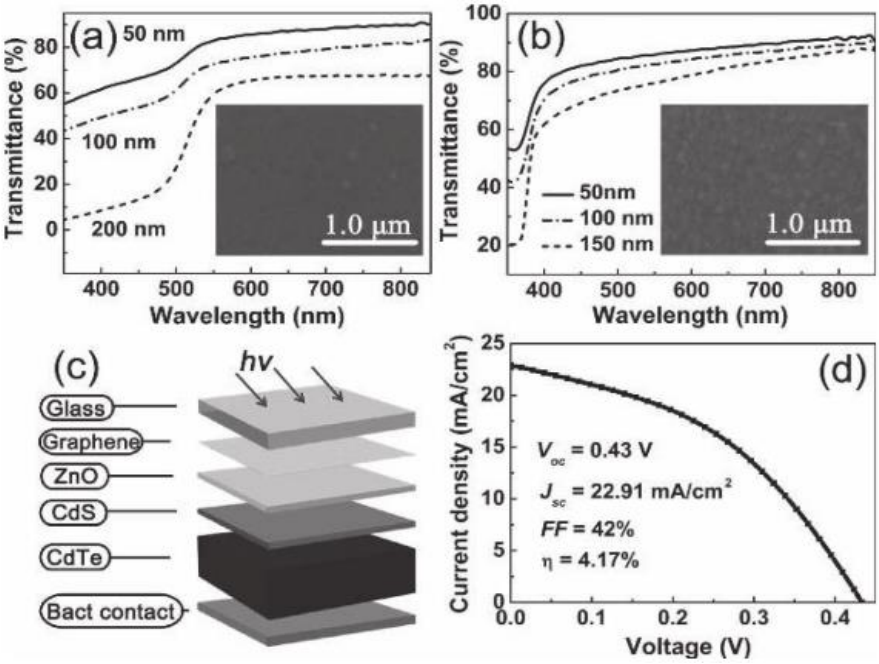

Figure 35. a) UV-vis spectra of the graphene/CdS composite films, and the SEM image of the graphene/(100 nm thick CdS) fi lm in the inset. b) UV-vis spectra of the graphene/ZnO films, and the SEM of the graphene/(100 nm thick ZnO) film in the inset. c) Schematic diagram and d) J–V characteristics of the glass/graphene/ZnO/CdS/CdTe/(graphite paste) solar cell [78]**.**

Table 2. Summary of work performed using graphene and rGO as electrode in solar cell

Material	R: Resistance , T: transmittance	PCE %	Ref
rGO	Transparent anode R=1.8 Ω /sq , T=70 %	0.26	[79]
rGO	Transparent anode R=3.2 Ω /sq , T=65 %	0.78	[80]
CVD graphene	Transparent anode R=0.25 Ω /sq , T=92 %	0.85	[81]
CVD graphene	Transparent anode R=3.5 Ω /sq , T=89 %	1.18	[82]
CVD graphene	Transparent anode R=0.08 Ω /sq , T=90 %	2.5	[83]
Al-TiO_2modified graphene	Transparent cathode R=01.2 Ω /sq , T=96 %	2.58	[84]
CVD graphene	Transparent cathode R=0.22 Ω /sq , T=84 %	4.17	[85]
CVD graphene	Transparent cathode R=0.3 Ω /sq , T=92 %	4.2	[86]

2.5.3 Graphene as electron transport layer

Jiang and his team reported that rGO was better suited to be used as the 2D electron transport layer better than 1D CNT composite base, as shown in Figure 36. They achieved the best performance when they loaded rGO [87].

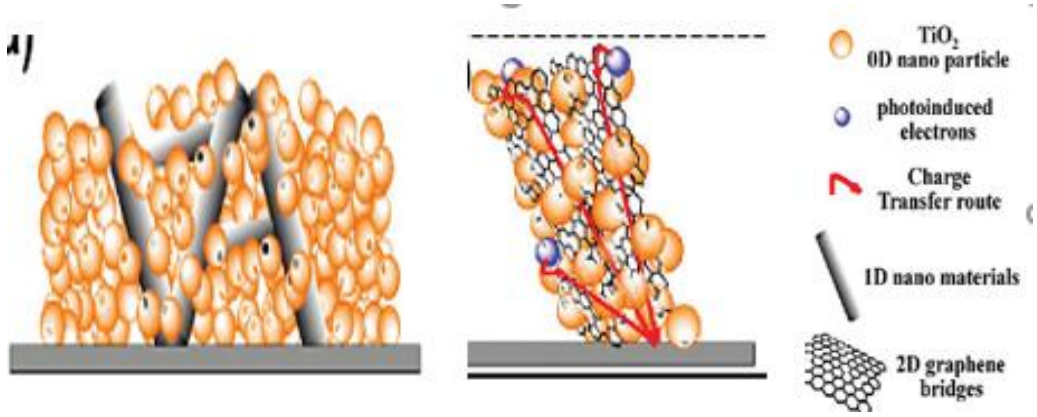

Figure 36 Schematic of using CNT and graphene [87].

Heeger and his team developed a novel stamping process, as shown in **Figure 37**, to directly transfer graphene onto the bulk heterojunction layer to the top of Al cathode. They achieved a PCE that was 6.8% higher, compared to pure TiO_2 [88].

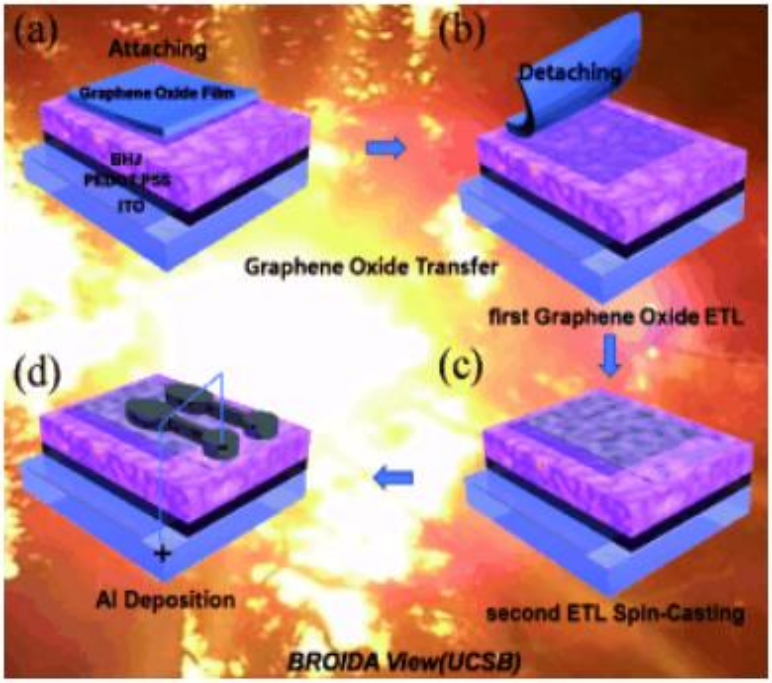

Figure 37. Stamping transfer method [88].

2.5.4 Graphene as a hole transport layer

Used as a hole transport layer in PV cells, graphene oxide and graphene oxide-based composite showed excellent properties, due to functionalized groups. Hung and his team have combined GO and SWCNTs at the hole transport layer of polymer solar cell. Figure 38shown the configuration of the layers .They achieved higher performance than when they used pure GO [89].

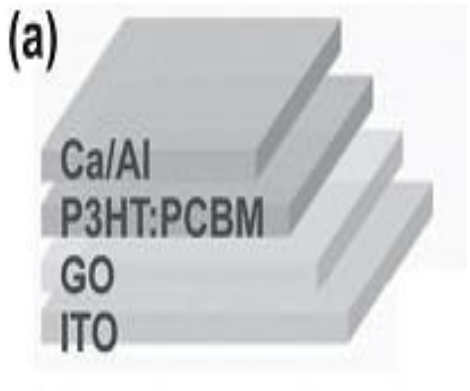

Figure 38. Configuration of layers [89].

Table 3. Summary of work done using graphene and rGO as charge transport layer in solar cell

Material	Function	PCE %	Ref
rGO	Electron transport layer	1.04	[90]
rGO	Electron transport layer	1.68	[91]
CVD graphene	Electron transport layer	7.5	[92]
rGO	Hole transport layer	0.61	[93]
GO-SWCNTs	Hole transport layer	4.1	[94]

2.6 Characterization of graphene

Raman spectroscopy, transmission electron microscopy (TEM), scanning electron microscope (SEM), atomic force microscope (AFM) and X-ray photoelectron spectroscopy (XPS) are used to characterize graphene quality as well as the number of layer of graphene and other different techniques. Raman spectroscopy has been used as the main characterization technique for graphene applications, perhaps because the method is simple and non-destructive [95][96]. From the Raman spectra, a great deal of details on the fine structure of graphene or graphite can be extracted. A typical Raman spectrum for graphene consists of two main bands and a few more very small bands. The two main bands are the G-band found at a Raman shift of ~1582 cm^{-1} and the 2D band found at ~2685 cm^{-1}. A third band although often very weak, the D-band, is found at ~1350 cm^{-1}. These bands are used to discern the quality, the defects, the number of layers and the doping in graphene films [96][97].

The D-band represents a disorder band and is sometimes called the defect band. It denotes a ring breathing mode from sp^2 carbon rings. The ring must be adjacent to a graphene edge or a defect for the band to be active [96][97]. The band is a result of a single phonon lattice vibrational process, and its intensity is an indication of the level of defects in graphene sample. The D-band is a dispersive band and thus its position and shape can be significantly influenced by the excitation laser frequencies. Meanwhile, the G-band is a resonant band and it represents the planar configuration sp2 bonded carbon that constitutes graphene. It arises from the E2g in-plane vibration of the atoms. Unlike the D-band, the G-band position is independent of the excitation laser frequencyو but depends on the number of graphene layers and perhaps the synthesis conditions. The position of the band shifts to the a lower

energy with increased layer thickness, which connotes softening of the bonds [97]. In addition, the position of the G-band is influenced by the addition of dopants as well as micro strain. These influences must be well considered if the graphene layer thickness is to be accurately evaluated.

The 2D-band (or G/ band as it is called in carbon nanotubes, etc.) is an overtone of the D-band and represents the second order of the D-band [98][99]. It is due to a two-phonon lattice vibrational process but, unlike the D-band, does not need to be close to a defect before being active. As a result, the 2D-band is always a strong one and is often present in graphene. This band is also used to estimate graphene layer thickness or the number of graphene layers. As pointed out with the G-band, care must be taken to ensure that the influences of micro-strain and synthesis conditions are considered, as the differences between single and bilayer graphene are more complex than a simple band shift in the 2D-band. Apart from the wave number shift to a higher value, the band shape changes due to an increased number of the active components. A single layer graphene has one active component while a bilayer graphene has up to four active components which causes a band shape distortion.

In a study reported by Li et al. [22] Raman spectroscopy was used to characterize graphene films with different numbers of stacked layers as shown in **Figure 39**. The graphene layers were deposited on Cu substrate and then transferred onto a 100 mm diameter silicon wafer containing 300 nm thick SiO_2. Based on the Raman plot, it is clear that the peak intensities of the G and 2D bands and the number of layers are well correlated. This behavior is attributed to the random orientations of the hexagonal lattices between any pairs of graphene layers. It is also observed that the 2D-band position shifts to the higher wave

number especially between a single and bilayer graphene. The ratio of the peak intensity of 2D-band to that of G-band (I_{2D}/I_G) has been used to distinguish monolayer graphene from others as well as to quantify the uniformity of the graphene layers (by Raman mapping) [100][101].

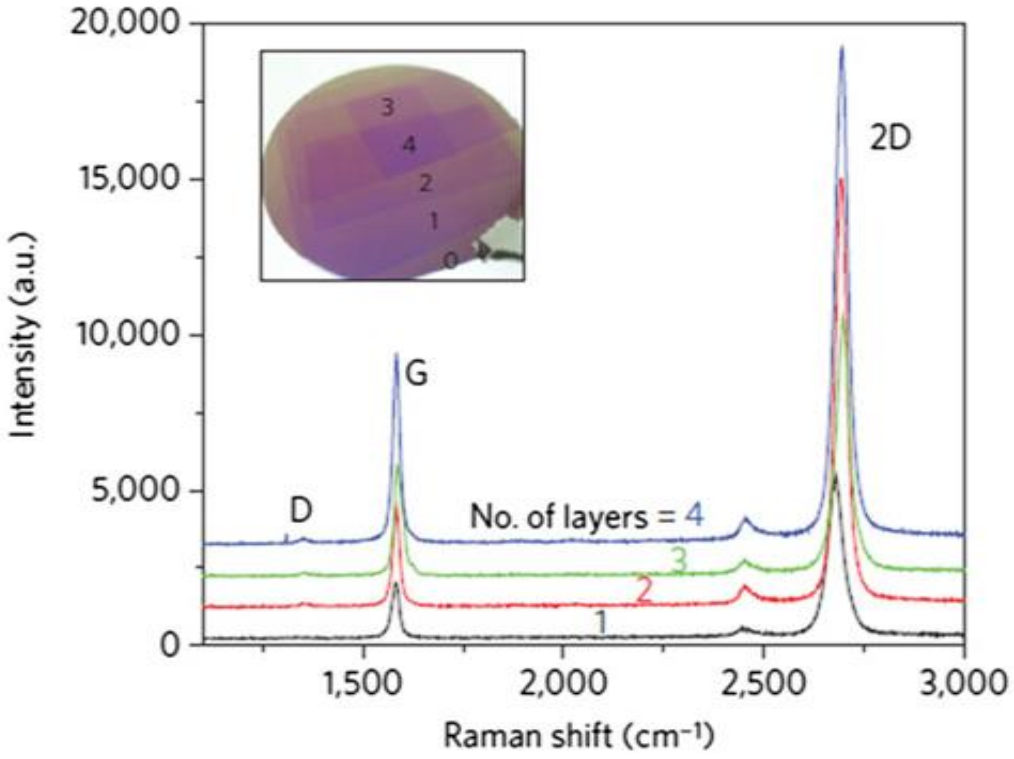

Figure 39. Raman spectra of graphene films with different numbers of stacked layers[22].

Intensity maps of the G band can also give further evidence of the uniformity of the as-grown graphene film [22]. Typically the G-peak intensity of graphene on copper is uniform except in regions corresponding to wrinkles or graphene grain boundaries [22]. An intensity ratio I_{2D}/I_G between ~1.8 and 4 is considered a fingerprint of monolayer graphene films[100][101]. In addition, a symmetric 2D peak located at 2698 cm^{-1} [100]or ~2700 cm^{-1} [102] is an indication of a monolayer film.

Yu, et al. [103] also had used Raman spectroscopy and mapping to study a single graphene grain, and two coalesced graphene grains as shown in **Figure 40**, respectively. They found that, almost all I_{2D} values were more than twice that of I_G, confirming single layer graphene samples. Furthermore, almost all I_D intensity values throughout the investigated areas were very small (indicating a low defect content), with the exception of a few notable isolated spots of relatively high I_D located mostly at the grain centers, edges and grain boundaries. They indicated later that high defect regions caused week localization and impede the electrical transport capability of synthesized graphene.

Raman mapping was also exploited by Li, et al. [22] to investigate monolayer, bilayer and multilayer graphene coverage percentages on the copper substrate surface. Their LPCVD graphene synthesis regime gave approximately 95% monolayer graphene coverage, while only small a fraction of bilayer and few-layer (<5%) was found on the copper surface, as can be observed from **Figure 41**. The growth parameters were as follows; H_2: 2 sccm, 40 mTorr (before reaction) and CH_4: 35 sccm, 500 mTorr (during reaction and cooling periods), and growth time was in the range from 10 to 60 minutes.

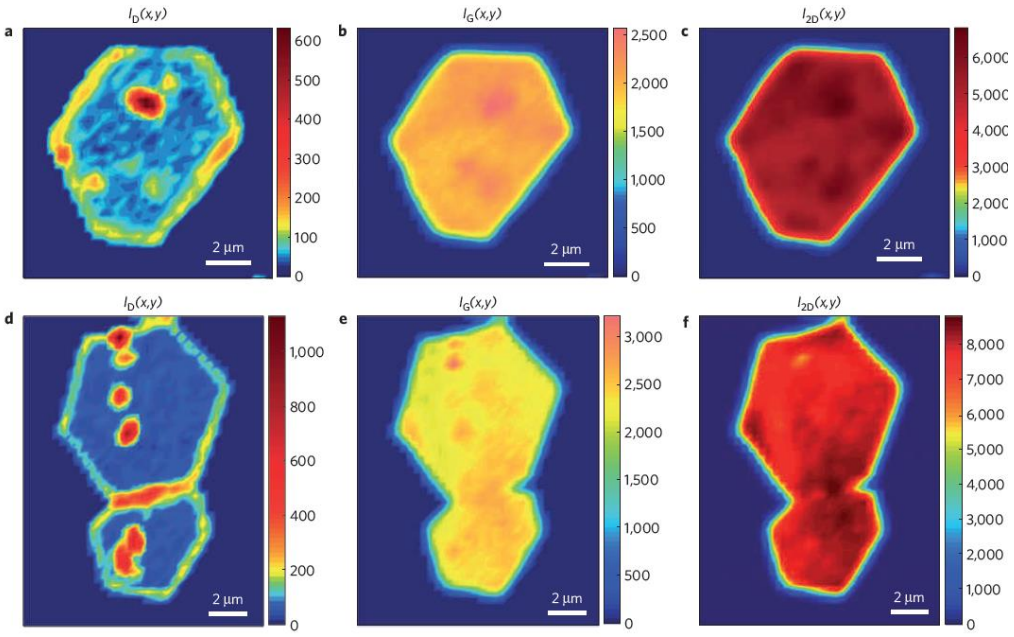

Figure 40. Spectroscopic Raman mapping of graphene grains and grain boundaries. a–c, Intensity maps of the 'D', 'G' and '2D' bands, respectively, for a two coalesced graphene grains with a single grain boundary [103].

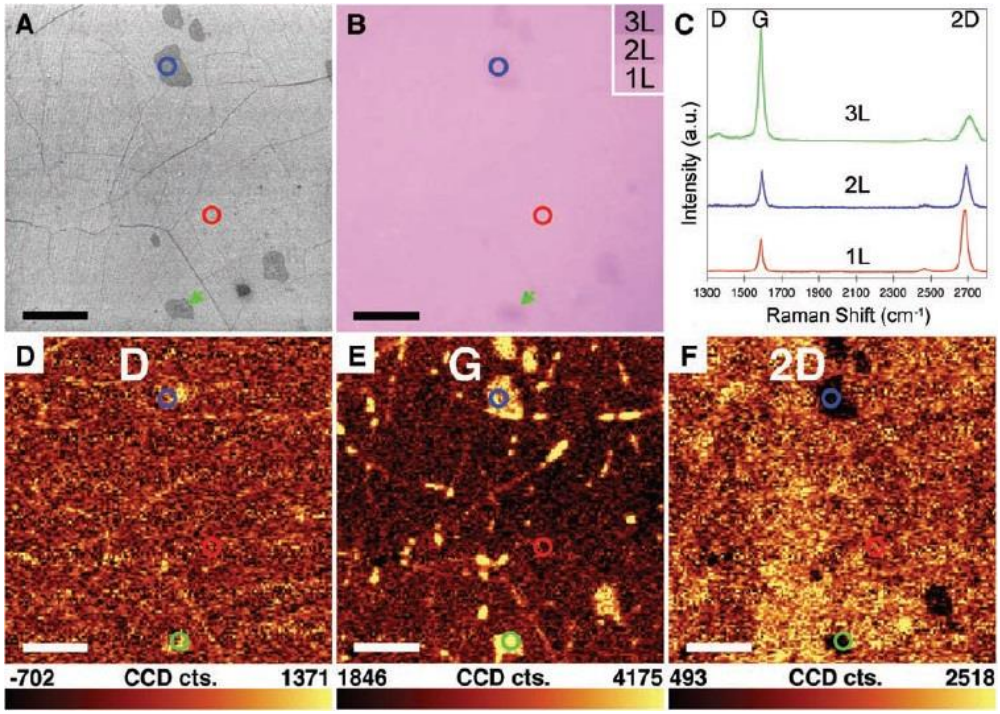

Figure 41. (a) SEM image of graphene transferred on SiO_2/Si (b) Optical microscope image of the same regions as in (a). (c) Raman spectra from the marked spots ,(d to f) Raman maps of the D , G and 2D bands [22].

2.7 Aim/objectives

The aim of the present work is to develop an enhanced CVD-grown graphene transfer method that yields good quality graphene film transferred onto SiO_2/Si target substrate for improved performance of related solar cell application. The specific objectives include:

- To select the best chemical etchant that can efficiently remove Cu substrate with minimum density of Cu-residues on the graphene layer/film.
- To optimize the PMMA deposition/removal parameters (spin-coating speed, PMMA concentration, acetone temperature, and time) to minimize the amount of PMMA residues on the transferred graphene layer.
- To enhance the graphene adhesion onto the target substrate (SiO_2/Si) using various surface pre-treatments (e.g. Piranha, HF, plasma, and NH_4OH) to reduce the various transfer-induced structural defects such as tears, cracks and wrinkles.
- To deposit graphene layer onto the surface of zinc oxide using the optimum transfer parameters
- To characterize the transferred graphene film using optical microscopy, FE-SEM, AFM, and Raman spectroscopy techniques.
- To determine the electrical and optical properties of graphene layer and graphene/zinc oxide combination.

CHAPTER 3
EXPERIMENTAL WORK

This chapter is devoted to explain all the experimental methods and techniques that conducted during graphene synthesis, transfer and characterization.

3.1 CVD graphene synthesis

Chemical Vapor Deposition (CVD) is a process where graphene is deposited on a metallic substrate, namely copper (Cu). CVD is the most commonly used technique as it produces a larger graphene surface. Graphene CVD consist of two main steps: Copper pre-cleaning and graphene synthesis process.

3.1.1 Copper pre-cleaning

Graphene was synthesized using CVD method on copper substrate from 25 μm thick, 99.8% purity from Alfa Aesar (Product No.13382). The copper foils were cut into 4x2 cm pieces and cleaned by being dipped into acetone, followed by iso-propanol alcohol (IPA) and then deionized (DI) water (for 5min each) using sonication during cleaning. This step is very important, as it removes any contamination on the surface of copper. The copper foil pieces were etched using a APS as copper etchant for pre-cleaning process with concertation of (0.2 M) for 30s. Ibrahim and his group reported in their paper [42] that using APS for 30s for pre-cleaning copper would result in a very smooth surface and also produce the highest quality of mono layer CVD graphene. Copper foil pieces were then dipped in DI water twice (for 5 min each) to make sure that absolutely no copper oxides or contamination remained. Finally, the pieces were dried with nitrogen gas.

3.1.2 CVD graphene synthesis process

The principle behind chemical vapor deposition is that the substrate is exposed to gaseous precursors, which, when in contact with the substrate at high temperatures, deposit on its surface, creating a thin film [104]. The quality of the materials obtained by CVD is greatly dependent on the process parameters such as gas temperature, pressure, and time. To achieve single layer graphene by CVD, with a quality similar to that of exfoliated graphene, these parameters have to be adjusted during the deposition process. In addition, the metal used as substrate will influence the entire process. Transition metals such as copper, nickel, platinum, ruthenium and iridium have been used to grow CVD graphene, however copper is more commonly used for this specific purpose [43][105].

In the chemical vapor deposition (CVD) process, the precursor is fed into the chamber at high temperature in the presence of the catalytic substrate, which results in the deposition of the desired film. As a result of this reaction some volatile by-products can be developed but they are removed from the chamber by the carrier gases. During this reaction the atmosphere inside the tube must be kept inert in order to avoid any reactions that may occur between oxygen and the reactive gases. Any CVD process requires/involves the use of three main components: (1) substrate, (2) precursor gases and (3) inert carrier gas.

CVD processes can be categorized as follows;

1. Atmospheric Pressure Chemical Vapor Deposition (APCVD)
2. Low Pressure Chemical Vapor Deposition (LPCVD)
3. Plasma Assisted Chemical Vapor Deposition (PACVD)

APCVD is one of the most common techniques used to synthesize graphene, because it is simple, and requires a short time to produce full coverage of graphene on the Cu substrate. On the other hand, this technique requires very delicate control over the gas flow rate, growth temperature and time, as it involves high amounts of gases at an elevated temperature. In the present work, all graphene samples are synthesized using APCVD. The process of APCVD is shown in **Figure 42**. Gases are controlled by valves, and the carbon source, methane (CH_4), is introduced at a high temperature of 1000°C in the presence of a thin transition metal (copper), which acts as a substrate as well as a catalyst. CH_4 will be decomposed into carbon, hydrogen, and these carbon atoms will be utilized for graphene nucleation and growth.

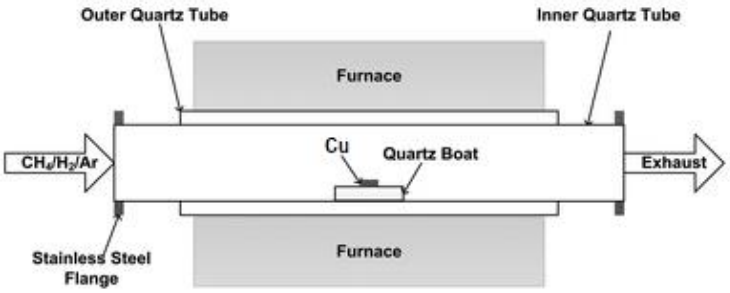

Figure 42. Schematic diagram of the CVD process [106]**.**

First Nano-CVD reactor with 3'' diameter quartz tube as shown in Figure 43 was used to grow graphene on Cu substrates.

Figure 43. First Nano-CVD reactor

Cu substrate is inserted into the CVD reactor and heated from room temperature to 1000^{o}C in the presence of argon (Ar) and hydrogen (H_2) gas mixture with a total flow rate of 1500 sccm. The ratio H_2: Ar = 37:1463 (sccm) is kept constant during heating and cooling steps for all prepared samples. After being heated to 1000^{o}C, the foil pieces are annealed for 30 min at H_2 which constitutes 2.5 % of the total gas mixture. Cu is annealed under Ar and H_2 at 1000^{o}C in order to improve its surface characteristics, as this step reduces surface oxides, volatile impurities and surface contaminations [107], [108]. Annealing also increases the grain size of Cu and hence reduces the overall density of grain boundaries, which, in turn reduces multilayer graphene nucleation on Cu grain boundaries. This is very important, since the grain size of Cu plays a crucial role in nucleation and growth of multilayer and/or amorphous graphene regions. After the annealing step, graphene growth starts by introducing CH_4 of 5 sccm in the reactor chamber (3'' in diameter) for 3 minutes, Throughout the process, Hydrogen constitutes 2.5 % of the total amount of gas in the

reactor chamber. The APCVD cycle, comprised of heating, annealing, growth and cooling, is shown in **Figure 44**

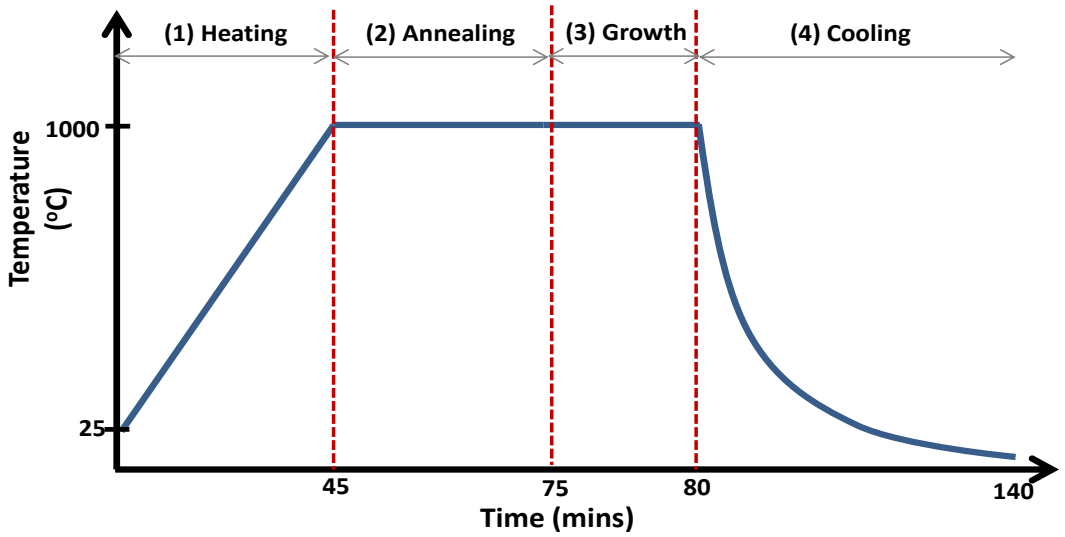

Figure 44. APCV growth cycle of graphene on Cu foils.

3.2 Copper etching techniques

Graphene/Cu samples were coated with polymethylmethacrylate (PMMA) using the spin-coating method in order to support and protect the graphene film during transfer step (details of PMMA process will be explained in section 3.4). The backside graphene is then removed by floating PMMA/graphene/Cu on an ammonium persulfate (APS) bath for 7 min, then rinsing it in DI water for 5 min. Next, the Cu substrate that holds the PMMA/graphene stack is etched away using different copper etchants APS(0.2M), Ferric chloride ($FeCl_3$) (0.2M) and Iron (III) nitrate ($Fe(No_3)_3$) (0.7 M). The first sample was left for 2h, the second for 4h, and the third for 8 h. The remaining PMMA/graphene stack is finally rinsed in 3 baths (for 10 min each) of DI water before being transferred it to the target substrate.

3.3 SiO_2/Si substrate treatment

Before transferring graphene onto SiO_2/Si substrate it is cleaned as follows: bare-substrate is cut into 2x2cm pieces and cleaned using sonication baths of acetone for 10 min and isopropanol for 5 min. Acetone and isopropanol help remove organic contaminants and clean oils that may be present on the SiO_2/Si substrate surface. Pieces are then rinsed using running de-ionized (DI) water and blow dried using compressed nitrogen. These cleaned SiO_2/Si substrates are then stored in a sealed container to prevent the accumulation of dust particles on their surfaces. SiO_2/Si surface is further pre-treated using various approaches (e.g. Piranha, hydrofluoric acid (HF), oxygen plasma or Ammonia solution (NH_4OH)) before scooping PMMA/graphene stack to enhance its hydrophilicity and hence help it better adhere to the target substrate. This may greatly reduce various transfer-induced structural defects on the graphene film such as tears, cracks and wrinkles.

3.3.1 Hydrofluoric (HF) dip treatment

Literature review shows that a 2 % HF solution is enough to carry out the surface treatment. A 48% HF solution was diluted to 2 % in order to carry out the treatment. Six cleaned 2x2cm SiO_2/Si samples were considered for surface treatment. Samples were sequentially dipped and gently stirred in the HF solution for 20 seconds. This was followed by immediate rinsing in running DI water and then blow drying using compressed nitrogen. The same procedure was repeated for the remaining samples, but dipping time was increased to 40, 60 and 80, 90 and 120 sec. for second, third, fourth, fifth and sixth sample, respectively [50].

3.3.2 Piranha treatment

Piranha is a 3:1 solution of 98 % sulfuric acid and 30% hydrogen peroxide. Six cleaned SiO2 10 mm by 10 mm samples were considered for surface treatment. The first sample was immersed in piranha solution for 10 minutes, the second sample was immersed for 15 mins and the third sample was immersed for 20 mins. All three samples were then rinsed with DI water and blow dried with compressed nitrogen.

3.3.3 Oxygen plasma treatment

Oxygen plasma treatment was used for 2, 5, 10 and 30 min with power of 18W applied to the RF coil. Oxygen plasma was used to remove any contamination and treat the surface of SiO_2/Si substrate to reduce the water contact angle. As shown in **Figure 45** the plasma cleaner model PDC-32G manufactured by (Harrick Plasma) has been used to clean the samples.

Figure 45. Plasma cleaner [109]**.**

3.3.4 Ammonia solution treatment

NH_4OH solution was used to treat the SiO_2/Si substrate. Samples were dipped in NH_4OH solution (2.5M) for 4h at 100°C to make the target substrate more hydrophilic. Water

contact angle measurement was then carried out using static contact angle by placing a droplet of DI water on the surface of the substrate.

3.4 PMMA removal process

3.4.1 Design of experiment for optimizing the parameters

As mention in Chapter 2 many parameters factors can affect the efficiency of PMMA removal, for example PMMA concentration, spin coating speed, acetone dissolving time and temperature, baking time and how many layers of PMMA have been used. This section covers changing one or more process variables (or factors) in order to observe the effect, the changes have on one or more response variables. The (statistical) design of experiments (DOE) is an efficient procedure for planning experiments so that the data obtained can be analyzed to yield valid and objective conclusions. DOE is used to determine the relationship between factors affecting a process and the output of that process. In other words, it is used to find cause-and-effect relationships.

In this study, of the many DOE methods, the Taguchi model has been used to identify the factors and their interactions that may affect the PMMA residuals are left behind from the transfer of graphene to its desired substrate. The level of PMMA residues greatly reduce the quality of graphene and hence it is vital to make sure there are no PMMA residuals left behind from the transfer process. It is influenced by factors such as temperature, spin coating rpm, acetone temperature and acetone time of the dissolving. By using orthogonal experimental design and analysis technique, the performance of this process can be analyzed more objectively through only a small number of simulation experiments.

The objective here is to select a combination of input parameters' values that result into minimum surface coverage of PMMA. After a lot of research through the literature review, the following factors and parameters were considered the most cited for PMMA removal. Our objective is to optimize these parameters, which are covered in detail in their different levels in **Table 4**

Table 4. Factors/parameters for PMMA removal DOE and their levels

Factors	Level 1	Level 2	Level 3
PMMA (% conc.)	4.5	8	12
Spin coating speed (rpm)	2500	3000	4000
Acetone dissolving temp (°C)	25	40	60
Acetone dissolving time (min)	5	20	60

Using design of experiments (DOE) is crucial in planning a set of PMMA deposition/removal experiment, as it specifies the most important parameters contributing to these processes. After that the experiments will be conducted on glass substrate first to calculate the area fraction on PMMA residues. Validating the results of DOE by conducting several PMMA-assisted graphene transfers onto SiO_2/Si substrates.

Amount of PMMA residues can be analyzed using atomic force microscopy (AFM) and image J software. Graphene was transferred using optimized parameters results from DOE. Graphene induced-structural defects were quantified using Raman spectroscopy after the transfer process. Amount of PMMA residues on graphene surface was analyzed using AFM and Image J software.

3.4.2 Graphene transfer parameters for PMMA removal

PMMA/graphene is transferred onto SiO_2/Si substrate and dried on hot plate for 15 min at 90^oC. This step is essential for removing any water residue between PMMA/graphene and the underlying SiO_2/Si substrate so that they improve adhere better. It is worth mentioning that before the transfer process, PMMA's deposition and/or removal parameters have to be optimized in order to achieve the lowest PMMA residuals in the final transferred graphene film. This is done by conducting design of experiment (DOE) on the deposition/removal parameters (spin coating speed, time, PMMA concentration, acetone time and temperature).

Following the above optimization results, PMMA is dissolved by acetone followed by isopropanol. Finally, the graphene/SiO_2/Si stack was placed in a DI a water bath for 10 min to remove any organic residuals then blow dried with nitrogen.

3.5 Transfer to zinc oxide (ZnO) substrate

An ultrathin layer of ZnO was deposited on a cleaned glass was fabricated RF sputtering using automatic sputter coater (model NSC-4000). A high purity zinc (99.999 %) target received from Semiconductor Wafer, Inc. was pretreated following a standard procedure (ultrasonication for 15 min in acetone followed by 15 min ultrasonic cleaning in methanol). In addition, the zinc target substrate was further cleaned before each experiment by a pre-sputtering process for 1 min. The base pressure in the chamber was kept at $\sim 2\times10^{-6}$ torr and the working pressure was set to 7×10^{-3} torr by adjusting the Ar and O_2 gas flow to 80 scum. The target substrate distance was maintained fixed at 10 cm. The graphene film was grown on copper foil using the chemical vapor deposition (CVD) method, then transferred

onto the ZnO file using the wet transfer method using PMMA as a supported layer. Ammonium persulfate (APS) was used over the period of two hours. as copper etchant.

3.6 Characterization of graphene

Graphene samples are characterized before and after transfer, for the purpose of: (1) evaluating the quality of graphene layer including the number of layers and the percentage of generated defects; and (2) measuring the optical and electrical properties of transferred graphene layer and correlate it to the quality of transferred graphene layer. There are a lot characterization methods and tools mentioned in literature, including Optical microscopy (OM), Raman spectroscopy, atomic force microscopy (AFM), Ultraviolet–visible spectroscopy (UV-vis), Hall effect measurement and scanning electron microscopy (SEM).

3.6.1 Optical microscopy (OM)

Optical microscopy (DXR™ 2 Raman Microscope) manufactured by (ThermoFisher Scientific) (as shown in

Figure 46), was used during the whole work basically to take Optical images of transferred graphene films onto SiO_2/Si and ZnO. It was utilized to give information regarding the graphene film continuity and uniformity.

Figure 46. DXR™ 2 Raman Microscope [110].

3.6.2 Raman spectroscopy

Raman spectroscopy is one of the most popular and powerful non-destructive technique utilized to identify and characterize the materials and their structural properties. Raman phenomenon effect was discovered in 1928 by C.V. Raman [111]. Raman effect is based on the fact that when a monochromatic light with frequency v_o encounters a molecule, most of the light scatters with the same frequency of the incident light due to elastic scattering (i.e. Rayleigh scattering). However, a very small portion of incident photons are inelastically scattered with an energy lower or higher than the incident energy. This shift in energy (i.e. hv) is equal to the vibrational energy of molecules, as illustrated in **Figure 47**. In other words, the shift energy; hv is related to the material properties

At room temperature, most molecules are in the ground vibrational states. When light interacts with these molecules, they become excited and their energy jumps from the ground vibrational state to a virtual state for a very short time, then they relax by emitting light with lower energy (i.e. hv_o- hv) called Stokes shift. However, a few of the molecules are naturally excited in a vibrational excited state. These molecules gain energy when they interact with the incident photons, so they become excited to a virtual energy level, and then relax to the ground state by radiating photons with higher energy (i.e.. . hv_o+ hv) called antiStokes shift [112].

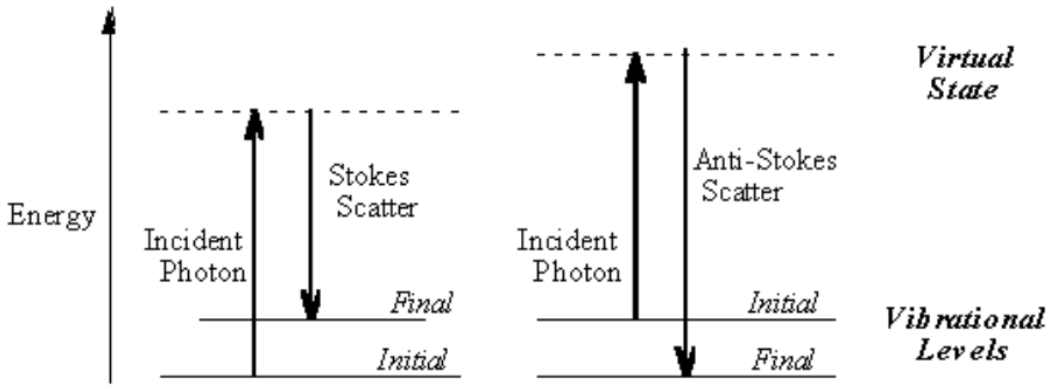

Figure 47. Diagram of the different possibilities of light scattering [112].

As depicted in **Figure 48**, Raman spectrometer consists basically of many devices and tools such as:

- A pulsed or continuous monochromatic light source with a wavelength in the UV. Visible or near IR wavelengths are used as excitation source. This light source is usually powerful laser.
- Laser line specific Rayleigh filters used to prevent Rayleigh scattering from entering the detector.
- A high quality optical set such as lenses, mirrors, or optical fibers utilized to direct and collect the light.
- A dispersing device (grating or prism) coupled with a charge-coupled device CCD.

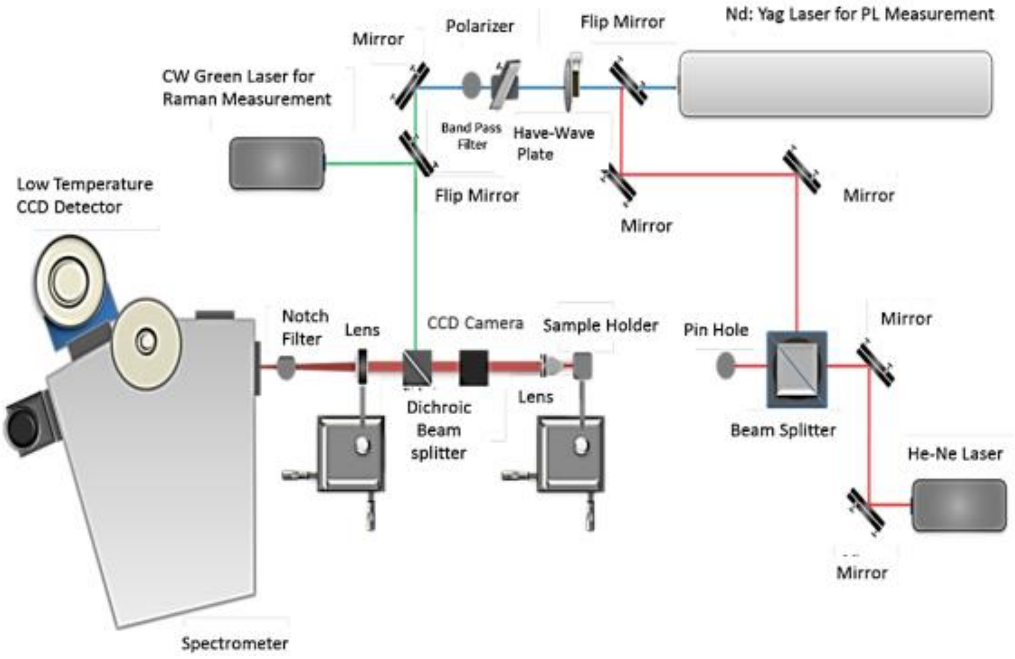

Figure 48. Schematic diagram of the Raman and PL spectroscopy system [113]**.**

Raman spectroscopy is very common for graphene characterization. Raman spectrum of any carbon allotropes contains basically three characteristics bands; from these bands we can identify the number of layers and quality of deposited graphene. The main advantages of Raman spectroscopy technique are that it is very simple, nondestructive and that is provides accurate results.

In present work, Raman spectroscopy Optical microscopy (DXR™ 2 Raman Microscope) manufactured by ThermoFisher Scientific (as shown in

Figure 46**),** is used to characterize as-grown graphene over Cu-substrates and as-transferred graphene on 300 nm SiO_2/Si wafers and ZnO.

3.6.3 Atomic force microscopy (AFM)

Atomic force microscopy is a type of scanning probe microscopy with nanometric resolution. It is used to obtain topographic images of surfaces [114].

Figure 49 shows the basic components and configurations of AFM. The AFM probes the sample surface with a nanometric tip which is attached to the end of the cantilever.

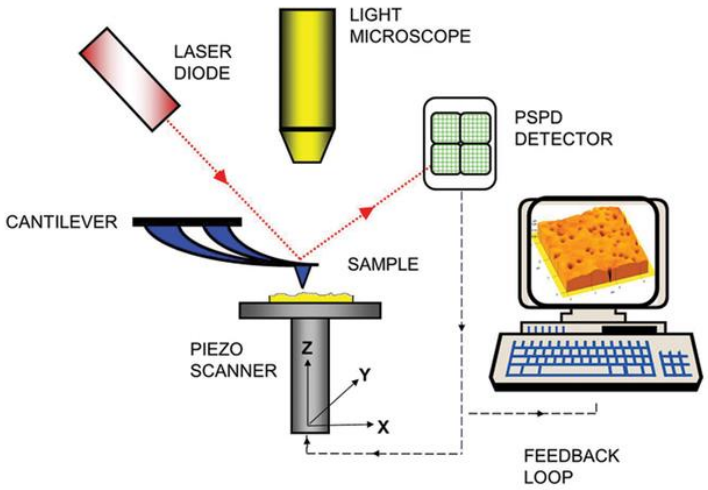

Figure 49. The basic components of AFM [115].

The cantilever deflects when the tip is brought close to the sample surface, due to the forces (such as Van der Walls or electrostatic forces) caused by tip-surface interactions. The deflection is measured by a photodetector that reflects an incident beam off the top of the cantilever. The direction of the laser beam is altered by changes in cantilever deflection. The topographic images are obtained by scanning the probe tip over the sample surface. Surface features (high and low points of the surface) cause alteration in tip-surface interaction which can be are measured by shifts in frequency, amplitude, phase and height[116].

AFM can operate in different modes, depending on the tip motion. In the contact mode, the tip is kept in close contact with the surface (around 10 angstroms from the surface) and the interatomic force between the surface and the cantilever is repulsive. On the other hand, in the non-contact mode the tip is kept at tens to thousands of angstroms from the surface and interatomic force between the cantilever and the surface is attractive. Although in contact mode the obtained images have a higher resolution, the tip is more susceptible to being damaged. A compromise between both modes is the tapping mode, in which the tip is oscillating up and down [113].

In tapping mode, also known as the intermittent contact mode, the probe scans the surface by gently tapping the substrate surface. One of the great advantages of this mode is that the tip is not dragged through the surface. Which helps avoid problems caused by friction, adhesion and electrostatic forces. The cantilever is excited to oscillate near its resonance frequency. When the tip is not in contact with the surface, the cantilever oscillates at higher frequencies. When it is brought closer to the surface, and reaches it, the tip-surface interactions cause the cantilever frequency to decrease, as the surface is scanned. The oscillation amplitude is dependent on tip-surface interaction forces. In tapping mode, the image is produced by retrieving the data related to the reduction in oscillation amplitude. A feedback loop keeps the oscillation amplitude constant, and when an elevated (or lowered area) is scanned, the amplitude is altered since the cantilever has more (or less) space to oscillate [113].

In this work we manipulated AFM (Dimension Icon- Bruker) to characterize the SiO_2/Si surface morphology evolution as influenced by different treatment methods. This is accomplished by using the Tapping mode. AFM was utilized to characterize as-transferred

graphene films onto SiO_2/Si wafers in order to check its morphology, uniformity, thickness and continuity.

In addition, the Nanoscope software was used in image processing and analysis of AFM images. Filters were applied to eliminate unwanted features from the images. Thus, to retrieve information about surface properties of samples, images were analyzed to obtain not only a 2D and 3D image of the scanned surface, but also data about depth and width, roughness, particles, and more.

3.6.4 Scanning electron microscopy (SEM)

Scanning electron microscopy (SEM) is used extensively to characterize the deposited graphene/Cu substrates. It gives very important information about the morphology, size and distribution of graphene domains deposited on Cu and as-transferred graphene.

In this work we utilized field emission scanning electron microscopy (FESEM) manufactured by (TSCAN-MIRA 3 LMP). The incident electron beam was accelerated by low voltage (1.5-5 kv).

3.6.5 X-ray photoelectron microscopy (XPS)

X-ray photoelectron spectroscopy (XPS) is an ideal technique for characterizing a material's surface chemistry with extreme selectivity. It can also identify chemical states on a surface, as well as measure the elemental composition, empirical formula, and electronic state of the elements present.

The elemental chemical composition of as-grown and as-transferred graphene were analyzed by XPS from Thermo Scientific, model (ESCALAB250Xi).

3.6.6 UV-Vis absorbance spectroscopy

UV-Vis spectroscopy is used to determine the absorption of the samples at different wavelengths. The absorbance, A, of the sample is a factor of the extinction coefficient at the specific wavelength, $\varepsilon \lambda$, refers to the concentration of the species in the sample, and b represents the path length of the light . Absorbance is a measure of the light that does not pass through the sample and it corresponds to the base ten logarithm of incident light, I_o, divided by light registered by the detector, I. This is known as Lambert-Beers law which is written as:

$$A = \log 10 (I_o / I) = \varepsilon \lambda c b \quad (3.1)$$

Absorption spectroscopy is a method of quantifying photoinduced changes by illuminating a sample with a pump light or laser and continually measuring the resulting absorbance. The changes registered from to the sample are a function of time and incident light. The illumination pathway is set perpendicular to the probe beam in order to prevent the light coming from the probe to reach the detector; as shown in **Figure 50**.

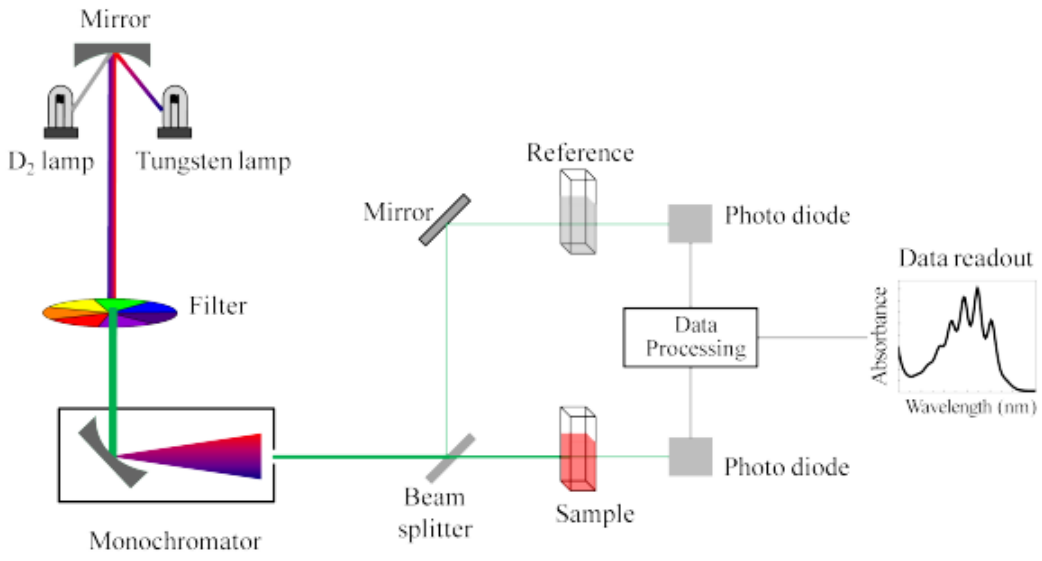

Figure 50. Schematic for a UV-Vis spectrophotometer[117]**.**

The absorption of the initial sample is measured and used as a baseline for the light induced state's absorption spectrum. This makes it possible to accurately measure the difference in absorption (ΔAbs) as a function of time, pump light intensity and excitation wavelength; **Figure 51** gives an example of a principal spectra. The subtraction of the initial spectra from the resulting state gives a difference spectrum where the changes are easier to follow. When two or more measurements coincide at some wavelength, that wavelength constitutes an isosbestic point. This occurs because the extinction coefficients of state 1 and 2 are equal.

In **Figure 51** the isosbestic points are positioned where the red and black lines cross; which can be seen in both the middle and rightmost picture. These points can be used to calculate the total concentration of a sample when the ratio of state 1 and 2 is unknown. If the isosbestic points are not maintained it is due to molecule destruction or the generation of further states[118].

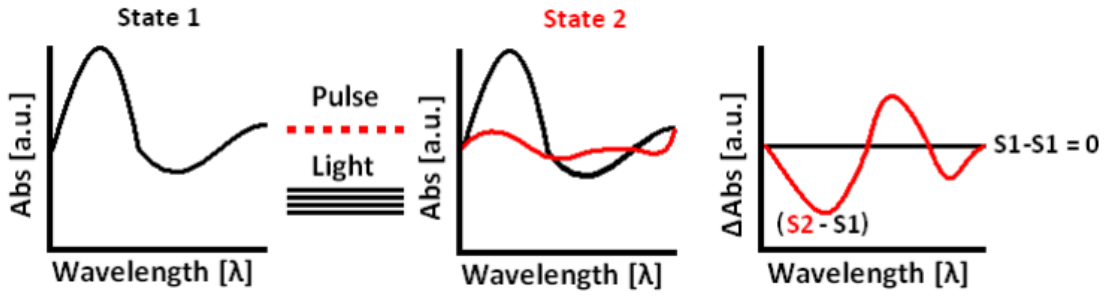

Figure 51. Example of absorption spectra. From the left; an initial sample (State 1), not illuminated, is recorded for comparison. A pump light or laser pulses is directed through the sample and the illuminated sample is recorded (State 2); the result is a difference spectrum depicting the change in absorption as a function of illumination time/pulse count [118].

In this work we used UV-VIS-NIR Spectrophotometer V-670 manufactured by (JASCO) to measure UV-Vis absorbance for all samples.

3.6.7 Hall effect measurement

The Hall effect is a long-known effect observed in conductors in an external magnetic field (H). It was discovered by Edwin Hall in 1879 [119]. The charge carriers carrying the current (I_q) within the conductor are detected by the Lorentz force and thus, if the charge carriers can accumulate at the interfaces (open boundary conditions), an electric field perpendicular to H and I_q is created. **Figure 52** Shows the principle of Hall effect: as electrons travel through the conductor that lies in a magnetic field, they will be experience a magnetic force, so they will be forced to travel closer to one side than the other because of the magnetic force. This side will be negatively charged, which will make the other side positively charged. The Hall effect voltage is known as the separation of the charge due to the voltage difference.

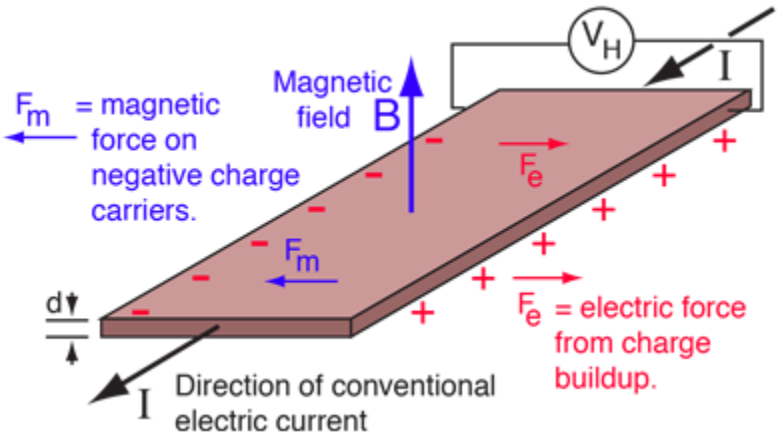

Figure 52. The principle of Hall effect [120].

Hall effect measurement system (LakeShore), shown in **Figure 53**, was used in the present work to measure resistance of the samples for resulting current-voltage curve.

Figure 53. Hall effect measurement system (LakeShore) [121].

Figure 54 shows a flow chart for the methodology followed in this work.

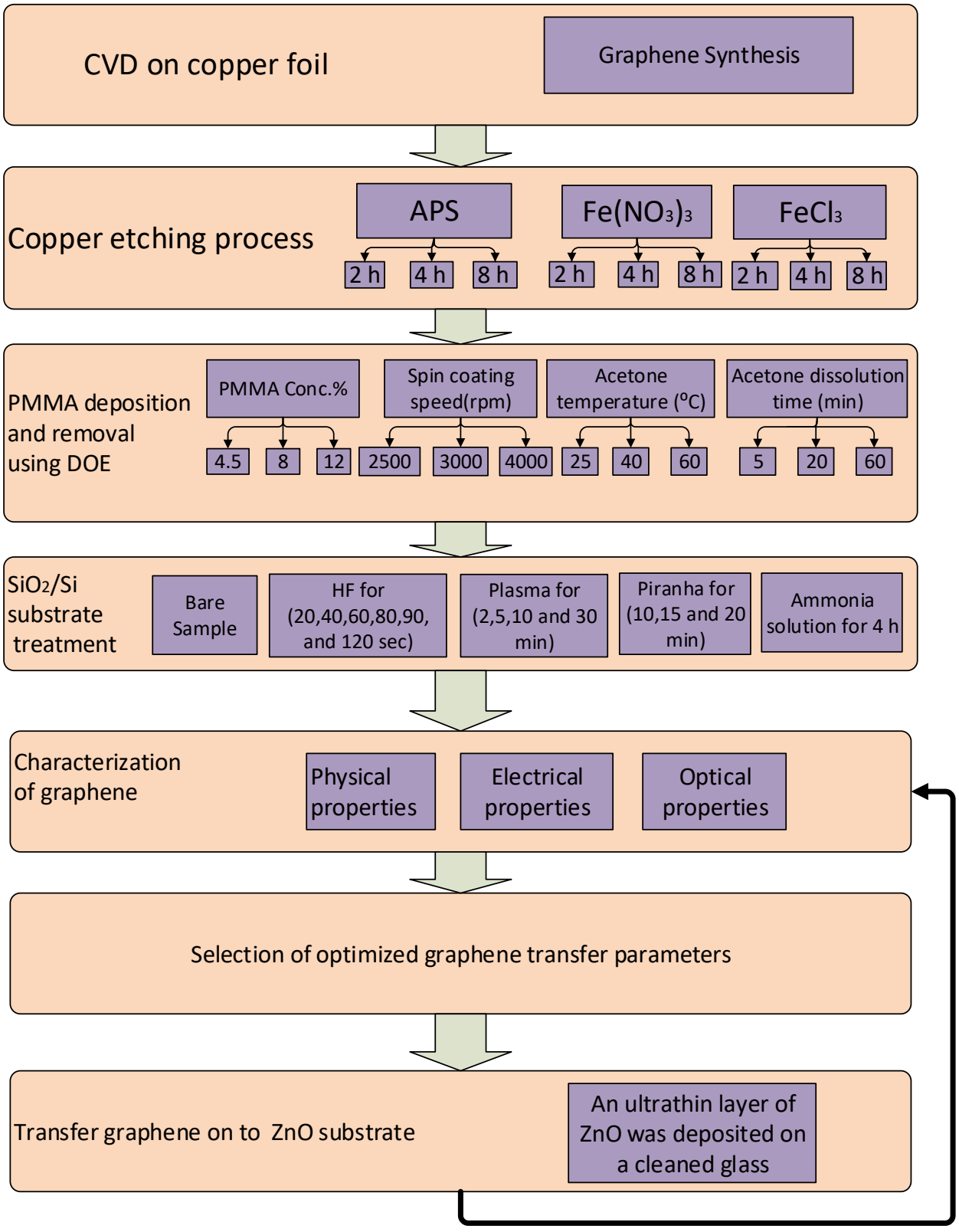

Figure 54 Thesis methodology summary

CHAPTER 4
RESULTS AND DISCUSSION

4.1 Copper residues of transferred CVD graphene

Metal residues (copper, nickel or iron) can significantly affect the electrical and electrochemical properties of graphene, especially in semiconductor devices, since a very small amount of metallic residues can alter the device parameters and cause problems [122][123].

In this section, the effect of the etching process using different copper etchants, namely (APS, $FeCl_3$ and $Fe(NO_3)_3$), on the as-transferred graphene onto SiO_2/Si substrate was investigated using Raman spectroscopy, XPS, SEM, UV-visible light absorption and hall effect measurement.

Optical microscopy images of as-transferred graphene show that using APS and $Fe(NO_3)_3$ for 2 and 4 hours each produce a uniform graphene layer with less cracks and tears, as shown in **Figure 55 (a, b) and Figure 57 (a, b).** Increasing the etching time to 8 hours**,** produced teas and creaks on graphene layer, as shown in **Figure 55 (c) and Figure 57 (c)**. In contrast, using $FeCl_3$ resulted in more copper residuals, as shown in **Figure 56 .** Raman spectra of graphene were taken in different positions and then plotted, as shown in **Figure 55 (c, f, and i), Figure 56 (c, f, and i) and Figure 57 (c, f, and i)** using APS (2, 4 ,8h) , $FeCl_3$ (2, 4, 8h) and $Fe(NO_3)_3$ (2, 4, 8h) respectively.

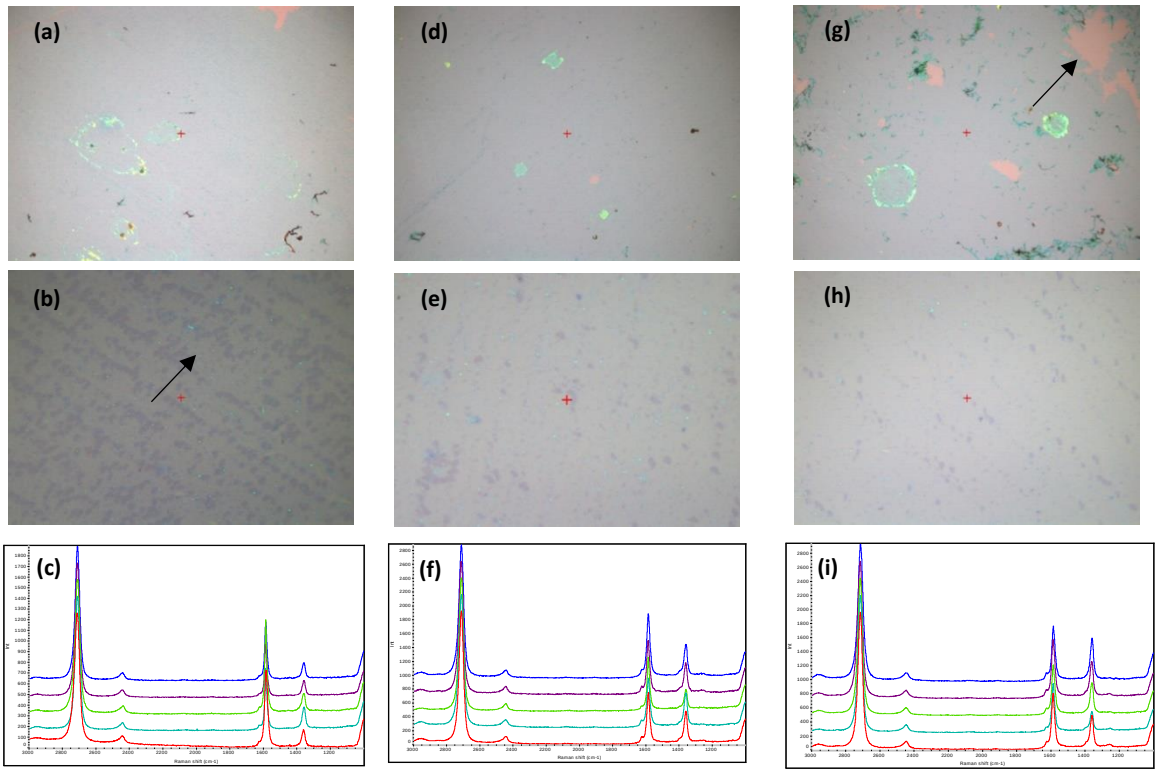

Figure 55. 10X and 100 X optical microscopy images and Raman spectra of APS for 2h (a,b and c) , 4h (d, e, and f) and 8h (g, h and i).

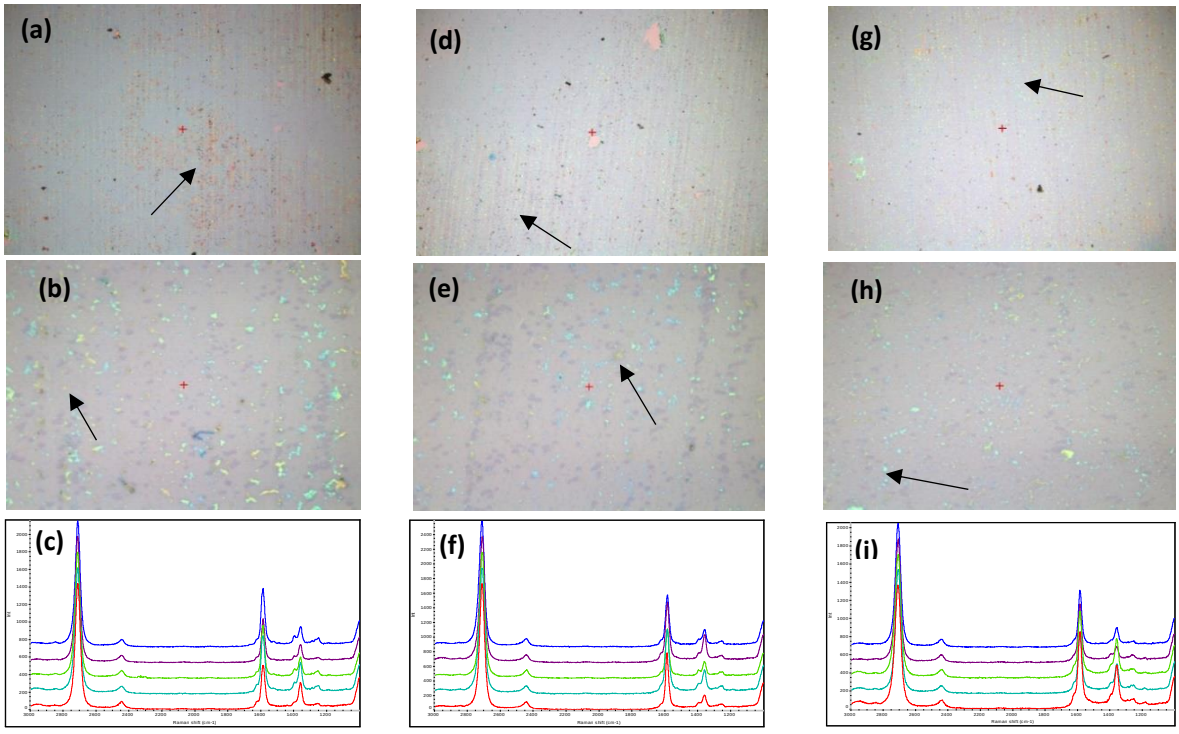

Figure 56. 10X and 100 X optical microscopy images o and Raman spectra of $FeCl_3$ for 2h (a, b and c), 4h (d, e, and f) and 8h (g, h and i).

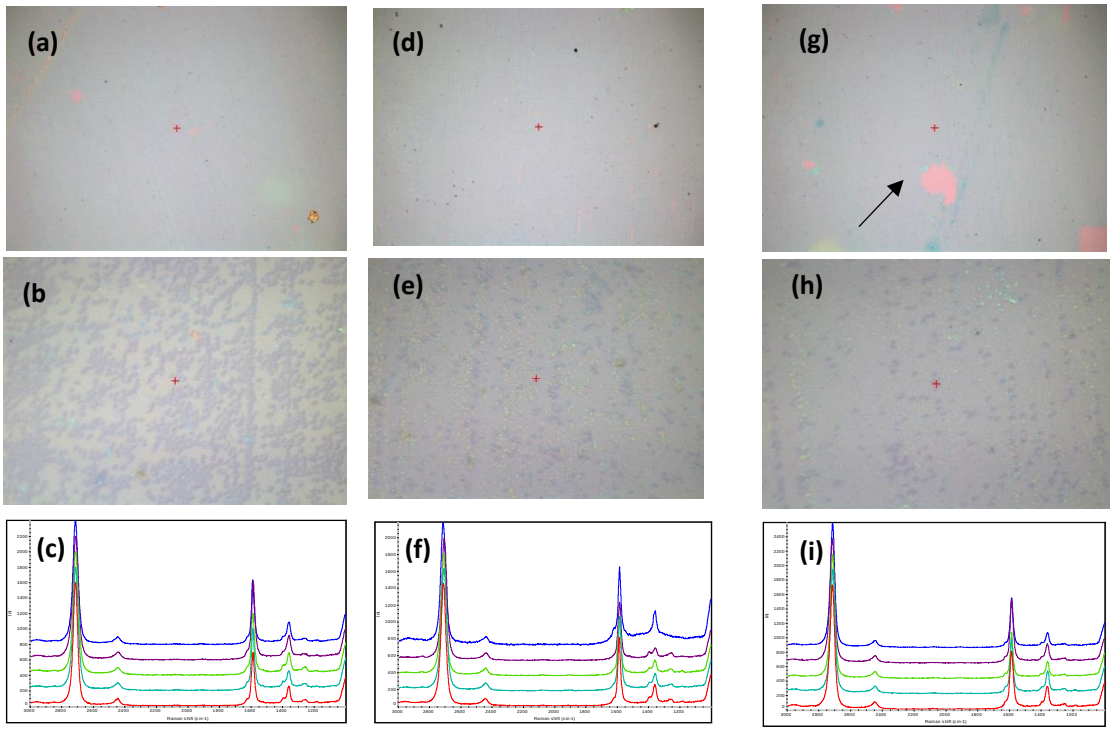

Figure 57. 10X and 100 X optical microscopy images o and Raman spectra of $Fe(NO_3)_3$ for 2h (a, b and c), 4h (d, e, and f) and 8h (g, h and i).

For further characterization of graphene layer, Raman mapping was carried out by taking 10x10μm, with an area of 100 μm^2, then I_D/I_G and I_{2D}/I_G were calculated for 100 spectra. **Figure 58** shows that increasing the time of etching increases the I_D/I_G ratio, which means that increases in defects lowers graphene quality [42]. In addition, APS and $Fe(NO_3)_3$ show a relatively small I_D/I_G ratio, compared with $FeCl_3$. Increasing the etching time to 4 hours does not significantly increase the I_D/I_G ratio. As shown in **Figure 59,** etching copper using APS for 4 hours produced the lowest I_D/I_G ratio with a value of ~ 0.26. In addition, using $Fe(NO_3)_3$ yielded a relatively moderate I_D/I_G ratio with a value of ~ 0.28. In contrast, using $FeCl_3$ for 4 hours gave a relatively high I_D/I_G ratio with a value of ~ 0.32, and yielded the lowest quality compared with APS-4h and $Fe(NO_3)_3$-4h.

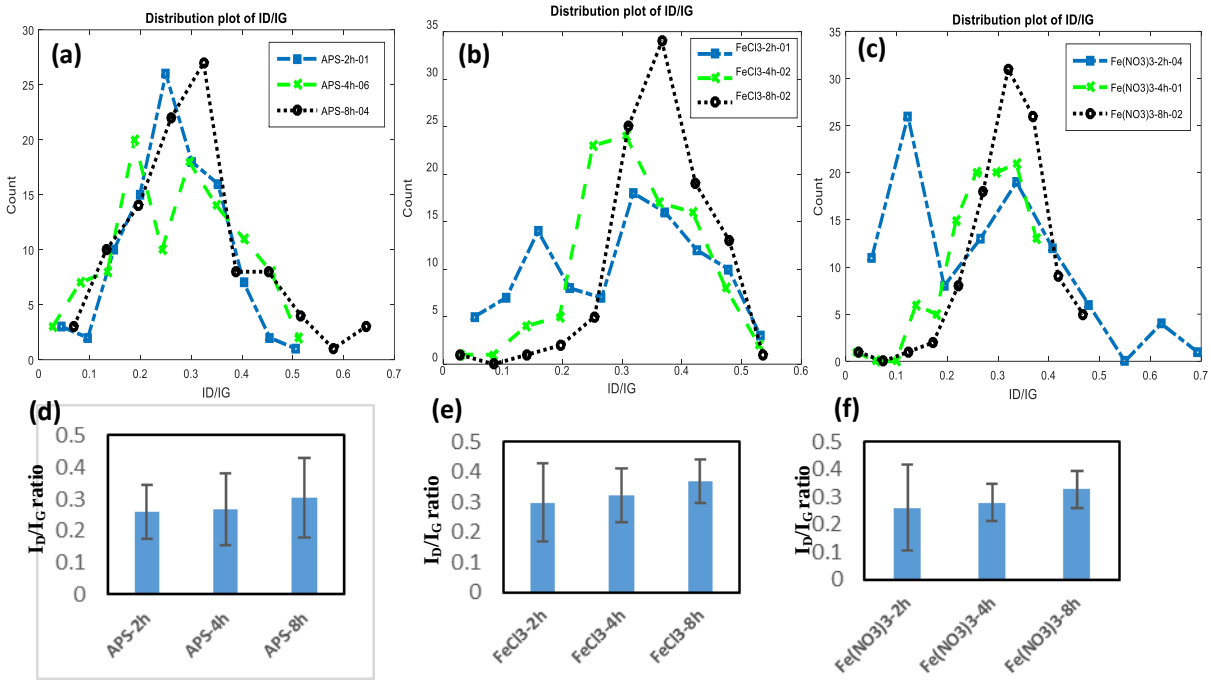

Figure 58. Histogram and Average plot of I_D/I_G for (a, c) APS (2, 4, 8 hour), (b,e) $FeCl_3$ (2, 4, 8 hour) and (c,f) $Fe(NO_3)_3$.

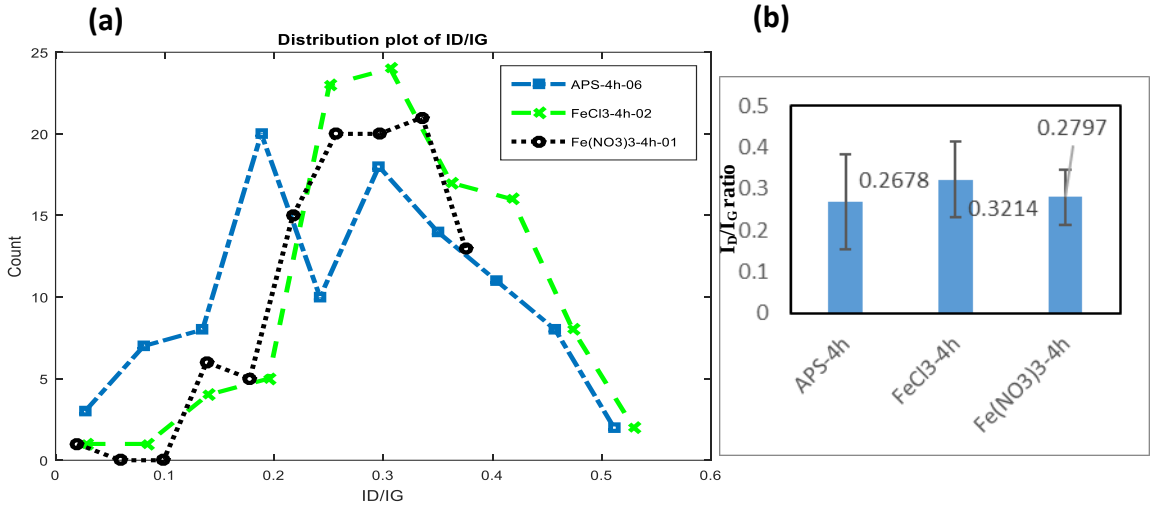

Figure 59. (a) Histogram and (b) average value of I_{2D}/I_G for using APS, $FeCl_3$, and $Fe(NO_3)_3$ for 4 hours.

The number of graphene layers was determined by I_{2D}/I_G, as shown in **Figure 60.** It is observed that all samples have a uniform distribution of layers, and that most of the

graphene area was dominated by monolayer or bilayer graphene, with only a few parts of multi-layer graphene.

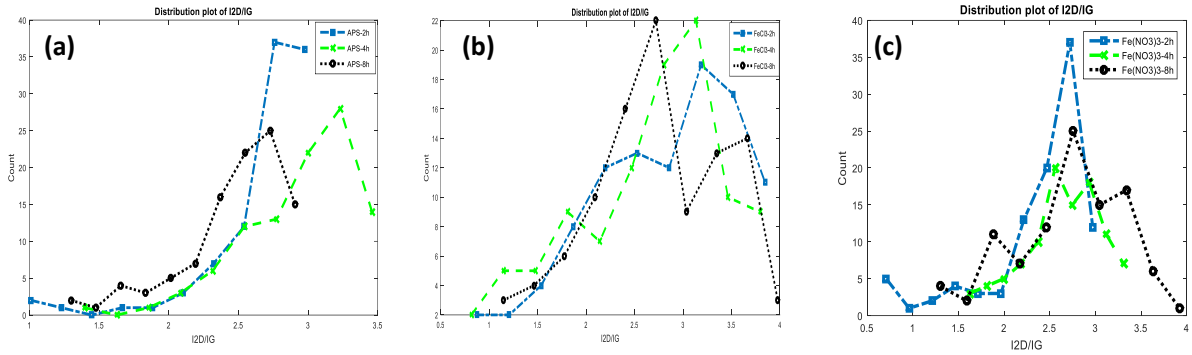

Figure 60. Histogram of I_{2D}/I_G for (a) APS (2, 4, 8 hour), (b) $FeCl_3$ (2, 4, 8 hour) and (c) $Fe(NO_3)_3$.

As-transferred graphene onto SiO_2/Si substrates using different copper etchants for different times was tested by UV-vis spectrophotometer absorbance test. The main UV-vis absorption peaks of as transferred graphene for all samples appeared at ~ 207, ~ 432, and ~ 682 nm, as shown in **Figure 61.** When APS solution was used, increasing the etching time from 2 to 4 hours decreased the absorption peaks intensity which appeared at ~ 374, ~ 432, and ~ 447 nm. In contrast, increasing the etching time from 4 to 8 hours increased the absorption peaks intensity. Using APS for 4 hours produced the lowest absorption

peaks intensity. When used for 4 hours to each copper, $FeCl_3$ and $Fe(NO_3)_3$, gave the lowest absorption peaks intensity compared with 2 and 8 hours' cases.

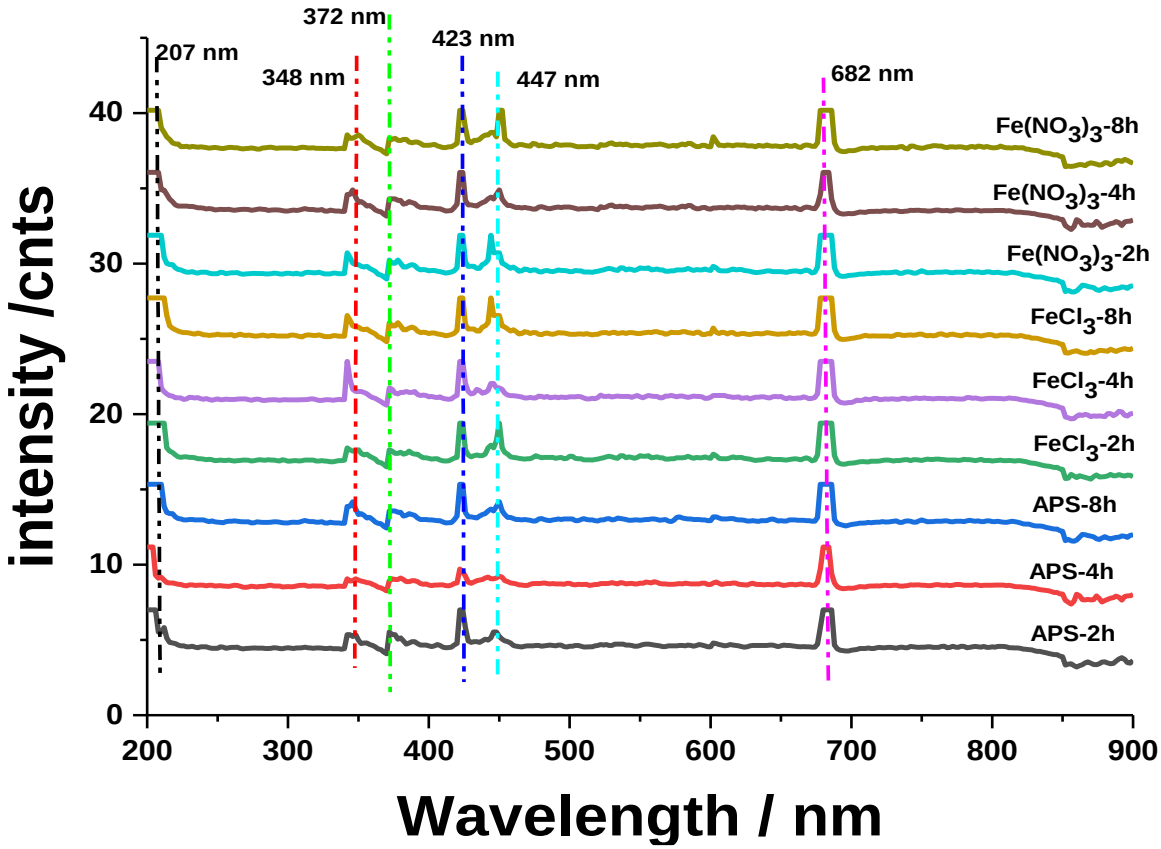

Figure 61. UV-visible spectroscopy of as-transferred graphene using different copper etchants.

The plot in **Figure 62** shows a comparison between UV-vis spectrophotometer absorbance result of as-transferred graphene using APS, $FeCl_3$ and $Fe(NO_3)_3$ for 4 hours. It is noticed that using APS for 4 hours resulted in the lowest absorbance compared with in $FeCl_3$ and $Fe(NO_3)_3$. APS-4h has lower UV-vis absorption peaks than those of other copper etchants at 384, 372, and 432.

According to UV-vis spectrophotometer absorbance results, using APS for 4 hours produced the most transparent as-transferred graphene onto SiO_2/Si substrates.

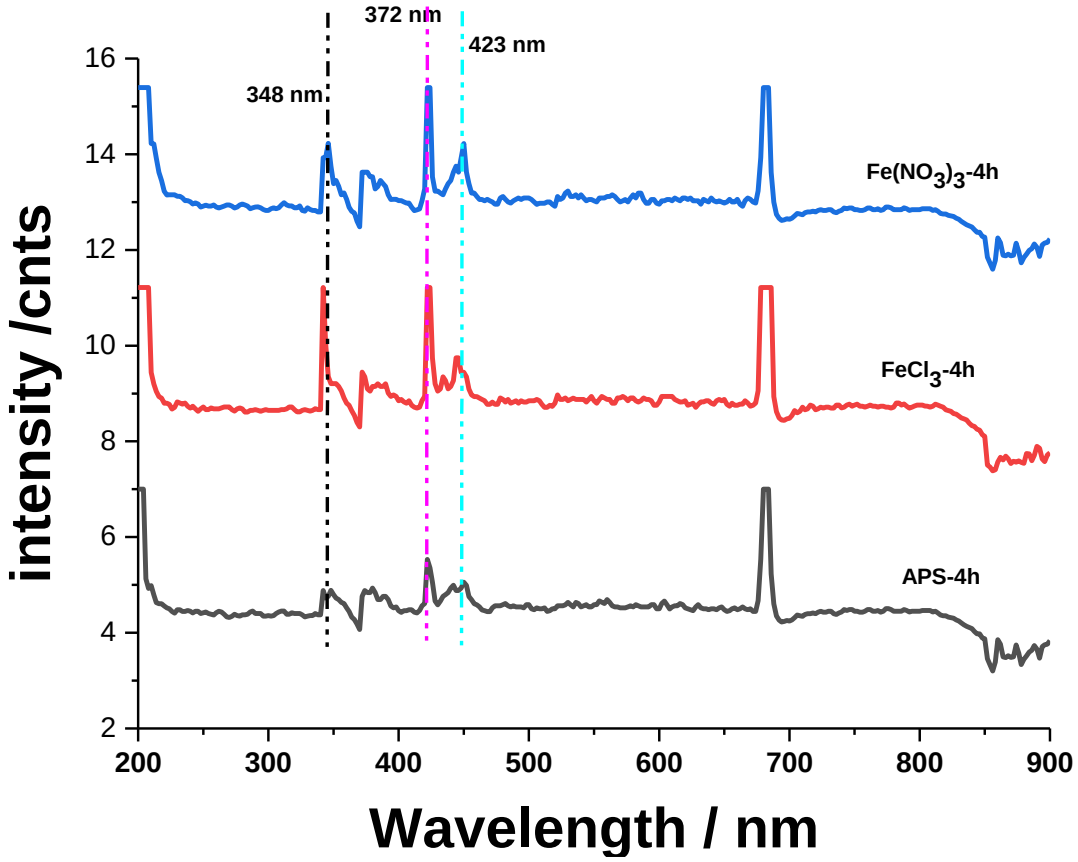

Figure 62. UV-visible spectroscopy of as-transferred graphene using APS, $FeCl_3$, and $Fe(NO_3)_3$ for 4 hours.

The electrical properties of the as- transferred graphene onto SiO_2/Si were also investigated using hall effect method. As-grown CVD graphene dominated by a monolayer area shows a sheet resistance of $(R_s) > 1\ k\Omega/sq$ because it has some a topological defects such as dislocations and grain boundaries [124], [125]. These defects can disrupt the sp^2 delocalization of π electrons in graphene and effectively scatter the charge carriers, forming highly resistive grain boundaries. Other defects such as wrinkles, folds, tears and cracks can also lead to a disrupted path of carrier transport, affecting the electrical resistivity [126]. In addition, copper residuals degraded graphene electrical properties when adopted and worked as an electrode material [123]. However,

the current- voltage (IV curve), shown in **Figure 63,** is linear, as expected for ohmic conduction also showed metallic behavior of graphene. Moreover, the IV results show that the electrical resistance decreases with increasing when etching time increased from 2 to 4 hours for APS, $FeCl_3$, and $Fe(NO_3)_3$ due to decrease in copper residuals [122] and I_D/I_G ratio changed slightly when etching time increased from 2 to 4 hours, as shown in **Figure 59.** In contrast, the electrical resistance increased when the etching time increased to 8 hours. Although the copper residuals decreased, the I_D/I_G ratio significantly increased to ~ 0.3 for all copper etchants. As shown in **Figure 63(d),** APS-4h yielded the lowest electrical resistance, ~ 10115 Ω, and $FeCl_3$ yielded the highest electrical resistance, ~ 29665 Ω.

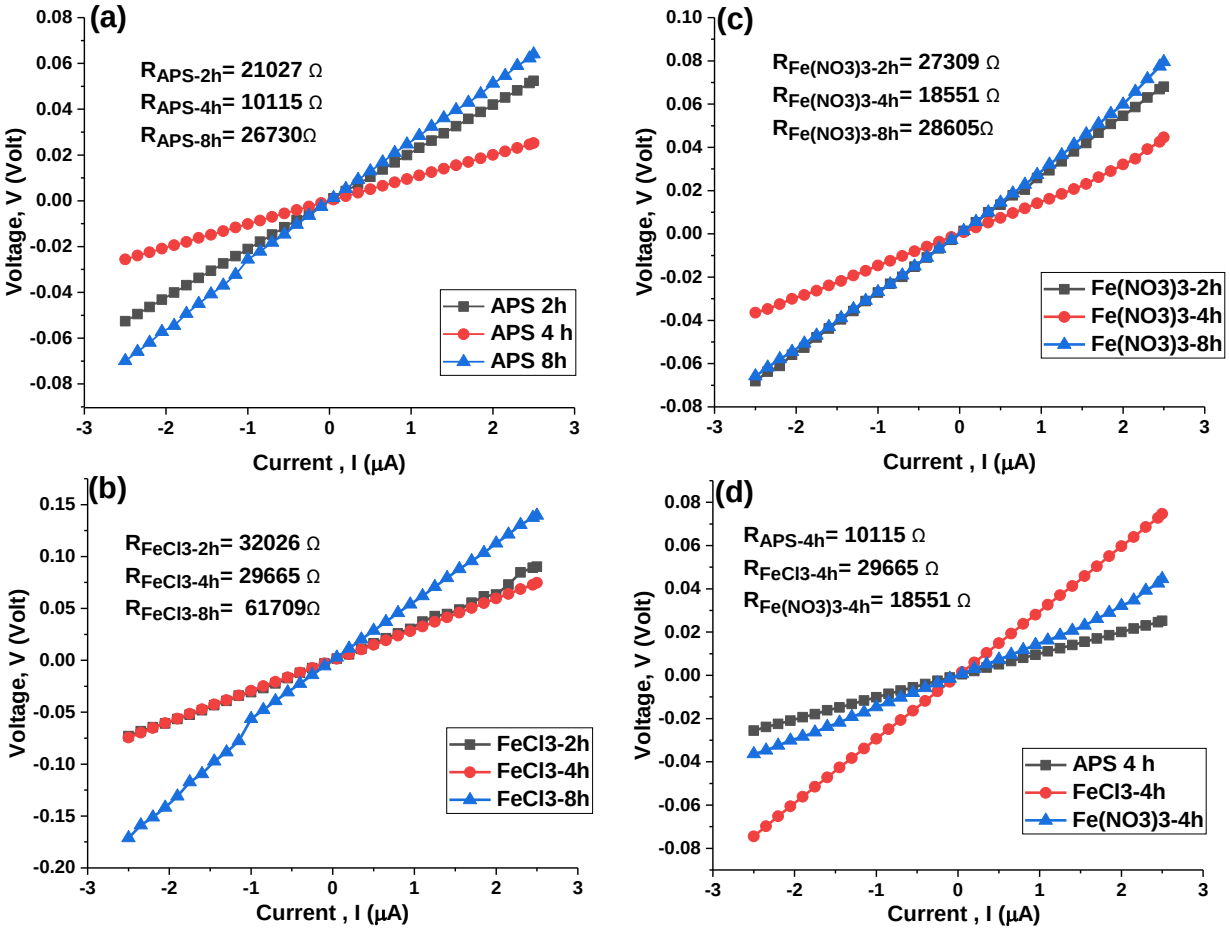

Figure 63. Hall effect measurement for as-transferred graphene using (a) APS (2, 4, and 8 hours), (b) $FeCl_3$ (2,4, and 8 hours), (c) $Fe(NO_3)_3$ (2, 4, and 8 hours), and (d) APS, $FeCl_3$, and $Fe(NO_3)_3$ for 4 hours.

Form the optical and electrical characterization of as-transferred graphene onto SiO_2/Si substrate, it is noticed that etching copper using APS, $FeCl_3$, and $Fe(NO_3)_3$ for 4 hours showed the lowest light absorption and electrical resistance. For further characterization of APS-4h, $FeCl_3$-4h, and $Fe(NO_3)_3$-4h samples, X-ray photoelectron spectroscopy (XPS) from Thermo Scientific, model (ESCALAB250Xi), was used to carry out XPS characterization. All spectra indicated the presence of carbon (C), silicon (Si) and oxygen (O), as shown in **Figure 64.** It is clear that the C peak came from the as-transferred graphene, the Si peaks come from the substrate, and that the O peak most probably came from the SiO_2 layer and the penetration of oxygen into graphene from the atmosphere, as

shown in **Figure 65 (a, b, and c)** respectively. In addition, nitrogen(N) peak appeared only for $Fe(NO_3)_3$-4h sample, which came from $Fe(NO_3)_3$ residuals on the graphene layer, as shown in **Figure 65 (d).**

It was concluded from XPS spectra survey that there are not Cu peaks for any of the samples, which means that the concentration of copper residuals is below the level that XPS spectroscopy can detect which is about 0.1 at % as mentioned in Ref.[126].

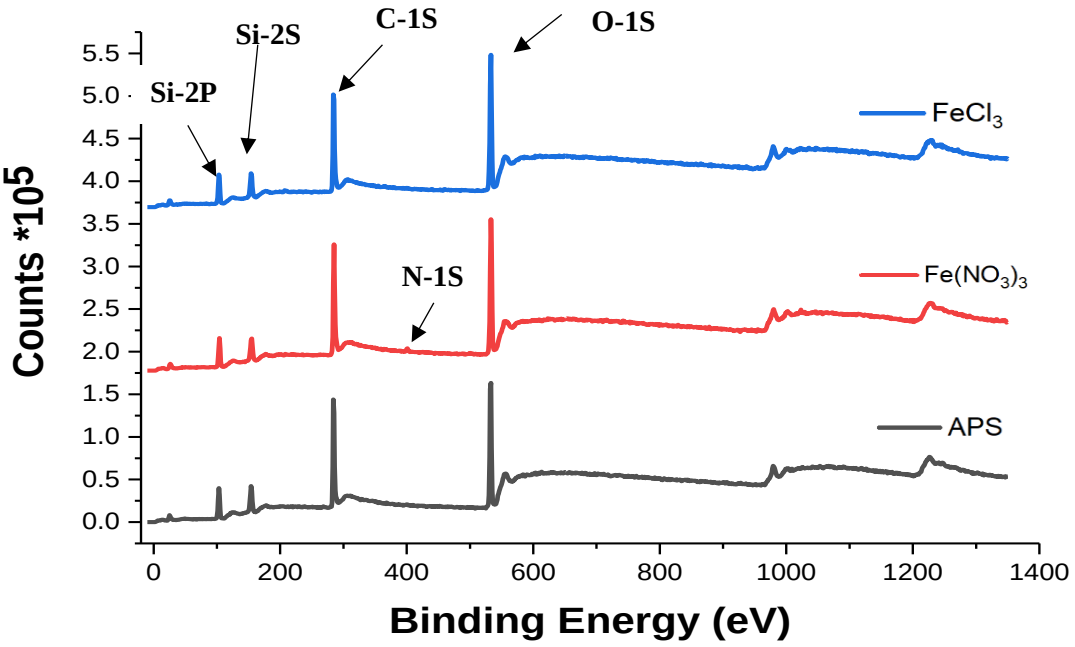

Figure 64. XPS spectra of as-transferred graphene onto SiO_2/Si substrate using APS, $FeCl_3$, and $Fe(NO_3)_3$ for 4 hours as copper etchant.

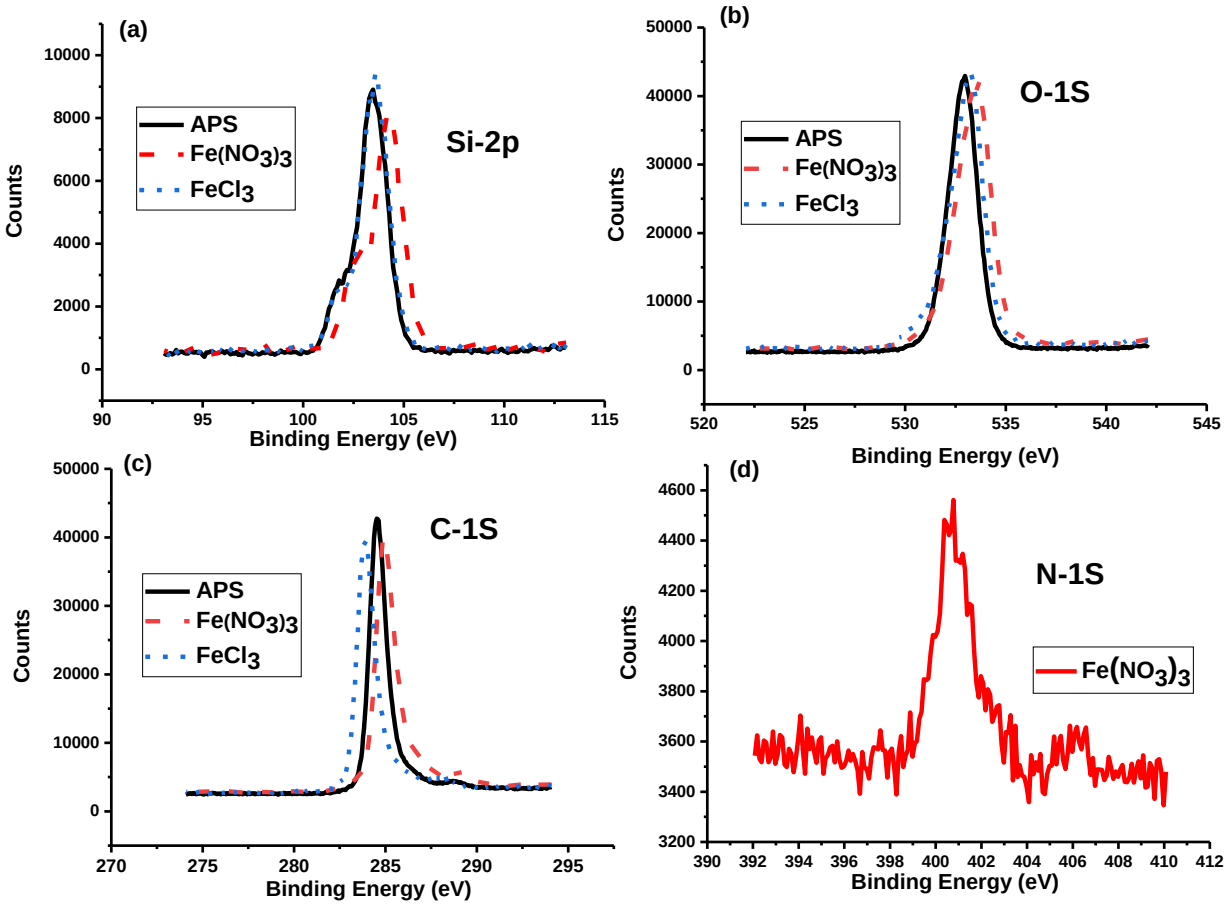

Figure 65. high resolution XPS for the (a) Si-2p peak, (b) O-1s peak, (C) C-1s peak, and (d) N-1s peak.

To further analyze the high resolution scanned of C1s peak, deconvolution of C1s peak was obtained by the profile into Gaussian–Lorentzian line shapes for all samples and their respective parameters are presented in **Figure 66**. Results of deconvolution were obtained using Origin 2017 software. From the deconvolution figures, it is noticed that APS-4h and $Fe(NO_3)_3$-4h had a sharp peak at ~ 284.6 eV binning energy and that $FeCl_3$-4h had a sharp peak at ~ 284 eV binding energy [127], which corresponds to graphene sp^2 C-C bonds. The slight shift in sp^2 position for $FeCl_3$ was due to the non-conjugated carbon in the hexagonal lattice, which in turn, was due to combination of C adatoms, non-aromatic C atoms and hydrogenation of carbon on the surface of the SiO_2/Si substrate[128]. The Sp^3 peak

represents the amorphous carbon and also hydrogenation of carbon on the surface of the substrate [129]. Furthermore, all samples presented a relatively lower intensity of O-C-O and O-C=O.

According to XPS, APS is the best copper etchant when used for 4 hours, as it yielded to the largest percentage of sp^2 ~82.6 %, with sharp peak at ~ 284.6 eV binding energy compared with other etchants ($FeCl_3$-4h and $Fe(NO_3)_3$-4h).

XPS results are consistent with Raman results, which confirms that using APS for 4 hours to completely etch the copper substrate produce the best quality and low defect graphene with the lowest electrical resistance and light absorption.

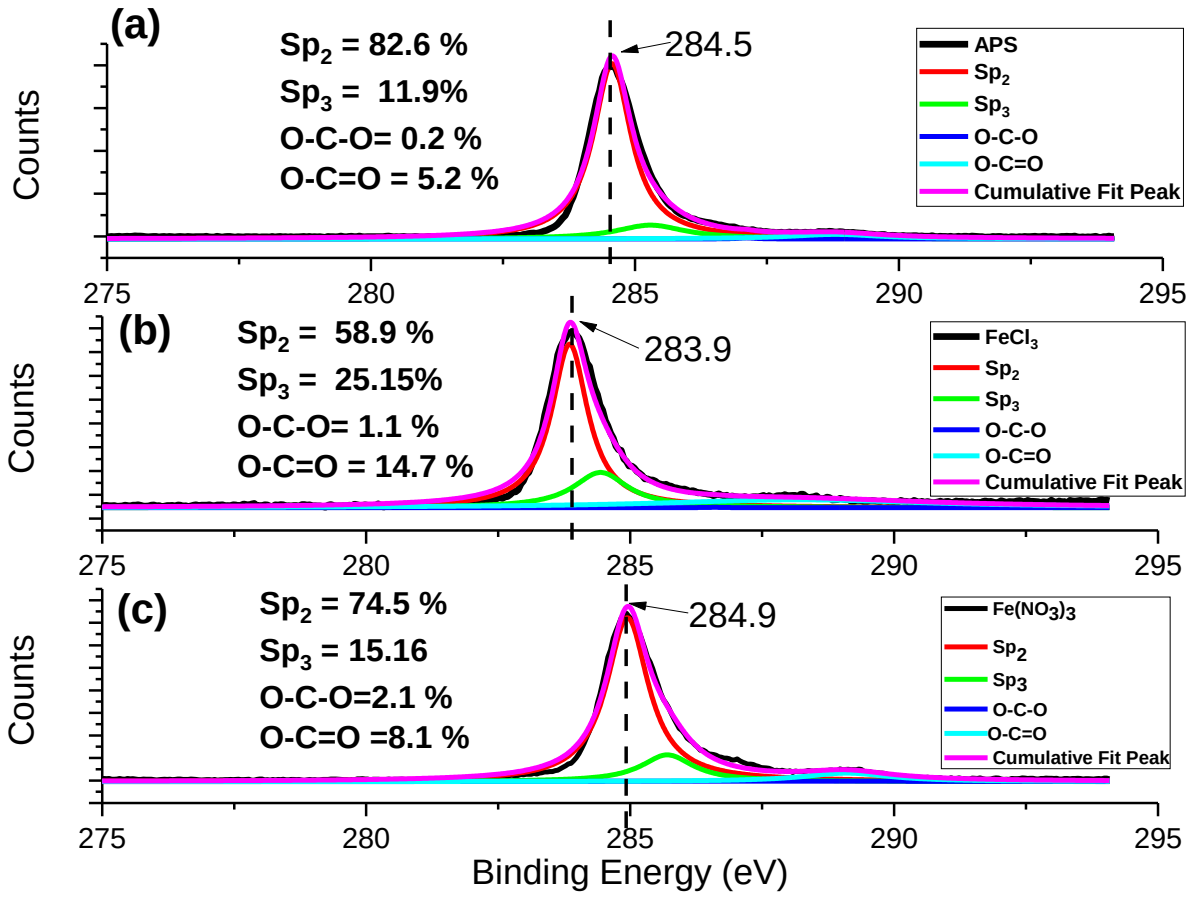

Figure 66. Deconvolution of peak of C-1s of as-transferred graphene using (a) APS, (b) $FeCl_3$, and (c) $Fe(NO_3)_3$ for 4 hours, as copper etchant.

4.2 PMMA removal

A lot of research has been done to investigate the influence of PMMA transfer method parameters on the final structure, morphology and quality of graphene, as mentioned in **Chapter 2**. PMMA residues degrade the quality of graphene, in terms of graphene properties. The results of optimizing PMMA parameters using design of experiment method are shown in this section.

4.2.1 Design of experiment for reducing PMMA residues

In one experiment, one or more process variables (or factors) were deliberately changed in order to observe how the changes affect one or more response variables. The (statistical) design of experiments (DOE) is an effective procedure for planning experiments so that the data obtained can be analyzed to yield valid and objective conclusions. DOE is used to determine the relationship between factors affecting a process and the output of that process. In other words, it is used to find cause-and-effect relationships.

In this study, of the many DOE methods, the Taguchi model has been used to identify the factors and their interactions that may affect PMMA residuals that are left behind during the transfer of graphene to its desired substrate. The level of PMMA residues greatly reduces the properties of graphene, hence it is vital to make sure there are no PMMA residuals left behind during the transfer process. PMMA residuals are influenced by factors such as temperature, spin coating rpm, acetone temp and dissolving time of the etching. By using orthogonal experimental design and analysis techniques, the performance of this process can be analyzed to reach more objective conclusions through only a small number of simulation experiments.

The Taguchi method, as shown in **Figure 67**, involves reducing the variation in a process through robust design of experiments. The overall objective of the method is to produce a high-quality product at low cost to the manufacturer. Poor-quality products affect not only the manufacturer but also the whole society, therefore high-quality products should be available at affordable prices. This method of designing experiments investigates how different parameters affect the mean and variance of a process performance characteristic that defines how well the process is functioning. The experimental design proposed by

Taguchi involves using orthogonal arrays to organize the parameters affecting the process and the levels at which they should be varied; it allows for the collection of the necessary data to determine which factors most affect product quality with a minimum amount of experimentation, thus saving time and resources. Analysis of variance on the collected data from the Taguchi design of experiments can be used to select new parameter values to optimize the performance characteristics [130].

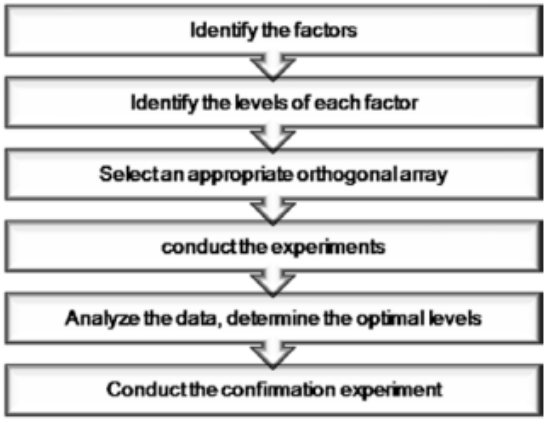

Figure 67. The Taguchi method steps [130]**.**

4.2.2 Detailed Design Description

The objective of this study is to select a combination of input parameters' values that will result in minimum PMMA surface coverage. After a lot of research through the literature review, the following factors and parameters were considered the most cited for PMMA removal, and our objective is to optimize these parameters. Details of the parameters and their levels are provided in **Table 5**.

Table 5. Factors affecting PMMA deposition/removal.

PMMA process	Factors	Level 1	Level 2	Level 3
Deposition	1- PMMA (% conc.)	4.5	8	12
	2- Spin coating speed (rpm)	2500	3000	4000
Removal	3- Acetone temp (ºC)	25	40	60
	4- PMMA dissolution time (min)	5	20	60

In the present reaction system, four operating parameters were selected, each at three levels, to evaluate the PMMA residue. This experiment was performed using the **Minitab 17 software**, and it was based on the Taguchi method, which assumes that there is no interaction between any two factors. In this experiment the factors are independent of one another. These are the sample experiments that were carried out in the lab. The suitable orthogonal array, L9, is shown in **Table 6**. The actual parameters' levels and values are also shown. The DOE reduced the number of experiments from actual number of experiments (For full coverage total number of experiments = n^k where n is the number of factors and k number of levels for each factor) $3^4 = 81$ to only 9 experiments (from Minitab software using Taguchi method).

Table 6. The actual parameters' levels and values.

# Sample	PMMA (%conc.)	Spin coating speed (rpm)	Acetone dissolving temperature (°C)	Acetone dissolving time (min)
1	4.5	2500	24	5
2	4.5	3000	40	20
3	4.5	4000	60	60
4	8	2500	40	60
5	8	3000	60	5
6	8	4000	24	20
7	12	2500	60	20
8	12	3000	24	60
9	12	4000	40	5

Based on this experimental design, each experiment was repeated four times to decrease random errors or errors due to experiments. Experiments were closely observed, and extreme care was taken to ensure that all parameters were accurately utilized, as the accuracy of analysis depends on the accuracy of data.

4.2.3 Analysis and Results

4.2.3.1 DOE results

After having carried out the 9 sets of experiments, atomic force microscopy was used to obtain the surface coverage of PMMA. **Figure 68** shows the AFM image of all the samples. The white spots represent the PMMA residues.

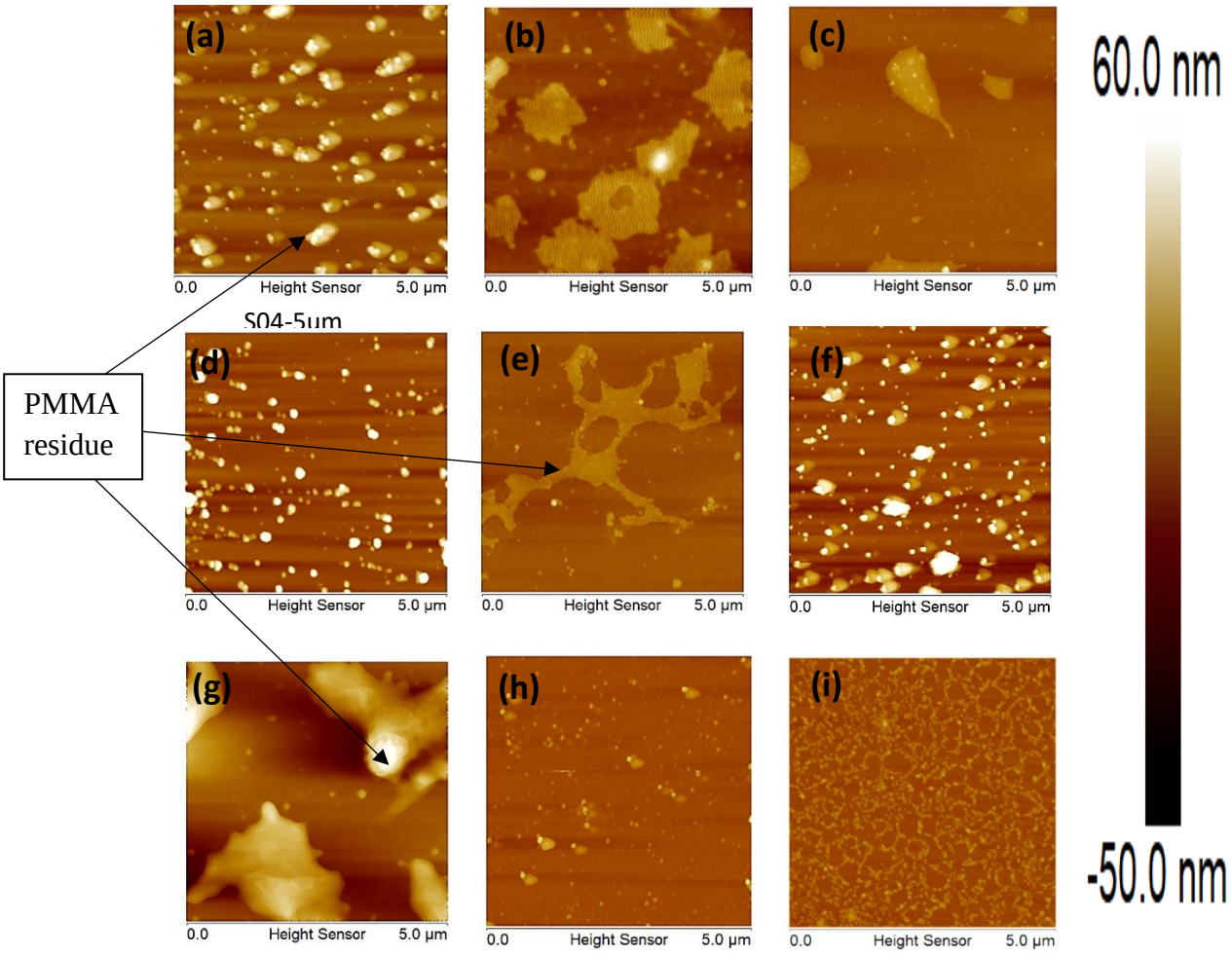

Figure 68. The presence of PMMA residues for samples (a, b, c, d, e, f, g, h and i) 1, 2, 3, 4, 5, 6, 7, 8, and 9 respectively.

It is observed from **Figure 68** that each experiment yielded PMMA residue area fractions of different sizes. The agglomeration of PMMA particles happened when a relatively higher temperature was used, as shown in **Figure 68 (c, e, and g)** on sample 3, 5, and 7 (increasing the temperate leads to agglomeration of the PMMA).

However, AFM cannot directly calculate the percentage of contaminant area. It needs to be converted into an image and analyzed using Image-J software to calculate the percentage of contaminated area. Using Image-J software, the above samples were converted to area

fraction, as shown in **Figure 69.** Many samples exhibited very low PMMA area fraction, around 7%. Compared to other samples, sample 8 gave the minimum residues, ~ 6.6 %.

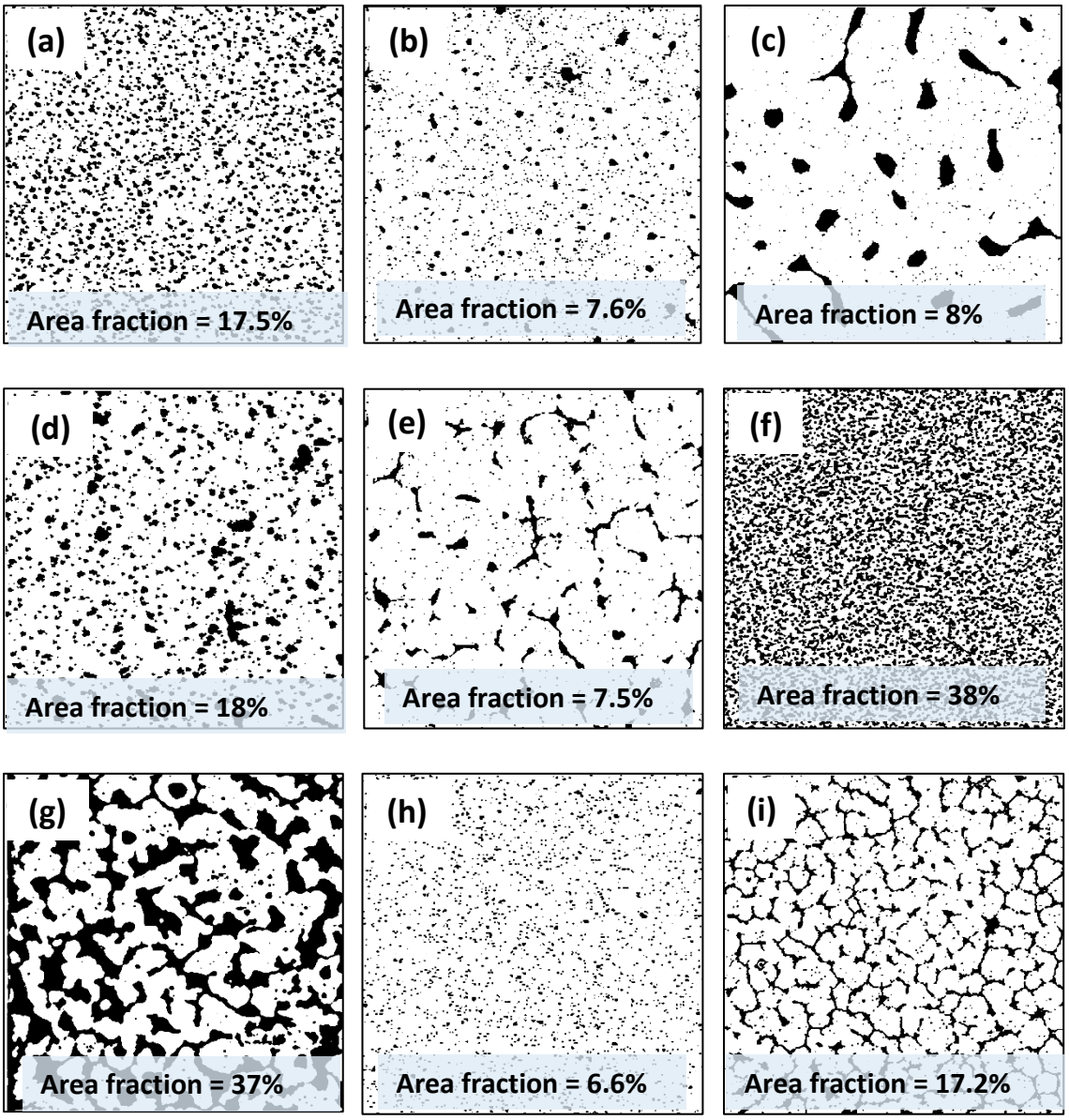

Figure 69. The area fraction of PMMA residue concentration obtained from the AFM images using Image-J for samples (a, b, c, d, e, f, g, h and i) 1, 2, 3, 4, 5, 6, 7, 8, and 9 respectively.

Each sample was analyzed using four representative AFM images of scan size 30 µm x 30 µm. Average values of measured PMMA area fractions for each sample revealed that S08

yielded the minimum PMMA residues (~ 5%) compared to other samples as, tabulated in **Table 7.**

Table 7. Results of PMMA area fractions

Sample	PMMA (%conc.)	Spin coating speed (rpm)	Acetone dissolving temperature (°C)	Acetone dissolving time (min)	Results of PMMA area fractions				Avg.
					Area1	Area2	Area3	Area4	
S01	4.5	2500	25	5	16.3	16.8	17.5	32.6	21
S02	4.5	3000	40	20	3.35	4.45	7.6	3.4	5
S03	4.5	4000	60	60	9.25	8.2	6.9	11.3	9
S04	8	2500	40	60	14.5	18	22	13	17
S05	8	3000	60	5	10.5	7.5	9.1	8.8	9
S06	8	4000	25	20	38	19.3	38.5	18.9	29
S07	12	2500	60	20	42.6	20.8	32	28.7	31
S08	12	3000	25	60	6.6	3.6	3.6	6.6	5
S09	12	4000	40	5	17.8	24.6	25.8	37.9	27

Taguchi experiments often use a 2-step optimization process. In step 1 the signal-to-noise ratio is used to identify control factors that reduce variability. In step 2, control factors that move the mean to target and have a small or no effect on the signal-to-noise ratio are identified. The signal-to-noise ratio measures how the response varies relative to the nominal or target value under different noise conditions. Different signal-to-noise ratios can be chosen depending on the goal of the experiment.

Signal-to-noise ratio (SNR) needs to be computed based on the design optimization requirements. In this case, since the goal is to minimize PMMA surface coverage, the-smaller-the-better approach is selected.

$$SN_s = -10\log\left(\frac{1}{n}\sum_{i=1}^{n} y_i^2\right) \tag{4.1}$$

Where y_i is the response of the i-th trial, and n is the number of trial/ repetition.

The SNR is calculated to compute the response, which is plotted, as shown in **Figure 70 a.** In order to verify the obtained results, the same analysis has been done using Mean plot directly from the software (**Minitab 17**). Results of SNR were identical with those of mean plot analysis, as shown in **Figure 70 b.**

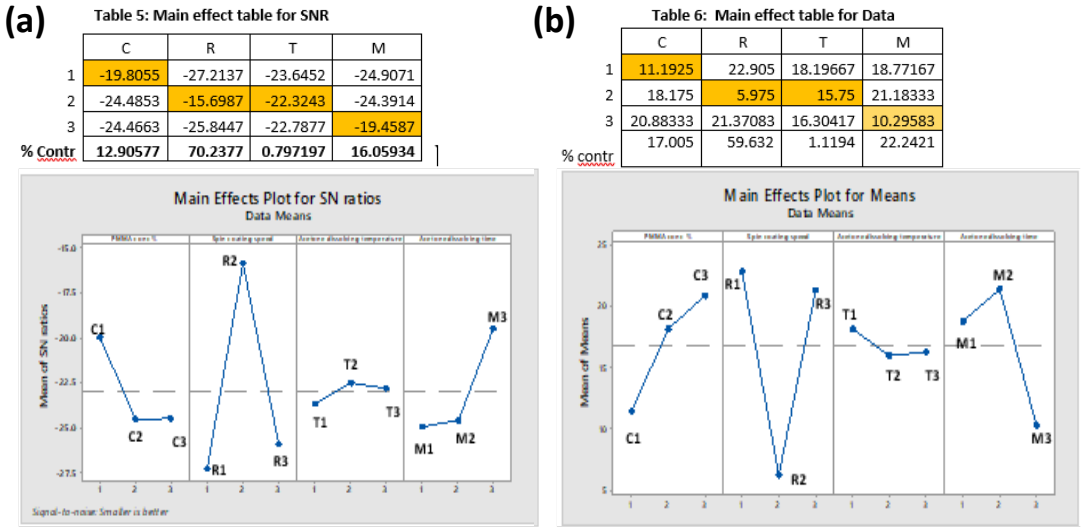

Figure 70. The main effects plots for (a) SNR and (b) means.

The next step is selecting a parameters' combination for minimum surface coverage. This is done by selecting the maximum value from each parameter in the Main Effect plot for SNR ratio or minimum points in the Main Effect Plot for Means. The combination is shown in **Table 8.**

Table 8. optimized PMMA parameters.

PMMA conc. %	spin rpm	acetone temp °C	acetone time (mins)
4.5	3000	40	60

Using analysis of variance (ANOVA) to estimate contribution, the contribution of each input parameter to the variation in the output has been evaluated as following.

ANOVA analysis

Table 9. PMMA Factors Information

Factor	Levels	Values
PMMA conc %	3	4.5, 8.0, 12.0
Spin coating speed (r.p.m)	3	2500, 3000, 4000
Acetone dissolving temperature(ºC)	3	24, 40, 60
Acetone dissolving time(min)	3	5, 20, 60

Table 10. Analysis of Variance for 4 factors

Source	DF	Adj SS	Adj MS	F-Value	P-Value
PMMA conc%	2	40.43	20.215	-	-
Spin coating speed (r.p.m)	2	229.724	114.86	-	-
Acetone dissolving temperature(ºC)	2	2.113	1.057	-	-
Acetone dissolving time(min)	2	55.877	27.938	-	-
Error	-	-	-		
Total	8	328.143			

Table 11. PMMA Factors contributions

PMMA conc %	Spin coating speed (r.p.m)	Acetone dissolving temperature(ºC)	Acetone dissolving time(min)
12.9 %	70.23 %	0.8 %	16.06 %

From ANOVA analysis, PMMA concentration contributes 13%, spin revolution 70%, acetone temperature 1% and dissolution time in acetone contributes 16%. The implication is that spin revolution is the most important parameter affecting the surface coverage.

As this experiment has 4 factors and each one consumes 2 DF with a total of 8 DF. Then, MSE could not be calculated and it's necessary for calculating the statistics tests (P and F). Removing factor of acetone dissolving temperature from the model because it has the smallest effect of the 4 factors on the S/N Ratios. This will free up 2 df for the error term. The new Anova analysis for remaining 3 factors (PMMA conc%, Spin coating speed and Acetone dissolving time) is shown in the following table.

Table 12. Analysis of Variance for 3 factors

Source	DF	Adj SS	Adj MS	F-Value	P-Value
PMMA conc%	2	40.43	20.215	19.13	0.050
Spin coating speed (r.p.m)	2	229.724	114.86	108.70	0.009
Acetone dissolving time(min)	2	55.877	27.938	26.44	0.036
Error	2	2.113	1.057		
Total	8	328.143			

Finally, projection of the improved performance was calculated. Results were obtained from the following equation.

$$\{\boldsymbol{SNR}\}_{\boldsymbol{proj}} = \{\boldsymbol{SNR}\}_{\boldsymbol{aver}} + \sum_{\boldsymbol{i=1}}^{\boldsymbol{n}}[\{\boldsymbol{SNR}\}_{\boldsymbol{i}} - \{\boldsymbol{SNR}\}_{\boldsymbol{aver}}] \qquad (4.2)$$

Where:

$\{SNR\}_{proj}$ represents the projected SNR.

$\{SNR\}_{aver}$ represents the average SNR calculated from the effect table.

$\{SNR\}_{i}$ represents the optimal SNR for each parameter.

n is the number of input parameters.

The projected SNR is therefore - 8.53, which translates to a minimum surface coverage of 2.7%.

4.2.3.2 Validation experiment results

PMMA has been deposited on a glass slice and removed using optimized parameter levels. Comparing to the projected SNR is therefore - 8.53, which translates to a minimum surface coverage of 2.7%, the validation experiment has an area coverage of PMMA residues of 2.87 % which is very close to the previously calculated one, as shown in **Figure 71**.

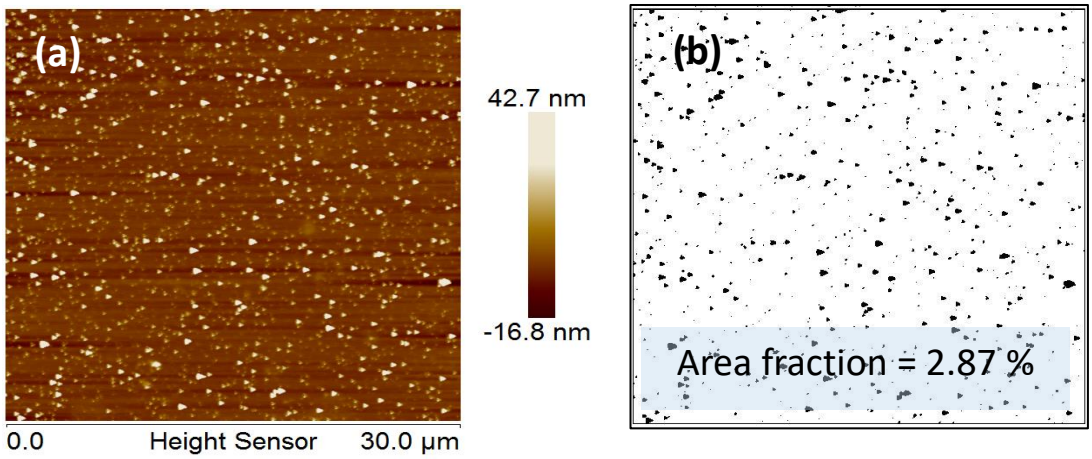

Figure 71. Validation experiment results (a) AFM image, and (b) Area fraction image calculated by Image-J software.

Using the same parameters of validation experiment, PMMA was deposited on the graphene layer, for graphene transfer experiment, and removed after graphene was transferred, and then compared with the worst-case scenario as tabulated in **Table 13**. Worst case scenario would be using 12% PMMA, at 2500 rpm, at 24ºC for 20 min in acetone, as shown in **Figure 72**. It is noticed from AFM images that using optimization parameter reduced the PMMA residuals, compared to the worst-case scenario. The AFM image of the optimized parameter case has an area coverage of ~ 3.42 % and the one in the worst-case scenario has ~ 9.23, about three times of the optimized parameters.

Table 13. Optimized and the worst-case parameters for PMMA removal.

Case	PMMA CONC	Spin coating speed	Temperature	Acetone time
Optimized case	4.5 %	3000 rpm	40ºC	60 min
Worst case	12 %	2500 rpm	24º C	20 min

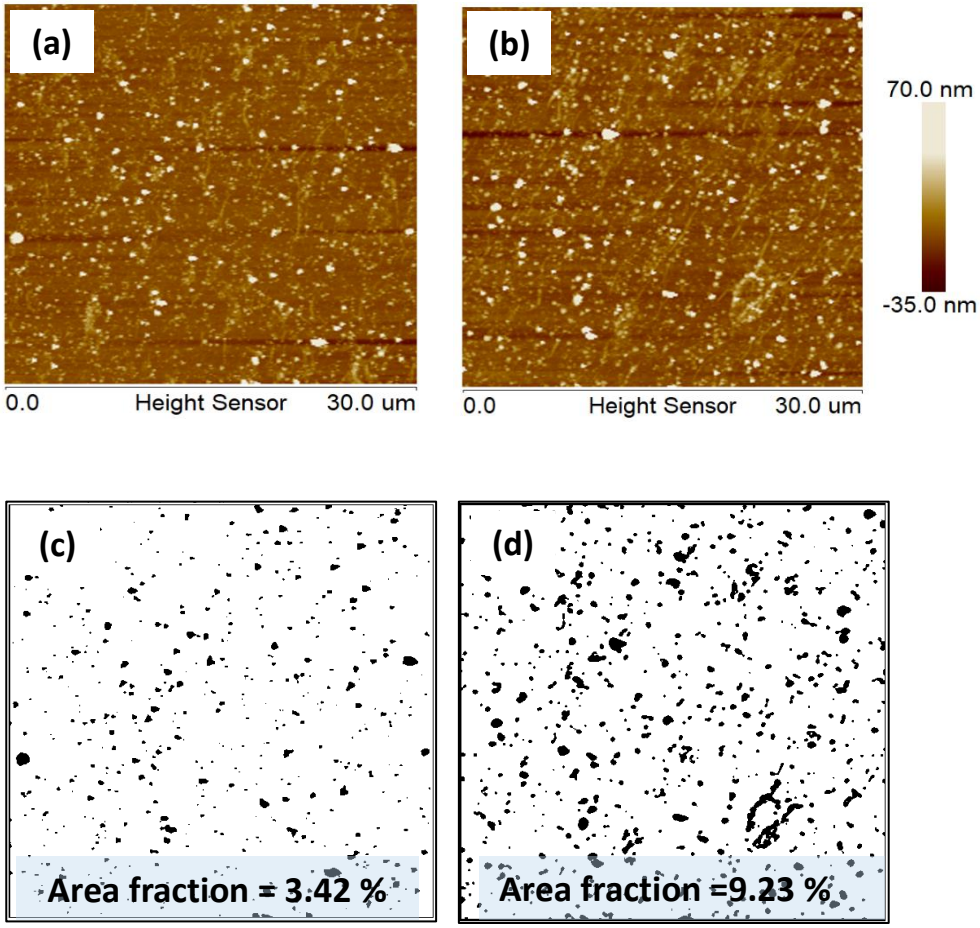

Figure 72. AFM images and area fraction for (a) optimized parameters (4.5%-3000 rpm- 40°C-60min) (b) worst case parameters (12%-2500 rpm-24°C-20 min).

4.2.4 Proposed PMMA transfer parameters

For an appropriate comparison, optimized and worst-case results are not enough. From DOE result, the contribution of spin coating speed was 70% and PMMA concentration was 13% and, based on the literature review, the most common PMMA transfer parameters were selected for a proper comparison, as shown in **Table 14**. The comparison will be in terms of graphene quality, electrical resistance and optical properties.

Table 14. Proposed PMMA transfer parameters.

Sample no.	PMMA %(conc.)	Spin coating speed (rpm)	Acetone temp (°C)	PMMA dissolution time (min)
S01	**2.5**	**4000**	**24**	**60**
S02	**4.5**	**3000**	**40**	**60**
S03	**12**	**2500**	**24**	**20**
S04	**12**	**3000**	**24**	**60**
S05	**12**	**4000**	**24**	**60**

In the graphene transfer process, the proposed PMMA transfer parameters were used. After removing the PMMA layer, the graphene layer was characterized using AFM to calculate PMMA residues. Raman mapping, UV-vis light absorption and Hall effect measurement were also carried out.

Optical microscopy images show the PMMA residues (bright spots), as shown in **Figure 73.** As shown in **Figure 73 a,** S01(2.5%-4000) and S02(4.5%-3000) contain less PMMA residues. On other hand, S03(12%-2500) contains a lot of PMMA residues, as shown in **Figure 73 c.** In addition, as OM shows in **Figure 73 (c, d, and e),** increasing the spin coating speed reduced the PMMA residuals, because increasing the speed produces a thinner layer of PMMA.

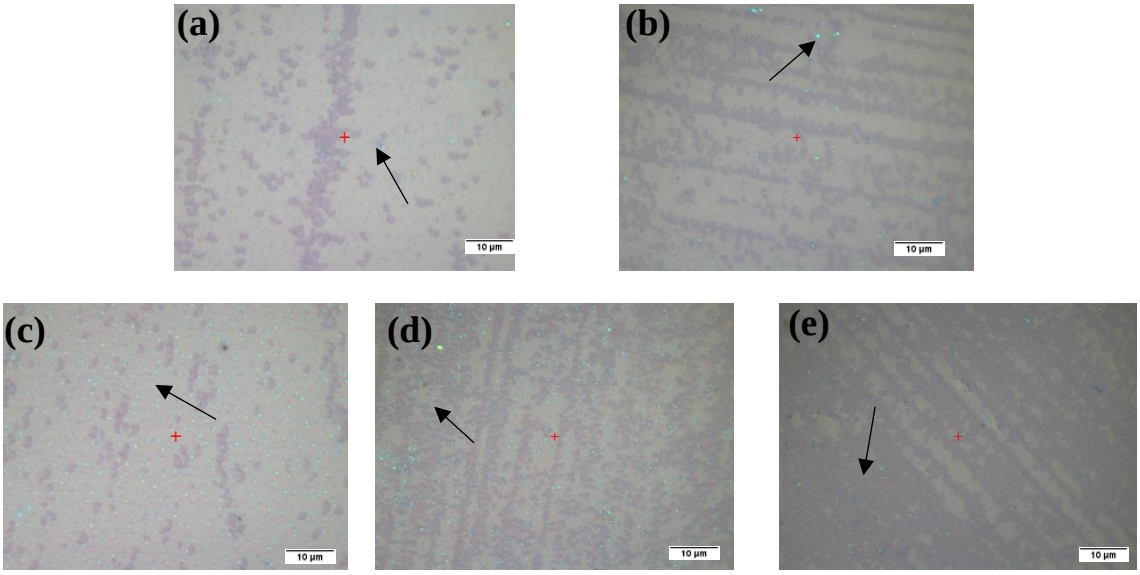

Figure 73. Optical images of (a) 2.5%-4000, (b) 4.5%-3000, (C) 12%-2500, (d)12%-3000, and (e)12%-4000.

AFM images were taken in a 30x30 µm area, using Image-J software to calculate area fraction of each sample. As shown in **Figure 74,** results confirm the OM images that S01 and S02 contain PMMA residues less than S03, S04 and S05.

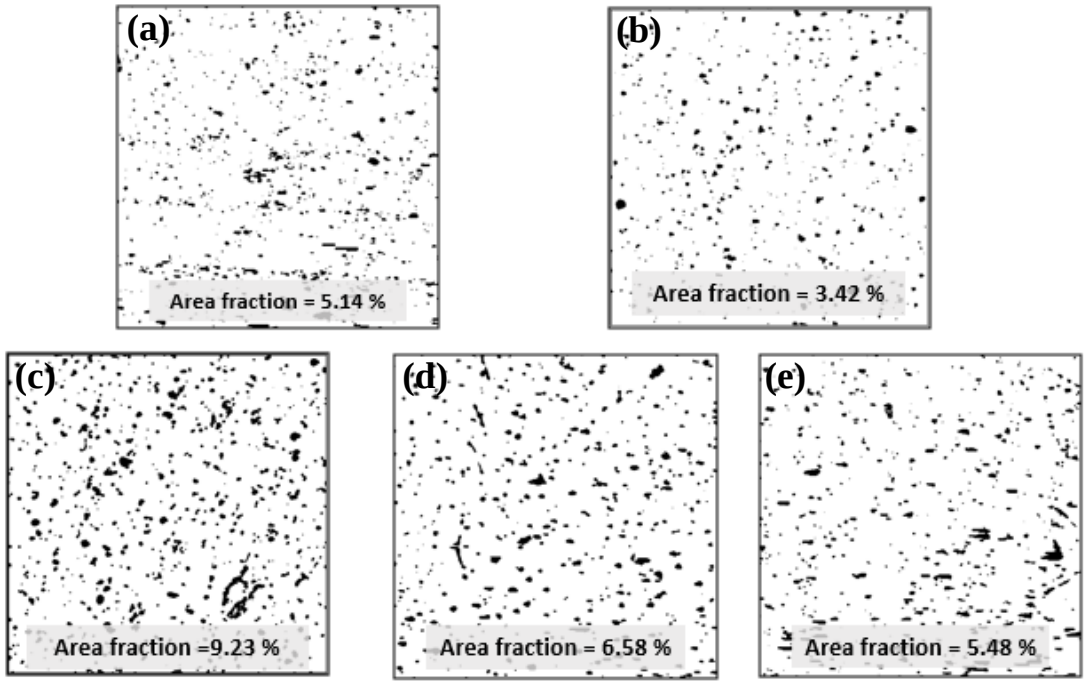

Figure 74. The area fraction of PMMA residue concentration obtained from the AFM images using Image-J for samples (a, b, c, d, and e) S01, S02, S03, S04 and S05 respectively.

Raman mapping measurements were conducted for all samples by investigating an area of 10x10 μm. A total of 100 μm^2 Raman spectra were collected and analyzed. The I_D/I_G ratio evaluate the quality of transferred graphene layers. The I_D/I_G histogram plots shown in **Figure 75 a** clearly show that the I_D/I_G decreased as PMMA concentration increased. S01, S02and S03 has a highest value of I_D/I_G ratio compared to S04 and S05. Average value of I_D/I_G was calculated for 100 spectra, as shown in **Figure 75 b**, and it showed that the quality of graphene layer was affected by the PMMA concentration and spin coating speed. S01 and S02, for example, have a very thin PMMA layer because a very small concentration of PMMA was used. However, even though they have the smallest percentage of PMMA residues, they have the highest I_D/I_G ratio, ~ 0.37, which means that the graphene layer contained higher defects. one of the factors that affect graphene quality is using a very thin

layer of PMMA, as this doesn't give enough support to graphene layer during the transfer process. Also, S03 has a high I_D/I_G ratio of ~ 0.32, even though it has a thick layer of PMMA (12%). This is because a high percentage of PMMA residue on the graphene surface can induce a p-doping effect and act as center of carrier scattering, decreasing carrier mobility and leading to a low-quality graphene [28][131]. In addition, PMMA could cause cracks and tears in weak monolayer graphene. As the PMMA coating on graphene dries, it holds the graphene rigid, keeping the ripples and folds on graphene that may have formed during the growth and cooling process. These ripples can hinder good contact between graphene and the transfer substrate, causing graphene to tear off as the PMMA layer is washed away [22]. On the other hand, S04 and S05 have a low I_D/I_G ratio of ~ 0.13 and ~ 0.18 respectively, which means that the graphene layer contains a less number of defects and that the PMMA layer provided a suitable support for the graphene layer during the transfer process.

The histogram plot in **Figure 75 c** shows that the intensity ratio of I_{2D}/I_G ranged from ~ 0.5 to ~ 3.5, which indicates that the graphene layer for all samples was dominated by a monolayers and bilayer graphene, with a small area of few-layer graphene. The I_{2D}/I_G histogram plot shows that all samples have the same distribution of graphene in terms of the number of layers for as-grown and as-transferred graphene.

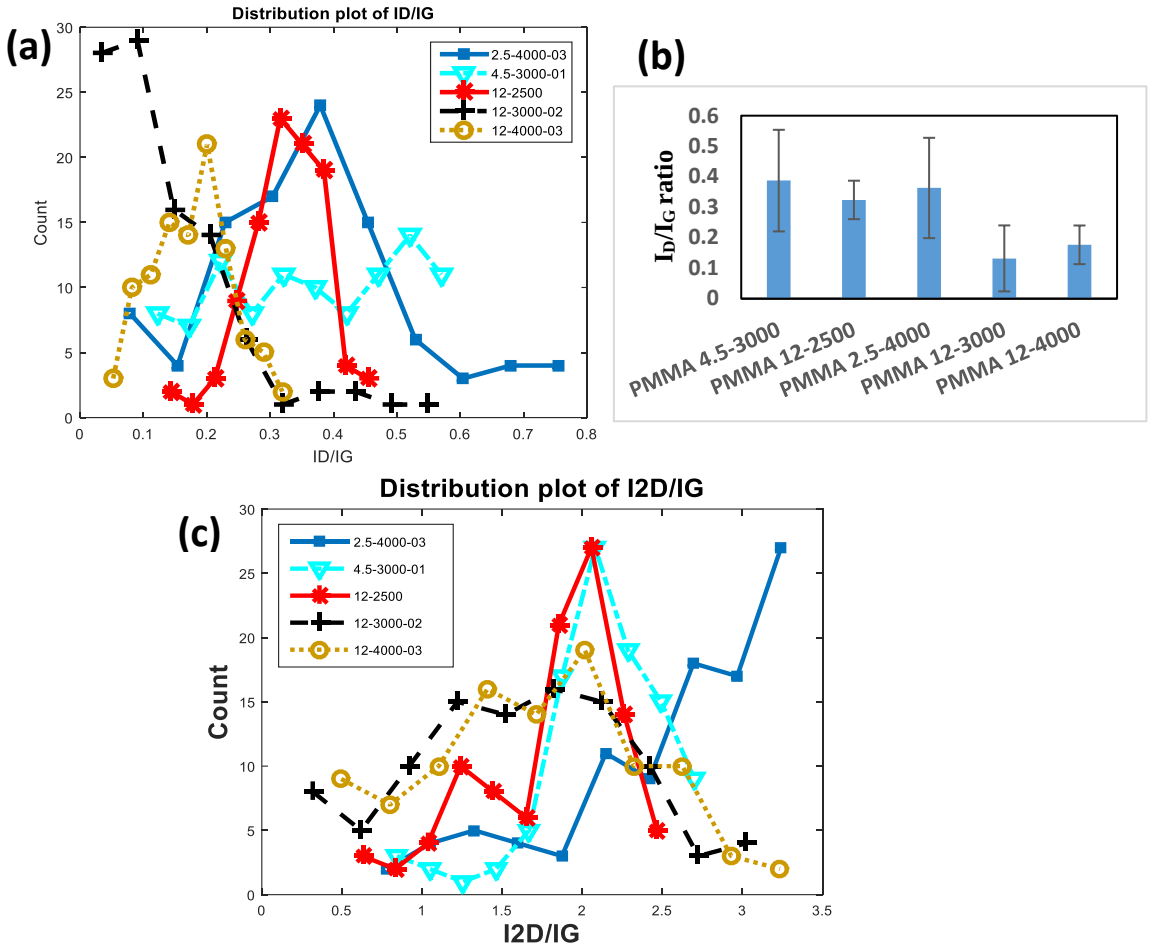

Figure 75. (a) Histogram plot of I_D/I_G, (b) plot of the average values of I_D/I_G and (e) histogram plot of I_{2D}/I_G for S01, S02, S03, S04, and S05.

To determine light absorption, UV-visible measurement was performed and plotted, as shown in **Figure 85**. Absorbance (represented by the vertical axis) measures the amount of light absorbed. The higher the value, the more a particular wavelength is being absorbed. All samples have highest peak of light absorption intensity at wavelength of ~ 682 nm. Also, S01, S02, S03 and S05 have five main absorption peaks of ~ 207, ~346, ~ 375, ~ 423 and ~ 447 nm. On the other hand, S04 has only the main peak at wavelength of ~ 682 nm, which makes it more transparent than other samples. This confirms that, after removing the supportive layer, as decrease the amount of PMMA residues I_D/I_G ratio will decrease, which improves the optical properties.

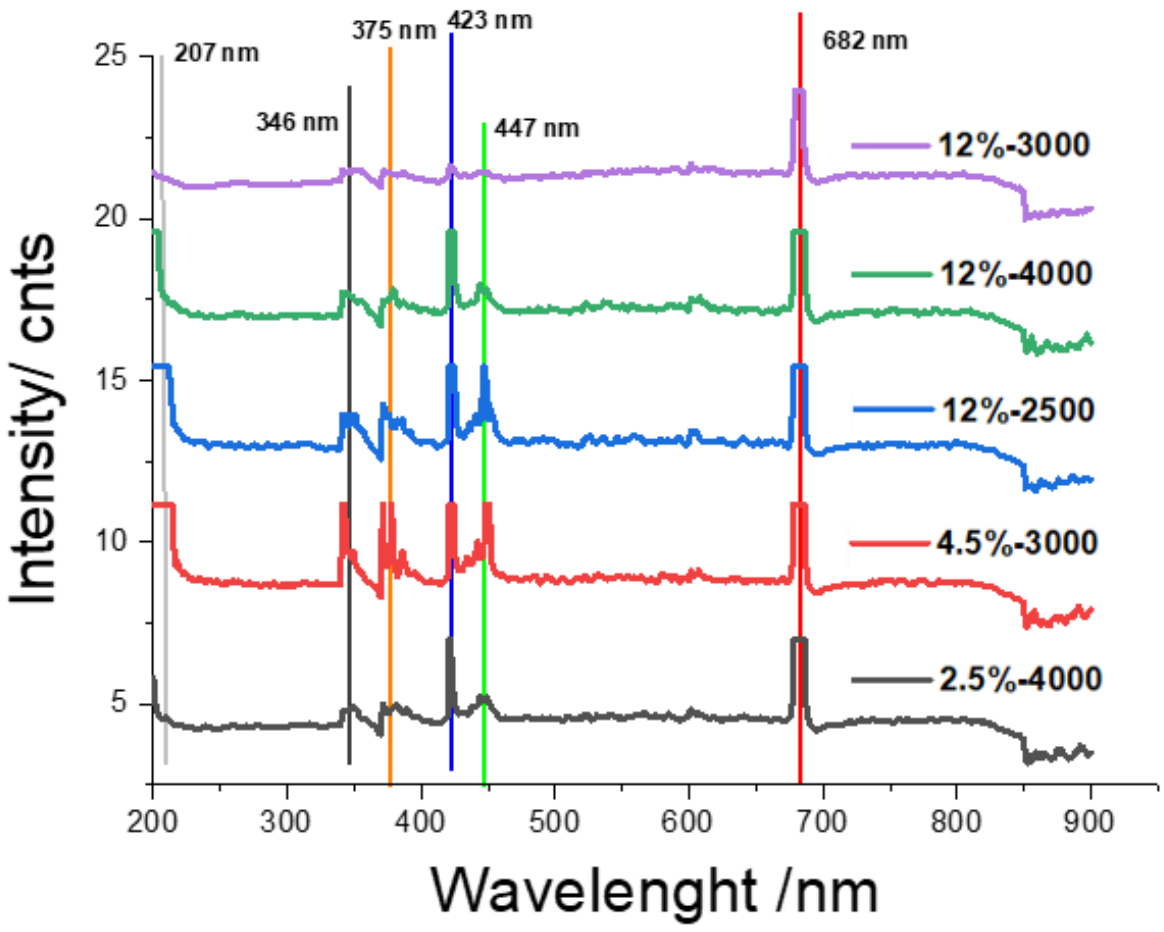

Figure 76. UV-Visible of S01, S02, S03, S04 and S05.

Electrical conductivity was measured for previous samples using Hall effect method to correlate the conductivity to the resistance of as-transferred graphene layer. **Figure 77** shows the current-volt plots of the as-transferred graphene layer onto SiO_2/Si samples using the proposed PMMA treatment parameter. It is seen that the S04 showed significantly smaller resistance of, ~ 8690.9 Ω, than the other sample. Also, S04 had the smallest I_D/I_G ratio, about 0.13 and an insignificant of PMMA residues with area fraction of about 6.5 %. Sample S03 had the highest percentage of PMMA residues and a relatively high I_D/I_G ratio of about 0.32 gives the highest resistance of 84672 Ω.

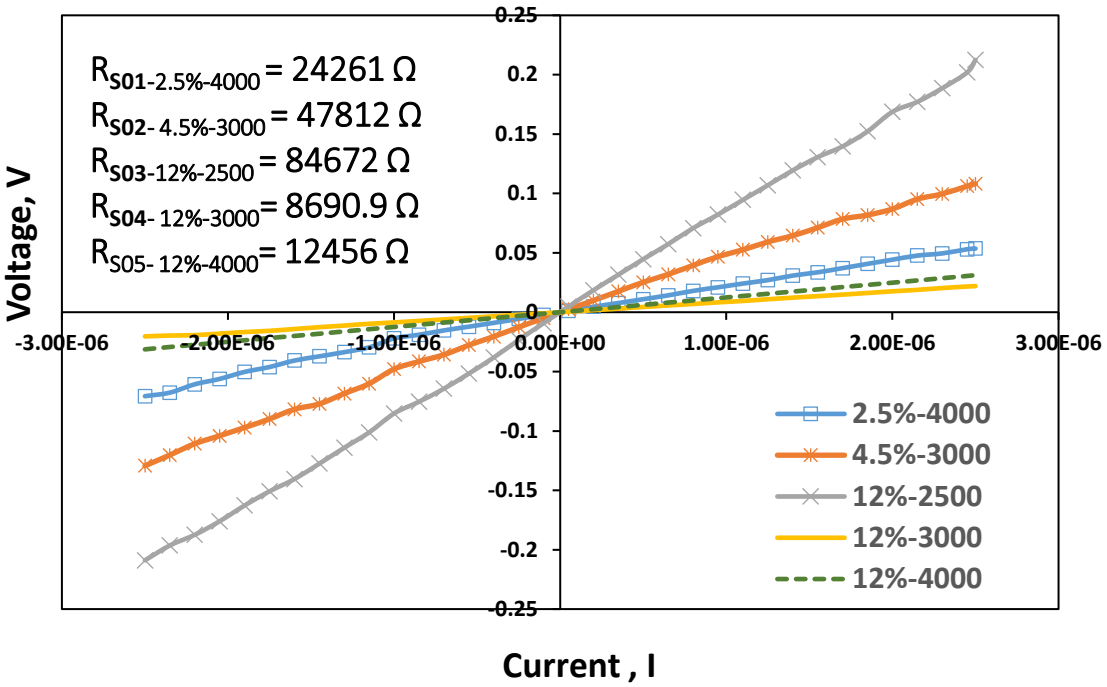

Figure 77. Hall effect measurement of S01, S02, S03, S04 and S05.

4.3 Effect of the hydrophilicity of SiO_2/Si substrate

A lot of work has been done by many researchers to study the effect of the substrate hydrophilicity on the graphene properties during the transfer process. Qine et al. [73] has studied the effect of substrate on the chemical reactivity of graphene. SiO_2 and Al_2O_3 have been used to investigate the effect of different substrates. They concluded that the type of substrate indeed affects chemical reactivity of graphene. K. Nagashio et al. [74] explain that although obtaining a hydrophilic surface of SiO_2/Si yielded a relatively large area of graphene layer, adhesion between the target substrate and graphene was too strong bonding which lessened the graphene mobility. Even though a large area of graphene was obtained using oxygen plasma treatment for SiO_2/Si substrate, the mobility was decreased. T. Yamahita et al. [132] also reported that graphene mobility was decreased due to the strong interaction and adhesion between graphene layer and SiO_2/Si substrate.

In contrast, Hyun et al. [30] explained that reducing the surface tension using some volatile liquids, for example heptane, reduced wrinkles and improved the quality and uniformity of graphene. Yun et al.[70] mentioned that controlling the hydrophilicity of the SiO_2/Si substrate by introducing micron-scale hole array (MSHA) on the target substrate reduced the water contact angle, which means that the surface become hydrophilic. They concluded that enhancing the contact between the SiO_2/Si substrate and graphene improved the quality of transferred graphene.

On the basis of the above-mentioned studies and studies mentioned in **introduction,** the importance of studying the effect of surface hydrophilicity on the graphene quality and properties, electrical and optical, was recognized. In this regard, the following experimental approach was adopted: First, cutting the SiO_2/Si substrate into 1x1cm. Second, cleaning the SiO_2/Si substrate using acetone followed by Isopropanol, rinsing using DI water, then drying all samples using compressed nitrogen. Third, applying different treatment techniques mentioned in detail in **Experimental work** using hydrofluoric acid, oxygen plasma, piranha solution and Ammonia solution.

It is well known that wettability is directly influenced by the morphology of the surface, micro-structure and chemical composition. When HF is used for SiO_2/Si substrate surface treatment, it changes the substrate's morphology and chemical composition, as indicated in the schematic in Figure 78. Hydrocarbon and hydroxyl groups are introduced to the surface, which makes it hydrophilic. In O_2 plasma treatment, removing of the water results in an interaction between OH and graphene, which leads to strong adhesion.

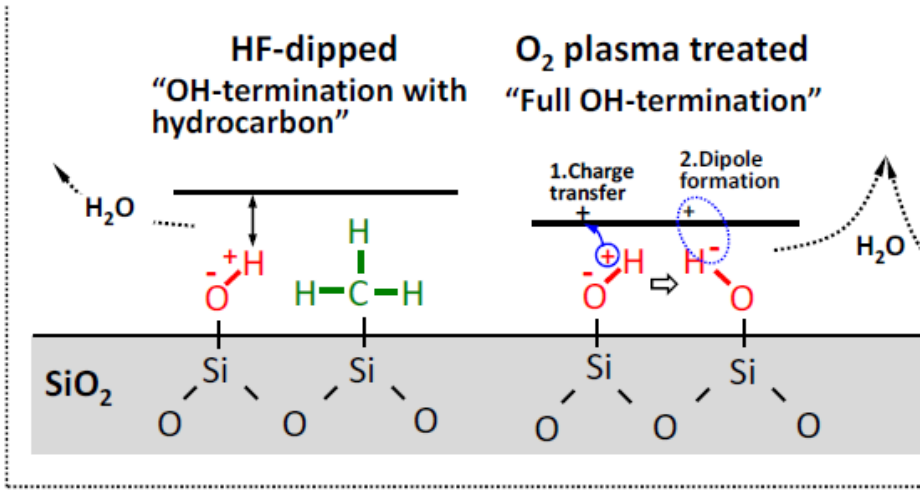

Figure 78. A model for a possible interaction model between graphene layer and SiO_2/Si substrate for HF and Oxygen plasma treatments [74].

Figure 79 shows the average water contact angle plotted for the various surface treatments. By comparing of the all samples, it can be seen that HF-80sec treatment gives the lowest average contact angle of ~ 3°. Piranha 15 min also gives a relatively average small angle among piranha solution treatment samples of ~ 44°. Plasma 10 min treatment also gives also a small angle among plasma treatment samples of ~ 15°.The ammonia solution sample gives an average water contact angle of ~ 12°. This indicates that the hydrophilic nature of the SiO_2/Si substrates is enhanced by different treatments processes. Therefore, these sample substrates have been selected for the graphene transfer process. In order to make a thorough comparison, another transfer process was carried out on a sample that was cleaned only, and it gives an average water contact angle of ~ 87°. All these treatments change the hydrophobic nature of the substrate surface to a hydrophilic surface, which results in a uniform distribution of the intermediate water layer between SiO_2/Si and PMMA/Graphene stack, during transfer, so that good adhesion can be achieved.

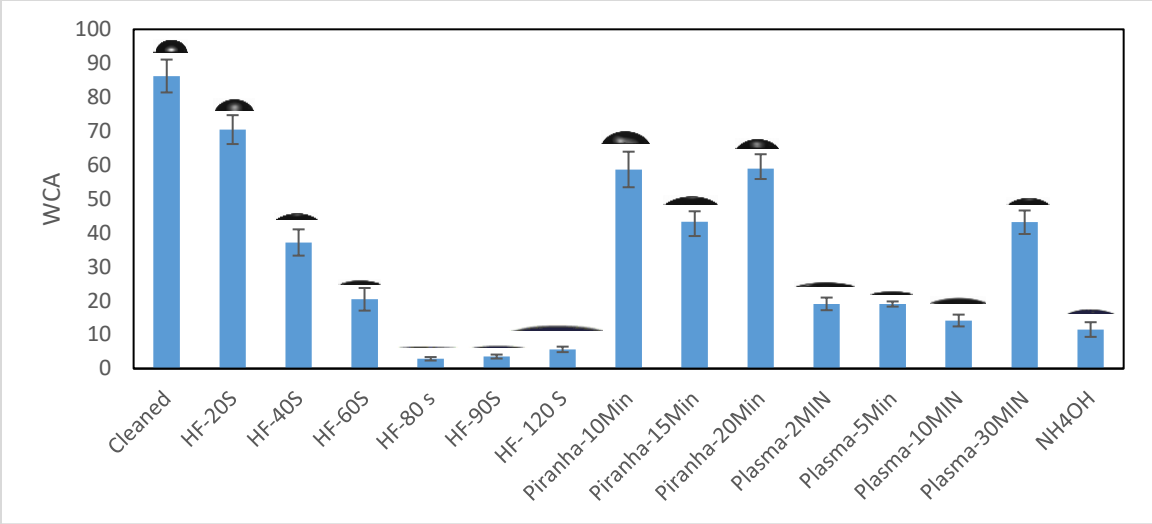

Figure 79. WCA measurement of SiO_2/Si bare and treated samples (HF, Piranha, plasma, and NH_4OH).

AFM images showing the effect of cleaning and surface treatment using HF, Piranha, plasma, and ammonia solution on the SiO_2/Si substrate are shown in **Figure 80.** It can be noticed form **Figure 80 (a, b and c)** that etching the substrate surface with Piranha solution affects the surface roughness. Piranha solution is a mixture of sulfuric acid (H_2SO_4) and hydrogen peroxide (H_2O_2), used to clean organic residues off substrates. Because the mixture is a strong oxidizer, it will remove most organic matter and also hydroxylate (add OH groups) most surfaces, making them extremely hydrophilic (water compatible) [133]. Using Piranha solution made the surfaces of SiO_2/Si substrates to be hydrophilic. Using Piranha solution to etch the substrate surface somewhat affects its roughness. As it shown in **Figure 80 (b and c)**, this process decreased surface roughness, which in turn, together with the added OH functional groups, decreased water contact angle. WCA measurement confirmed this result. On the other hand, increasing the Piranha solution treatment time to 20 min increased the etching effect. Surface roughness increased for samples treated with Piranha for 20 min, which increased water contact angle to about ~ 60^o. **Figure 80 (e)**

shows the AFM image of SiO_2/Si substrate treated with NH_4OH**.** This hydrophilization treatment removed adsorbed contaminants and built up an additional silanol group (Si–O–H) that made the surface more hydrophilic [130]. NH_4OH treatment affected the surface roughness, it slightly decreased the surface roughness to ~380 pm. It also dramatically decreased the WCA to ~ 12^o**. Figure 80 (f, g, h, i, j, and k)** shows the effect of cleaning and treatment of SiO_2/Si substrates using HF. **Figure 80 (f, g, h, I, j, and k)** clearly show how HF etching/treatment affected the substrate surface roughness. The HF removes the native oxide (which is hydrophilic), which leaves Si with some Si-F bonds. Very quickly the native oxide is formed again. The fresh oxide needs time to form Si-H bonds, after which the oxide surface becomes hydrophilic again. Fresh oxides (e.g. PECVD oxide) also show hydrophobic behavior as soon as they come out of the reactor. It takes some time in ambient air or a water rinse for the oxide to become hydrophilic, as the proposed conversions mechanism of treatment using HF [134], as shown in **Figure 80**. It can be observed form AFM images of HF for 20 sec. reduced its surface roughness directly from ~ 402 pm to ~ 334 pm. However, when HF treatment time was increased to 40 sec, surface roughness increased to ~ 713 pm. After that surface roughness started to decrease again as HF etching time increased to 60 and 80 sec. Surface roughness reached ~ 393 pm when HF etching treatment time increased to 80 sec, and this yielded the lowest water contact angle, ~ 3^o. It increases again until it reached ~ 685 pm. Water contact angle also slightly increased to ~ 5^o when HF treatment time increased to 120 sec. **Figure 80 (l, m, n, and o)** shows the AFM images of oxygen-plasma treated samples. Oxygen-plasma treatment improves the hydrophilicity of the SiO_2/Si substrates surface by increasing the OH group and removing hydrocarbon contamination on the samples, as shown in **Figure 80.** AFM

images show a remarkable decrease in surface roughness, from ~ 402 pm to ~ 230 pm, after using oxygen-plasma for 2 min. After 5 min oxygen-plasma treatment, roughness increased slightly to ~ 250 pm. It is noticed that using oxygen-plasma for 10 min produced the smoothest surface, ~ 188 pm, which resulted in the lowest WCA of ~ 15^{o}. In contrast using oxygen-plasma for a longer time (30 min) increased surface roughness to ~ 379 pm, resulted in a WCA of ~ 43^{o}.

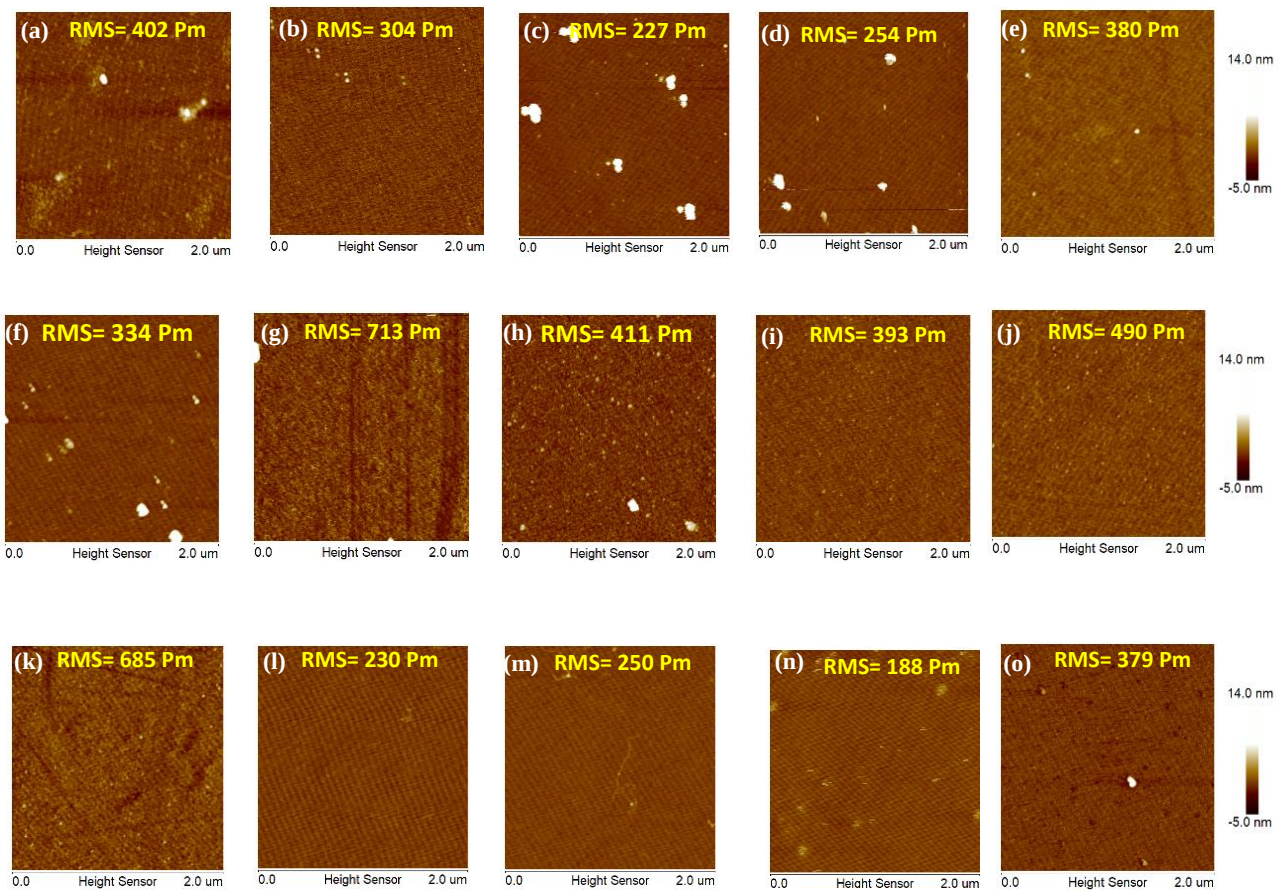

Figure 80. AFM Images of SiO_2/Si(a) bare sample, (b, c, and d) treated with piranha solution for 10, 15 and 20 min respectively, (e) treated with NH_4OH, (f, g, h, i, j, and k) treated with HF for 20, 40, 60, 80, 90 and 120 sec respectively (l, m, n, and o) treated with oxygen plasma for 2 ,5, 10 and 30 min respectively.

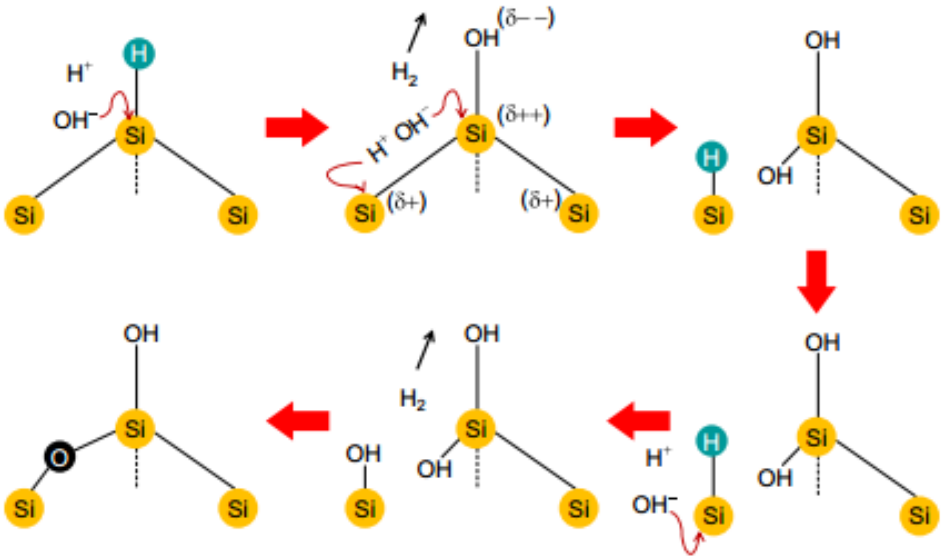

Figure 81. the proposed conversions mechanism of treatment using HF [134].

The chosen samples were graphene transferred onto bare sample, Piranha 15-min, HF 80 sec, Plasma 10-min and NH_4OH. Optical images of graphene transferred on selected substrates show the difference and effect of the surface hydrophilicity on the formation of wrinkles, as shown in **Figure 82**. For all samples except the bare sample, the substrate with a low contact angle has lower cracks and wrinkles, which means that a more hydrophilic surface enhances graphene's adhesion and quality (i.e. less cracks and wrinkles). From **Figure 82 (a)** it can be seen that there are a lot of wrinkles and cracks on graphene.

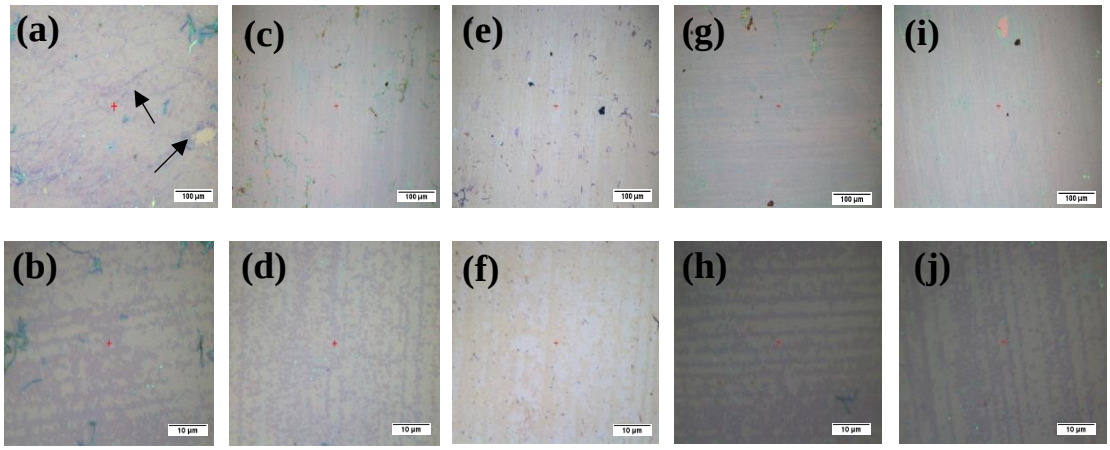

Figure 82. Optical microscopy images, low (10 X) and high magnification (100 X) of (a, b) bare sample, (c, d) HF 80-sec, (e, f) NH_4OH, (g, h) Plasma 10- min, and (i, j) Piranha 15-min.

To further characterize the graphene quality, Raman spectroscopy was performed and represented in **Figure 83** for each substrate (Bare, HF-80sec, Plasma 10-min, NH_4OH, and piranha 15- min each). Raman maps were carried out for 10x10 μm with a total area of 100 μm^2 for each sample. It is noticed from Raman maps contour of I_D/I_G, which evaluate the quality of transferred graphene layers, that the graphene layer is uniformly distributed, as shown in **Figure 83 (a c, e, g, and i). The** small red areas represent higher I_D/I_G ratio. These defects are higher than those blue areas. It is obvious that most of the graphene layer has an I_D/I_G ratio of less than 0.15. The I_D/I_G histogram plots in **Figure 84 (a)** clearly show that the I_D/I_G maintains almost the same low I_D/I_G ratio / value all over the samples. Average value of I_D/I_G was calculated for 100 spectra and showed that the quality of graphene transferred onto SiO_2/Si substrate is very similar to the quality of as- grown graphene on copper. Average value of I_D/I_G was less than 0.15 for all samples, which means a low defect intensity for as-grown graphene and as-transferred graphene. To conclude that enhanced the hydrophilicity of the SiO_2/Si substrate and adhesion between graphene and SiO_2/Si substrate does not influence the quality of the graphene layer in terms of I_D/I_G ratio.

The I_{2D}/I_G contour maps estimate the number of graphene layers, as shown in **Figure 83 (b, d, f, h, and j)**. It is obvious that all images of as-transferred graphene onto SiO_2/Si substrate glass are dominated by a brighter color (green color). This color represents I_{2D}/I_G spectra of < 1.8, which indicates an area of bi-layer and few-layer graphene, with a small percentage of monolayer graphene as represented by red color for both as-grown and as-transferred graphene. The histogram plot in **Figure 84 (b** shows that the intensity ratio of I_{2D}/I_G ranges from 0.2 to 2.5, which indicates an area of few-layer and bi-layer, in addition to a small percentage of monolayer graphene. The I_{2D}/I_G histogram plot shows that all samples have the same graphene distribution in terms of the number of layers for as-grown and as-transferred graphene. From I_D/I_G histogram and contour plots**,** reducing water contact angle of SiO_2/Si substrate does not affect on the quality of graphene in terms of physical properties.

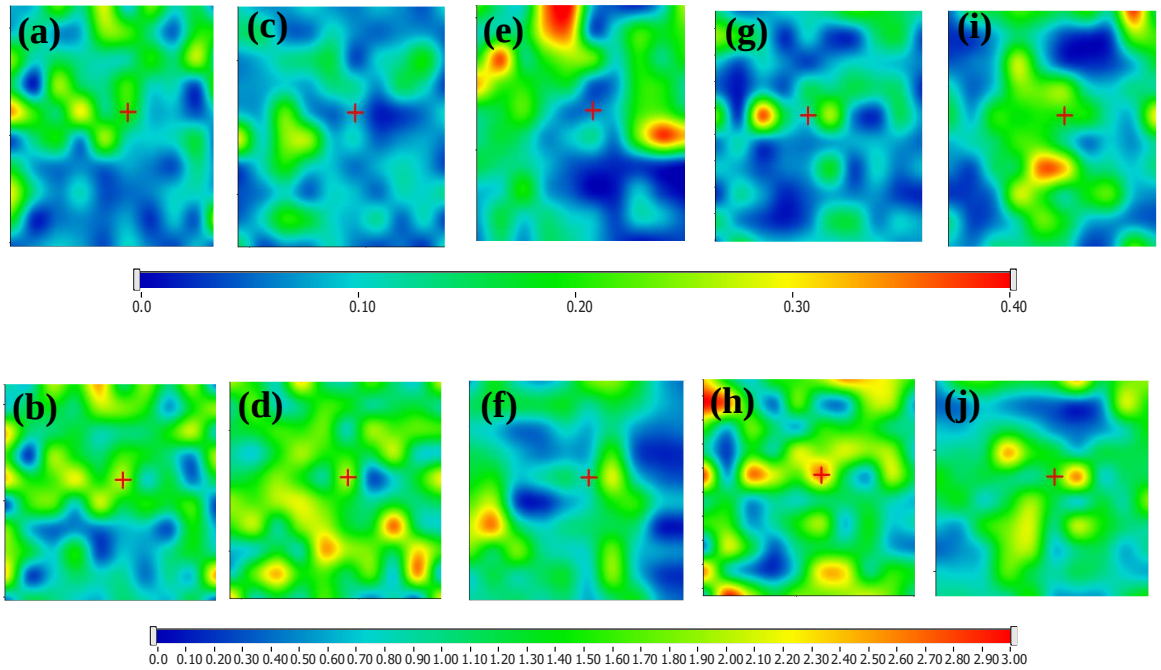

Figure 83. Raman mapping images of I_D/I_G and I_{2D}/I_G ratio of (a, b) bare sample, (c, d) HF 80-sec, (e, f) NH_4OH, (g, h) Plasma 10- min, and (i, j) Piranha 15-min.

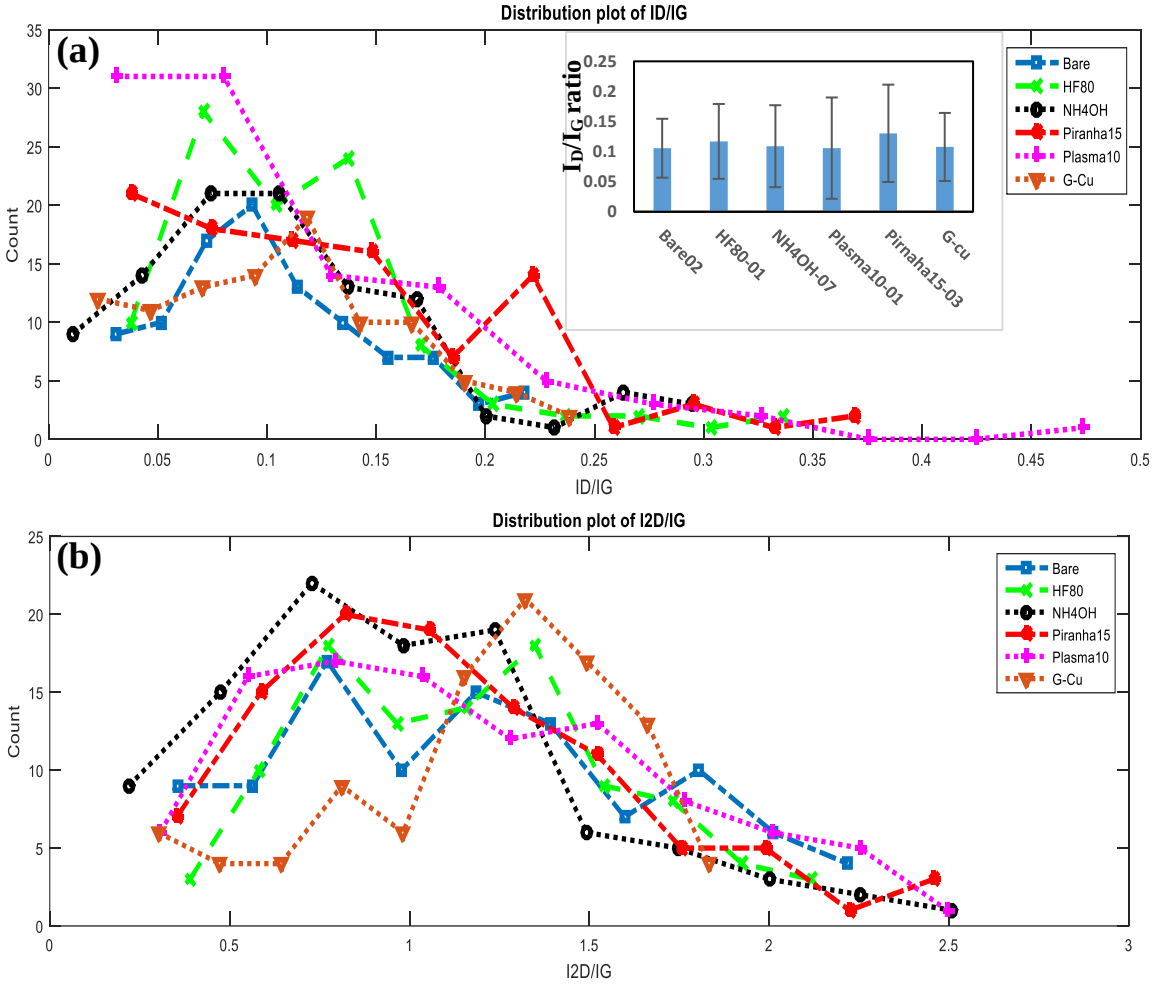

Figure 84. (a) histogram plot of I_D/I_G, inside plot of the average values of I_D/I_G and (e) histogram plot of I_{2D}/I_G for bare sample, HF-80 sec, NH_4ON, piranha-15 min, plasma-10 min and as-grown graphene on copper substrate.

The absorption of light, UV-visible measurement, was performed and plotted, as shown in **Figure 85**. Absorbance (represented by the vertical axis) measures the amount of light absorbed. The higher the value, the more a particular wavelength is being absorbed. All samples have highest peak of light intensity absorption at wavelength of ~ 680 nm, in addition to two main absorption peaks of ~ 446 and ~ 345 nm. On the other hand, samples treated with HF for 80 sec. and Piranha for 15 min have relatively lower light absorption than other samples at wavelength of ~424 and ~207 nm. This definitely confirms that enhancing the adhesion between as-transferred graphene layer and treated SiO_2/Si substrate

using piranha and HF-80 sec decrease the light absorption and enhance the transparency of graphene layer.

Electrical conductivity was measured for previous samples by using Hall effect method to correlate the conductivity to the resistance of as-transferred graphene layer. **Figure 86** shows the current-volt plots of the as-transferred graphene layer onto treated SiO_2/Si samples. It is seen that the treated samples showed significantly lower resistance than that of the bare sample. Treatment of SiO_2/Si using different treatment methods led to an increase in the electrical conductivity of as-transferred graphene layer, since 10-min plasma treatment decreased the as-transferred graphene layer resistance from 13525 Ω to about 7892 Ω, as depicted in **Figure 86 .**

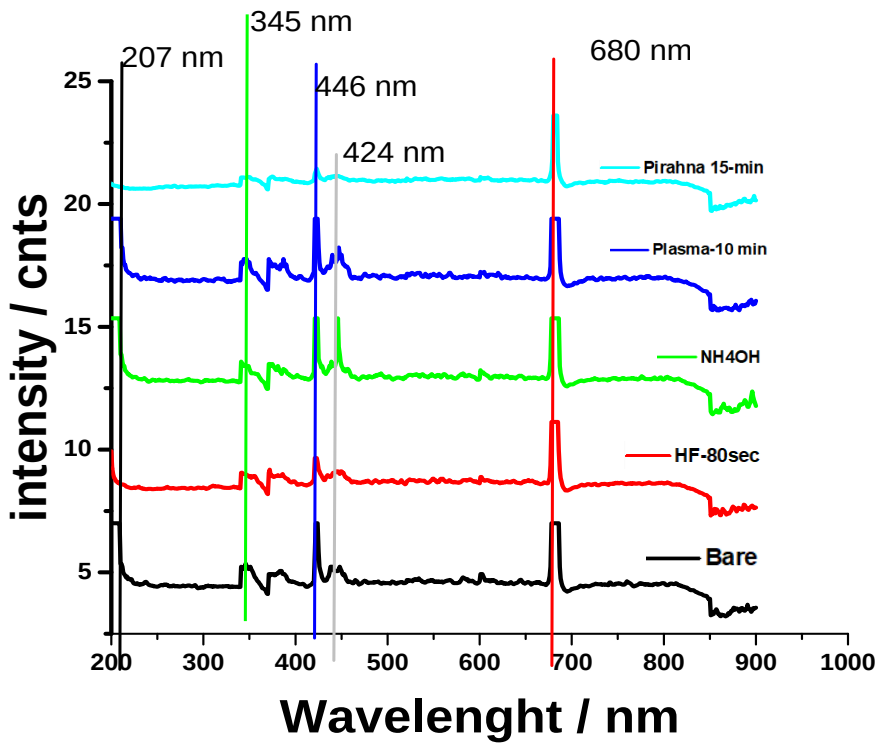

Figure 85. UV-Visible of bare, HF-80 sec, NH_4OH, Plasma- 10 min and piranha-15 min.

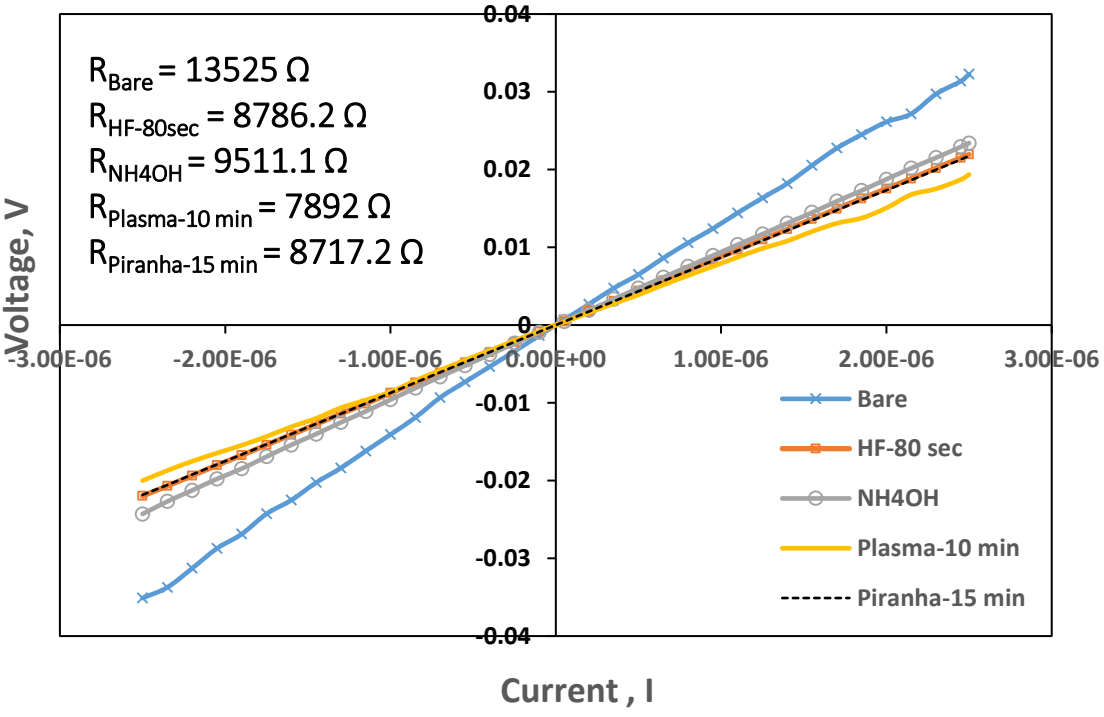

Figure 86. Hall effect measurement of bare, HF-80 sec, NH_4OH, Plasma- 10 min and piranha-15 min.

Table 15and **Table 16** show the optimized parameters of graphene transfer onto SiO_2/Si substrate for electrical and optical properties respectively.

Table 15. optimized graphene transfer parameters for electrical properties.

Optimized graphene transfer parameters for electrical properties	
Copper etching	APS for 4 h.
PMMA deposition parameters	Using PMMA concertation of 12%, at 3000 rpm.
PMMA dissolving parameters	For dissolving PMMA layer using Acetone at room temperature for 60 min.
SiO2/Si substrate treatment	Using Piranha for 15 min or HF for 80 sec.

Table 16. optimized graphene transfer parameters for optical properties.

Optimized graphene transfer parameters for optical properties	
Copper etching	APS for 4 h.
PMMA deposition parameters	Using PMMA concertation of 12%, at 3000 rpm.
PMMA dissolving parameters	For dissolving PMMA layer using Acetone at room temperature for 60 min.
SiO2/Si substrate treatment	Using plasma treatment for 10 min.

4.4 Enhanced electrical and optical properties of zinc oxide using graphene layer for solar cell application

In recent years, zinc oxide (ZnO) has attracted a great deal of attention in the field of nanodevices as an important semiconductor. This is due to its unique optical, structural and electronic properties. It is especially significant as a semiconductor because of its wide band gap (3.37 eV), large excitation binding energy (60 meV) excellent transparency (>90 %), high electron mobility (100 cm^2/Vs), good photoconductivity, etc. [135]–[138]. ZnO has been a promising material in the development of exciton-based optoelectronic devices,

such as a light emitting diode and photovoltaic cells, because of its band gap and binding energy that facilitate to collect carrier effectively [139]. Its properties have been studied since the early days of semiconductor electronics, but the use of ZnO as transparent conducting oxide (TCO) in optoelectronic devices has been hindered because of low carrier transport characteristics. On the other hand, graphene, single layer graphite with closely packed hexagonal lattice, has received a wide attention due to its unique carrier transport properties [140]. It is an excellent electrical conductor and it has a high aspect ratio, which makes it a great material for use in optoelectronic application[141]. Considering a crucial challenge to improve the efficiency of solar cells by enhancing the way excitons are collected and transported, it would obviously infer to have a TCO of best carrier collection and transport capabilities. Therefore, a heterostructure of ZnO and graphene is expected to serve the purpose. It is indispensable to understand the inherent characteristics of ZnO-graphene heterostructures to be implemented as TCO in solar cell application.

Figure 87 shows AFM images of G/ZnO on glass displaying 2D and 3D images. The thickness of ZnO film is about 50 nm, and that of graphene is about 175 nm. **Figure 88** shows AFM images of sputtered ZnO on glass as well as graphene on ZnO film. AFM image showed that ZnO film was very smooth with maximum height of 5.6 nm and the surface roughness was about 6.25 nm as shown in **Figure 88a**. Using the free transfer method caused the graphene layer to fold on itself in some regions. Further 3D imaging confirmed maximum step height to be 20.7 nm with surface roughness to be about 30 nm, as shown in **Figure 88d**.

Raman scattering measurement was carried out to reconfirm the presence of the ZnO layer as well as proper transfer of Graphene on as-fabricated ZnO. ZnO transverse optical mode

A1(TO) at 425 cm^{-1} and longitudinal optical mode A1(LO) at 591 cm^{-1} was observed, as shown in **Figure 89a**.[142]. The inset corresponds to the optical image captured simultaneously in the Raman measurement system. The Raman characterization of graphene on ZnO\glass confirmed the characteristic peaks to be around 1355, 1585, and 2700 cm^{-1}, corresponding to the D, G, and 2D peaks respectively, as shown in **Figure 89b** [143].

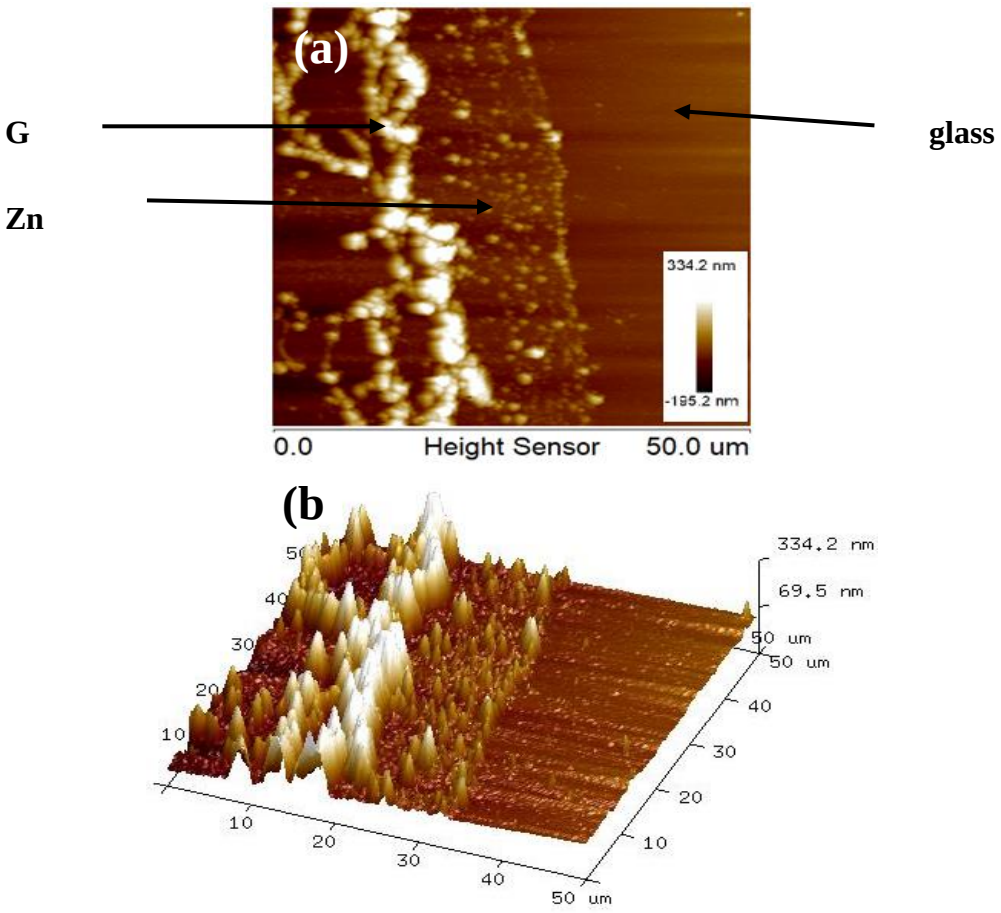

Figure 87. AFM spectroscopy of G/ZnO on glass substrate (a) 2D image (b) 3D image.

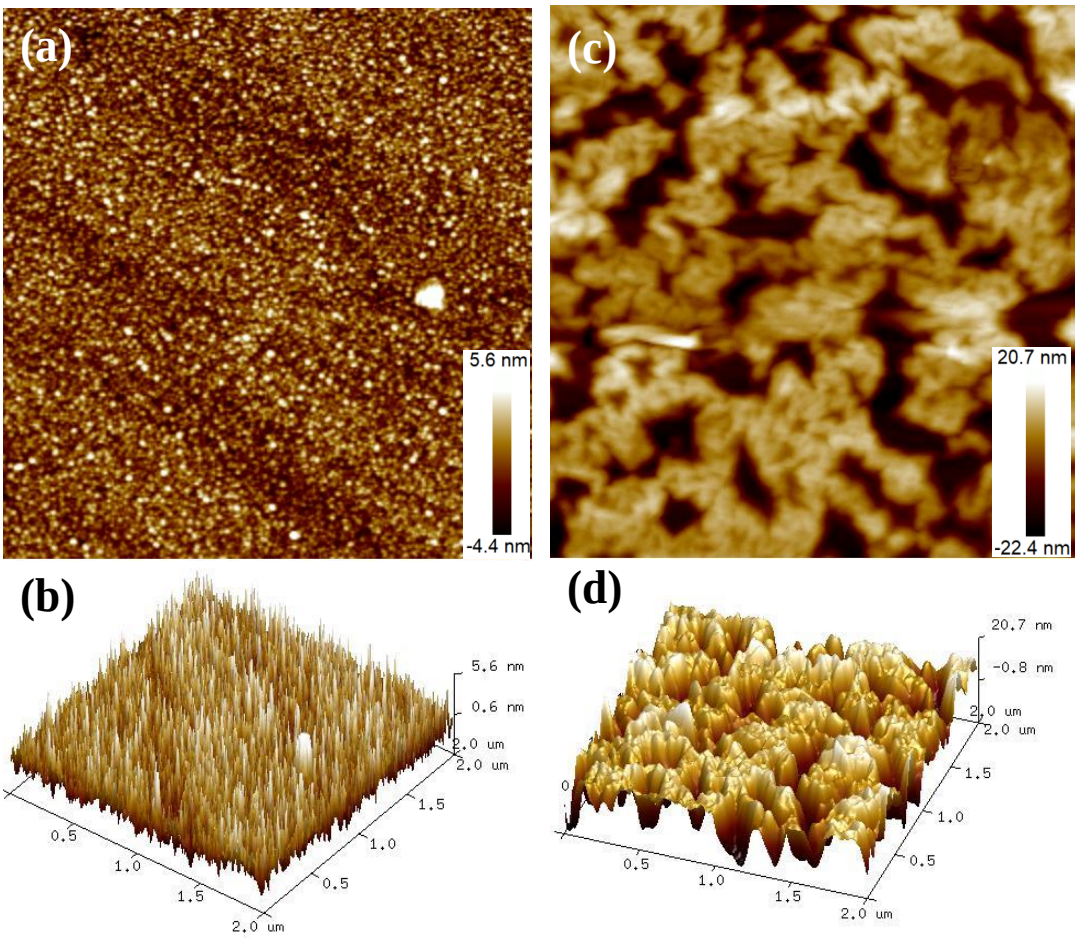

Figure 88. AFM spectroscopy of (a)-(b) ZnO and (c)-(d) G/ ZnO film.

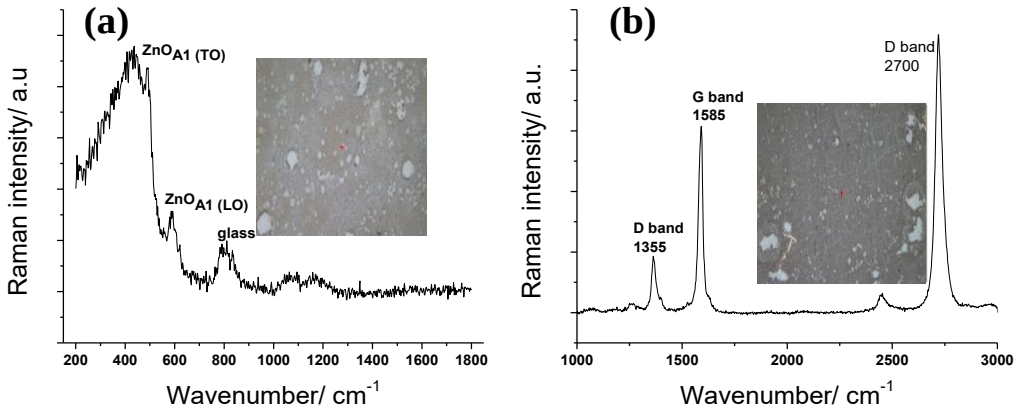

Figure 89. Raman scattering measurements of (a) ZnO\glass, inset: optical microscope image, and (b) graphene\ZnO\ glass, inset: optical microscope image.

From the Raman spectra, a great deal of details on the fine structure of graphene or graphite can be extracted. A typical Raman spectrum for graphene consists of two main bands and a few more very small bands. These bands are used to discern the quality, the defects, number of layers and the doping in graphene layers [96][97], and to give better vision into as-transferred graphene onto ZnO and glass. Raman mapping of the graphene/glass and graphene/ZnO/glass was carried out in order to evaluate the quality and the average number of layers of the as-transferred graphene layers onto ZnO and glass, as shown in **Figure 90**. The mapping measurements were conducted for all samples by investigated an area of 10x10 μm, a total of 100 μm^2 Raman spectra were collected and analyzed.

The contour maps of I_D/I_G evaluate the quality of transferred graphene layers as shown in **Figure 90 (a and b)**, which showed clearly uniform distribution of the graphene layer. The small red areas represent higher I_D/I_G ratio; the defects are higher than blue areas. It is obvious that most of the graphene layer has an I_D/I_G ratio of less than 0.2. The I_D/I_G histogram plots shown in **Figure 90 e**. clearly show that the I_D/I_G maintains almost the same value all over the samples and low value of I_D/I_G ratio. Average value of I_D/I_G was calculated for 100 spectra, and it showed that the quality of graphene transferred onto ZnO is very similar to the quality of graphene which was transferred on glass. Average value of I_D/I_G was 0.18 and 0.176 for graphene/glass and graphene/ZnO/glass, respectively.

The I_{2D}/I_G contour maps estimate the number of graphene layers, as shown in **Figure 90 (c and d)**. It is obvious that both images of graphene/glass and graphene/ZnO/glass are dominated by a brighter color (green color). This color represents I_{2D}/I_G spectra of < 1.8, which indicates an area of multilayer graphene. The histogram plot in **Figure 90 f**, shows that the intensity ratio of I_{2D}/I_G ranged from 0.2 to 1.8, which indicates an area of multilayer

and bilayer graphene. These results confirm that using the free transfer method caused the formation of folds and multilayer graphene.

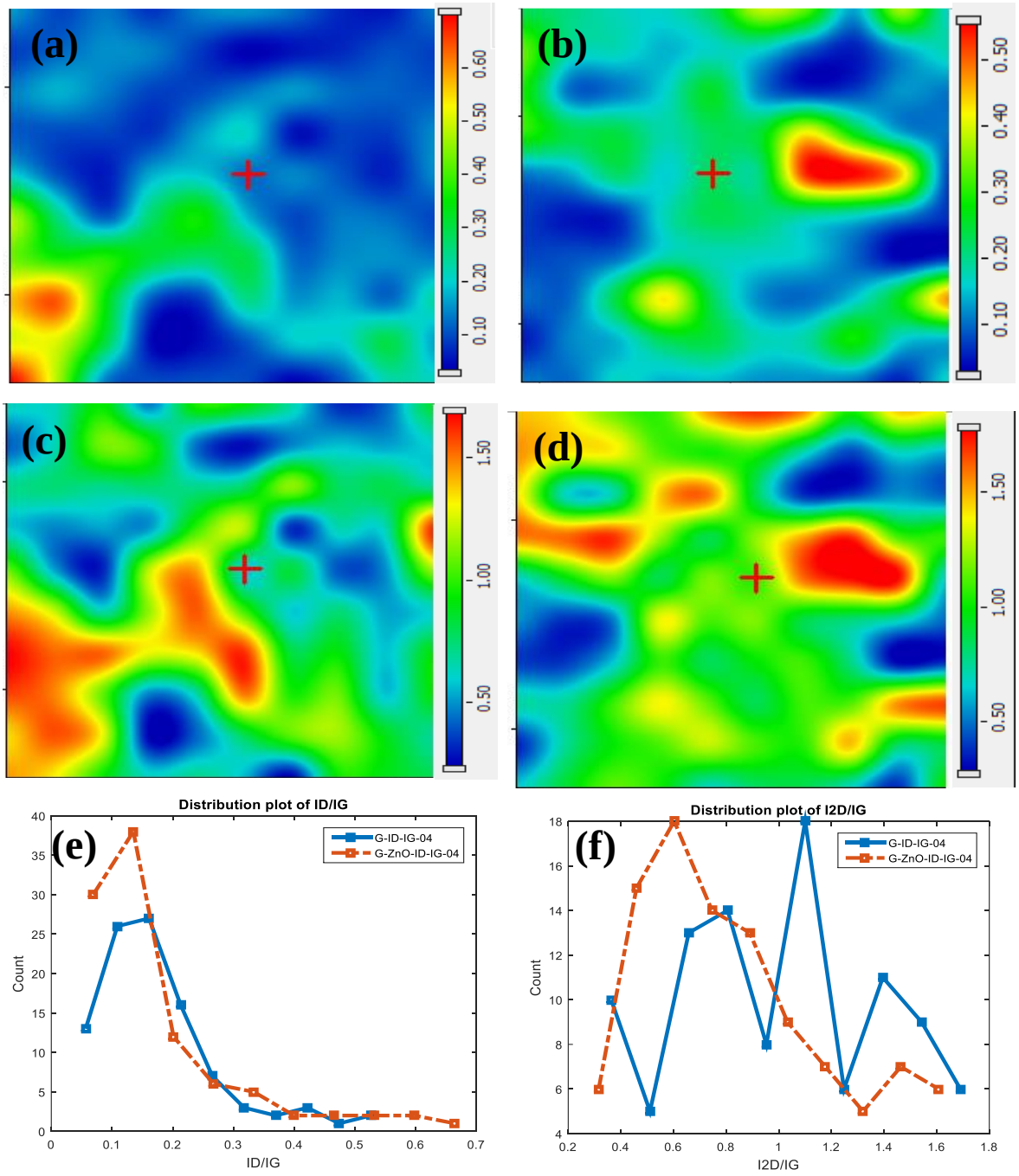

Figure 90. Raman mapping (a, b) I_D/I_G ratio (c, d) I_{2D}/I_G ratio, (e) histogram plot of ID/IG and (f) histogram plot of I2D/IG for G and G/ZnO. Pera5889515

Graphene layer could be used as a transparent electrode in photovoltaic cells, as it is

transparent material and only absorbs about 3 % of visible light [144]. As shown in **Figure 91** the absorption of light, UV-visible measurement was performed, Absorbance (represented by the vertical axis) measures the amount of light absorbed. The higher the value, the more a particular wavelength is being absorbed. Graphene layer has low absorption of light about 0.05 at wavelength of 268 nm. On the other hand, the ZnO film has a relatively high light absorption, about 0.36 at wavelength of 205 nm. The Hybrid structure of G/ZnO has a medium absorption level that lies in between graphene layer and zinc oxide film about 0.21 at wavelength of 205 nm. The absorption of light for ZnO film was decreased from 0.36 to 0.21 after transferring graphene onto the ZnO/glass. This definitely confirms that graphene/ZnO/glass light transparency was enhanced compared to ZnO/glass only.

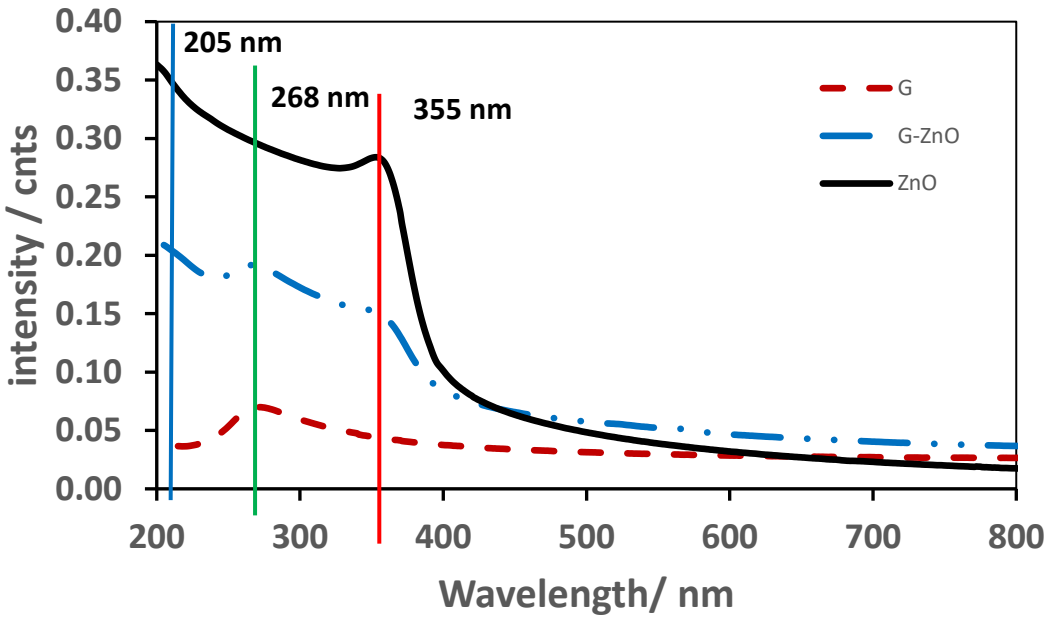

Figure 91. UV-Visible of G, ZnO, and G/ZnO.

Electrical conductivity was measured for previous samples by using Hall effect method to correlate the conductivity to the resistance of the prepared thin films. **Figure 92 (a and b)**

shows the current-volt plots of ZnO/glass, graphene/glass and graphene/ZnO/glass. It is seen that ZnO/glass sample exhibited a fluctuation behavior with average resistance value of 3.349 $\times 10^6$ Ω. However, graphene/glass showed significantly small resistance value ~ 0.317$\times$ 10^5 Ω as compared to ZnO/glass sample. Adding graphene layer onto ZnO/glass led to an increase of the electrical conductivity of ZnO/glass sample, since its resistance was decreased from 3.349 $\times 10^6$ Ω to 2.758 $\times$ 10^5 Ω as depicted in **Figure 92 6b**

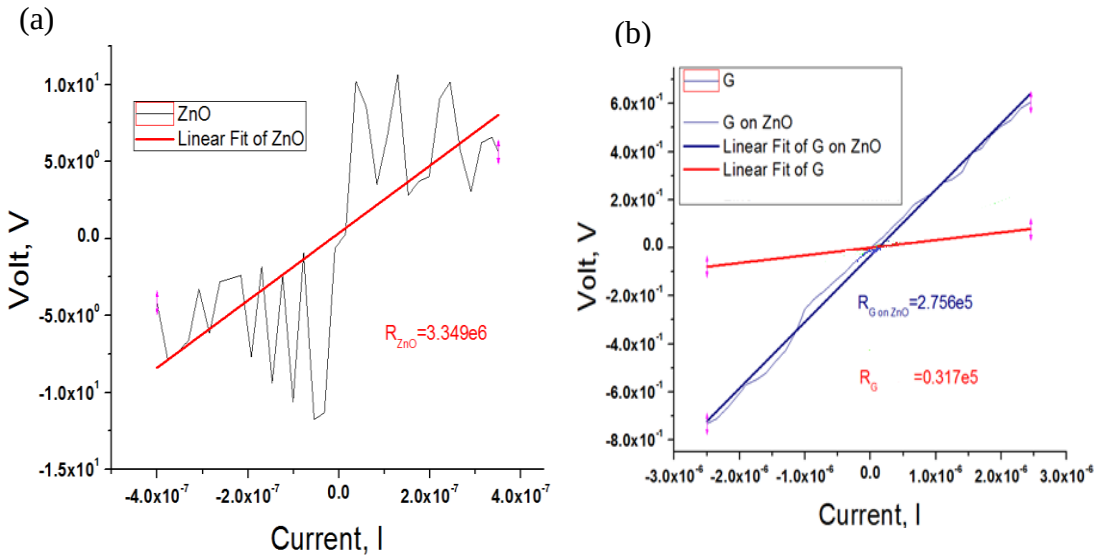

Figure 92. Hall effect measurement (a) ZnO (b) G, and G/ZnO on glass.

In conclusion, an ultrathin layer of ZnO was sputtered on a glass substrate yielding a thickness of 50 nm as measured by AFM with a surface roughness of 6.25 nm. Absorption was measured to be 0.36. Resistance of ZnO was calculated from IV curve to be equal 3.349 ×106 Ω. After the transfer of CVD-developed graphene layer on the surface of ZnO which it had a thickness of 175 nm with surface roughness of about 30 nm as measured by AFM. The value of the G/ZnO hybrid structure light absorption was 0.21 and resistance of 2.758 × 105 Ω. It is noticed that a substantial enhancement in transport properties for such

heterostructure was obtained. Such G/ZnO heterostructure would be a good candidate as TCO for solar cell application.

CHAPTER 5
CONCLUSIONS AND RECOMMENDATIONS

5.1 Conclusions

In conclusion, our results reveal that metallic and polymeric residuals, and surface hydrophilicity of the substrate play a crucial role on the as-transferred graphene quality and properties in terms of electrical resistance and optical transparency.

Our copper etching study investigate the effect of different copper etchants (APS, $FeCl_3$, and $Fe(NO_3)_3$ used for different time (2, 4, and 8h). It was concluded that etching with APS for 4 hours produces the best graphene layer quality in terms of physical, optical and electrical conductivity. In addition, it decreases the number of defects, as confirmed from XPS and Raman results. APS-4h had the lowest electrical resistance, of ~ 10115 Ω compared with other copper etchants.

Using the design of experiments analysis, our PMMA graphene transfer study demonstrate that using a 12% PMMA, 3000 rpm, room temperature, for one hour in acetone to dissolve the PMMA, shows the best optical properties with low light absorption. This confirms that, after removing the supportive layer, decreasing the amount of PMMA residues yields improved quality of graphene in terms of I_D/I_G ratio. It gives the smallest I_D/I_G ratio, about 0.13, and an insignificant amount of PMMA residues with area fraction of about 6.5 %. In addition, using the above parameters, a very small electrical resistance of ~ 8,691 Ω is obtained. In contrast, using 12% PMMA, 2500 rpm, room temperature, for 20 min in

acetone yields the highest percentage of PMMA residues and a relatively high I_D/I_G ratio of about 0.32 giving the highest electrical resistance of 84,672 Ω.

In addition, we have investigated the influence of SiO_2/Si hydrophilicity on the as-transferred graphene quality and properties, using various substrate cleaning and different surface treatment methods. The substrates with the lowest water contact angle are selected for the transfer process. Graphene, grown by chemical vapor deposition, is transferred onto SiO_2/Si substrate using the wet transfer process with PMMA as a supporting layer. It is found that graphene layer adheres well to the more hydrophilic surface with contact angle of about ~3 degree using HF treatment for 80 sec, which results in minimum number of wrinkles and cracks on graphene layer. In addition, it exhibits a low electrical resistance of 7,892 Ω using plasma treatment for 10 min and a low UV- light absorption for samples treated by Piranha for 15 min and HF for 80 sec. Therefore, it can be concluded that hydrophilicity of the substrate surface plays a direct role on the transfer process and the quality of transferred graphene layer.

An ultrathin film of ZnO is sputtered on a glass substrate yielding a thickness of 50 nm as measured by AFM with a surface roughness of about 6 nm. For such a film, the light absorption is measured to be 0.36, while the electrical resistance is calculated from IV curve to be equal to 3.349×10^6 Ω. Then, a graphene layer is transferred on the surface of the ZnO film, with a thickness of 175 nm and surface roughness of about 30 nm. The measured value of light absorption for the G/ZnO hybrid structure is 0.21 and a calculated electrical resistance of 2.758×10^5 Ω, which are much lower than that of ZnO film.

It is noticed that a substantial enhancement in transport properties for such heterostructure is obtained. It is concluded that such G/ZnO heterostructure would be a good candidate as

a transparent conductive oxide (TCO) for solar cell application.

5.2 Recommendations for future work

Based on the above in-depth study towards the wet-transfer method of graphene using PMMA, the following recommendations are made for future work.

- A separate study on metallic residuals should be conducted to compare different copper etchants using time-of-flight secondary ion mass spectroscopy and total reflection x-ray fluorescence to obtain elemental fingerprints of metallic residuals with sensitivity of 10^9 atoms/cm^2, and also to correlate the number of atoms of copper residuals and graphene quality.
- Other parameters for PMMA transfer method (such as number of PMMA layers, concentration of each layer, baking time and temperature) should be included in the design of experiment method to further enhance the process of PMMA residuals removal.
- Graphene should be transferred to different substrates with different hydrophilicity levels in order to investigate their effect on graphene quality and properties.
- The effect of zinc oxide deposition parameters on the graphene quality and properties should be investigated.

References

[1] M. Macucci, A. Betti, and P. Marconcini, “Graphene as a material for nanoelectronics,” *Adv. Mater. Sci.*, vol. 15, no. 4, p. 67, 2015.

[2] M. S. Ashutosh Tiwari, *Graphene Materials Fundamentals and Emerging Applications*. Wiley-Scrivener, 2015.

[3] Z. (Chemist) Liu and X. Zhou, *Graphene : energy storage and conversion applications*. CRC.

[4] K. S. Novoselov *et al.*, “Two-dimensional gas of massless Dirac fermions in graphene,” *Nature*, vol. 438, no. 7065, pp. 197–200, Nov. 2005.

[5] K. S. Novoselov *et al.*, “Electric Field Effect in Atomically Thin Carbon Films,” *Science (80-.).*, vol. 306, no. 5696, pp. 666–669, Oct. 2004.

[6] S. A. Kazmi, S. Hameed, A. S. Ahmed, M. Arshad, and A. Azam, “Electrical and optical properties of graphene-TiO2 nanocomposite and its applications in dye sensitized solar cells (DSSC),” *J. Alloys Compd.*, vol. 691, pp. 659–665, 2017.

[7] T. Mahmoudi, Y. Wang, and Y.-B. Hahn, “Graphene and its derivatives for solar cells application,” *Nano Energy*, vol. 47, pp. 51–65, May 2018.

[8] J. L. G. Mahmood Aliofkhazraei , Nasar Ali William I. Milne , Cengiz S. Ozkan Stanislaw Mitura, *GRAPHENE SCIENCE HANDBOOK Nanostructure and Atomic Arrangement*. CRC Press, 2016.

[9] J. Chen, Z. Bo, and G. Lu, *Vertically-oriented graphene: PECVD synthesis and applications*. 2015.

[10] X. Wang, L. Zhi, and T. et Al., "Transparent Carbon Films as Electrodes in Organic Solar Cells," *Angew. Chemie Int. Ed.*, vol. 47, no. 16, pp. 2990–2992, Apr. 2008.

[11] L. I. N. E. T. Al, "ARTICLE A Direct and Polymer-Free Method for Transferring Graphene Grown by Chemical Vapor Deposition to Any," no. 2, pp. 1784–1791, 2014.

[12] F. Hao, D. Fang, and Z. Xu, "Mechanical and thermal transport properties of graphene with defects," *Appl. Phys. Lett.*, vol. 99, no. 4, p. 041901, Jul. 2011.

[13] E. P. (Ernest P. DeGarmo, J. T. Black, and R. A. Kohser, *Degarmo's materials and processes in manufacturing*. .

[14] Y. Song, W. Fang, R. Brenes, and J. Kong, "Challenges and opportunities for graphene as transparent conductors in optoelectronics," *Nano Today*, vol. 10, no. 6, pp. 681–700, 2015.

[15] Y.-M. Lin *et al.*, "Wafer-Scale Graphene Integrated Circuit," *Science (80-.).*, vol. 332, no. 6035, 2011.

[16] E. Quesnel *et al.*, "Graphene-based technologies for energy applications, challenges and perspectives," *2D Mater.*, vol. 2, no. 3, p. 030204, Aug. 2015.

[17] S.-H. Bae, Y. Lee, B. K. Sharma, H.-J. Lee, J.-H. Kim, and J.-H. Ahn, "Graphene-based transparent strain sensor," *Carbon N. Y.*, vol. 51, pp. 236–242, 2013.

[18] J. Park *et al.*, “Porous graphene-based membranes for water purification from metal ions at low differential pressures,” *Nanoscale*, vol. 8, no. 18, pp. 9563–9571, 2016.

[19] S. Stankovich *et al.*, “Graphene-based composite materials,” *Nature*, vol. 442, no. 7100, pp. 282–286, Jul. 2006.

[20] C. Chung, Y.-K. Kim, D. Shin, S.-R. Ryoo, B. H. Hong, and D.-H. Min, “Biomedical Applications of Graphene and Graphene Oxide,” *Acc. Chem. Res.*, vol. 46, no. 10, pp. 2211–2224, Oct. 2013.

[21] Y. Hernandez *et al.*, “High-yield production of graphene by liquid-phase exfoliation of graphite,” *Nat. Nanotechnol.*, vol. 3, no. 9, pp. 563–568, Sep. 2008.

[22] X. Li *et al.*, “Large-Area Synthesis of High-Quality and Uniform Graphene Films on Copper Foils,” *Science (80-.).*, vol. 324, no. 5932, pp. 1312–1314, Jun. 2009.

[23] X. Li, W. Cai, L. Colombo, and R. S. Ruoff, “Evolution of Graphene Growth on Ni and Cu by Carbon Isotope Labeling,” *Nano Lett.*, vol. 9, no. 12, pp. 4268–4272, Dec. 2009.

[24] Q. Yu, J. Lian, S. Siriponglert, H. Li, Y. P. Chen, and S.-S. Pei, “Graphene segregated on Ni surfaces and transferred to insulators,” *Appl. Phys. Lett.*, vol. 93, no. 11, p. 113103, Sep. 2008.

[25] T. Hallam, N. C. Berner, C. Yim, and G. S. Duesberg, “Strain, Bubbles, Dirt, and Folds: A Study of Graphene Polymer-Assisted Transfer,” *Adv. Mater. Interfaces*, vol. 1, no. 6, pp. 1–7, 2014.

[26] Y. Chen, X. L. Gong, and J. G. Gai, “Progress and Challenges in Transfer of Large-

Area Graphene Films," *Adv. Sci.*, vol. 3, no. 8, pp. 1–15, 2016.

[27] S. Bae *et al.*, "30 inch Roll-Based Production of High-Quality Graphene Films for Flexible Transparent Electrodes," vol. 5, no. June, pp. 1–5, 2009.

[28] D.-Y. Wang *et al.*, "Clean-Lifting Transfer of Large-area Residual-Free Graphene Films," *Adv. Mater.*, vol. 25, no. 32, pp. 4521–4526, Aug. 2013.

[29] C. W. Bay and H. Kong, "Use of Hydrophobic-Hydrophobic Interactions for Direct Graphene Transfer," pp. 1–17.

[30] H. H. Kim, S. K. Lee, S. G. Lee, E. Lee, and K. Cho, "Wetting-Assisted Crack- and Wrinkle-Free Transfer of Wafer-Scale Graphene onto Arbitrary Substrates over a Wide Range of Surface Energies," pp. 2070–2077, 2016.

[31] A. Ibrahim, "SYNTHESIS AND CHARACTERIZATION OF GRAPHENE FABRICATED BY CHEMICAL VAPOR DEPOSITION METHOD," KFUPM, 2015.

[32] L. A. David, "Synthesis of large-area few layer graphene films by rapid heating and cooling in a modified apcvd furnace," Thesis, Kansas State University, 2011.

[33] W. Regan *et al.*, "A direct transfer of layer-area graphene," *Appl. Phys. Lett.*, vol. 96, no. 11, p. 113102, Mar. 2010.

[34] E. Rollings *et al.*, "Synthesis and characterization of atomically thin graphite films on a silicon carbide substrate," *J. Phys. Chem. Solids*, vol. 67, no. 9–10, pp. 2172–2177, 2006.

[35] 2012. [Online]. Available: I. ENTEGRIS, "SuperSiC and http://www. entegris. com/Resources/assets/620.-6116-0412. pdf. [Accessed 1 11 2012], “No Title.”

[36] P. R. Somani, S. P. Somani, and M. Umeno, “Planer nano-graphenes from camphor by CVD,” *Chem. Phys. Lett.*, vol. 430, no. 1–3, pp. 56–59, 2006.

[37] F. Yang, Y. Liu, W. Wu, W. Chen, L. Gao, and J. Sun, “A facile method to observe graphene growth on copper foil,” *Nanotechnology*, vol. 23, no. 47, p. 475705, Nov. 2012.

[38] A. W. Robertson and J. H. Warner, “Hexagonal Single Crystal Domains of Few-Layer Graphene on Copper Foils,” *Nano Lett.*, vol. 11, no. 3, pp. 1182–1189, Mar. 2011.

[39] X. Li *et al.*, “Graphene Films with Large Domain Size by a Two-Step Chemical Vapor Deposition Process,” *Nano Lett.*, vol. 10, no. 11, pp. 4328–4334, Nov. 2010.

[40] J. Zhang *et al.*, “CVD growth of large area and uniform graphene on tilted copper foil for high performance flexible transparent conductive film,” *J. Mater. Chem.*, vol. 22, no. 35, pp. 18283–18290, Aug. 2012.

[41] A. Ibrahim, S. Akhtar, M. Atieh, R. Karnik, and T. Laoui, “Effects of annealing on copper substrate surface morphology and graphene growth by chemical vapor deposition,” *Carbon N. Y.*, vol. 94, pp. 369–377, 2015.

[42] A. Ibrahim, G. Nadhreen, S. Akhtar, F. M. Ka, and T. Laoui, “Study of the impact of chemical etching on Cu surface morphology , graphene growth and transfer on SiO 2 / Si substrate,” vol. 123, pp. 402–414, 2017.

[43] A. Reina *et al.*, “Large Area, Few-Layer Graphene Films on Arbitrary Substrates by Chemical Vapor Deposition,” *Nano Lett.*, vol. 9, no. 1, pp. 30–35, Jan. 2009.

[44] A. Reina *et al.*, “Large Area, Few-Layer Graphene Films on Arbitrary Substrates by Chemical Vapor Deposition,” *Nano Lett.*, vol. 9, no. 1, pp. 30–35, Jan. 2009.

[45] Y.-C. Lin, C. Jin, J.-C. Lee, S.-F. Jen, K. Suenaga, and P.-W. Chiu, “Clean Transfer of Graphene for Isolation and Suspension,” *ACS Nano*, vol. 5, no. 3, pp. 2362–2368, Mar. 2011.

[46] X. Li *et al.*, “Transfer of Large-Area Graphene Films for High-Performance Transparent Conductive Electrodes,” *Nano Lett.*, vol. 9, no. 12, pp. 4359–4363, Dec. 2009.

[47] W.-H. Lin *et al.*, “A Direct and Polymer-Free Method for Transferring Graphene Grown by Chemical Vapor Deposition to Any Substrate,” *ACS Nano*, vol. 8, no. 2, pp. 1784–1791, Feb. 2014.

[48] Y. Wang *et al.*, “Electrochemical Delamination of CVD-Grown Graphene Film: Toward the Recyclable Use of Copper Catalyst,” *ACS Nano*, vol. 5, no. 12, pp. 9927–9933, Dec. 2011.

[49] J. Ryu *et al.*, “Fast Synthesis of High-Performance Graphene Films by Hydrogen-Free Rapid Thermal Chemical Vapor Deposition,” *ACS Nano*, vol. 8, no. 1, pp. 950–956, Jan. 2014.

[50] X. Liang *et al.*, “Toward Clean and Crackless Transfer of Graphene,” no. 11, 2011.

[51] X. Li *et al.*, “Transfer of Large-Area Graphene Films for High-Performance

Transparent Conductive Electrodes," *Nano Lett.*, vol. 9, no. 12, pp. 4359–4363, Dec. 2009.

[52] J. W. Suk *et al.*, "Transfer of CVD-Grown Monolayer Graphene onto Arbitrary Substrates," *ACS Nano*, vol. 5, no. 9, pp. 6916–6924, Sep. 2011.

[53] W. Regan *et al.*, "A direct transfer of layer-area graphene," *Appl. Phys. Lett.*, vol. 96, no. 11, p. 113102, Mar. 2010.

[54] X. D. Chen *et al.*, "High-quality and efficient transfer of large-area graphene films onto different substrates," *Carbon N. Y.*, vol. 56, pp. 271–278, 2013.

[55] a. . Fallis, "Etch Rates for Micromachining Processing," *J. Chem. Inf. Model.*, vol. 53, no. 9, pp. 1689–1699, 2013.

[56] H. H. Kim, S. K. Lee, S. G. Lee, E. Lee, and K. Cho, "Wetting-Assisted Crack- and Wrinkle-Free Transfer of Wafer-Scale Graphene onto Arbitrary Substrates over a Wide Range of Surface Energies," *Adv. Funct. Mater.*, p. n/a-n/a, 2016.

[57] G. B. Barin, Y. Song, I. D. F. Gimenez, A. G. S. Filho, L. S. Barreto, and J. Kong, "Optimized graphene transfer: Influence of polymethylmethacrylate (PMMA) layer concentration and baking time on grapheme final performance," *Carbon N. Y.*, vol. 84, no. C, pp. 82–90, 2015.

[58] H. Li and C. Mazet, "Iridium-Catalyzed Selective Isomerization of Primary Allylic Alcohols," *Acc. Chem. Res.*, vol. 49, no. 6, pp. 1232–1241, Jun. 2016.

[59] J. H. Worne, H. Gullapalli, C. Galande, P. M. Ajayan, and D. Natelson, "Local charge transfer doping in suspended graphene nanojunctions," *Appl. Phys. Lett.*, vol.

100, no. 2, p. 023306, Jan. 2012.

[60] A. Pirkle *et al.*, "The effect of chemical residues on the physical and electrical properties of chemical vapor deposited graphene transferred to SiO $_2$," *Appl. Phys. Lett.*, vol. 99, no. 12, p. 122108, Sep. 2011.

[61] Y.-C. Lin, C. Jin, J.-C. Lee, S.-F. Jen, K. Suenaga, and P.-W. Chiu, "Clean Transfer of Graphene for Isolation and Suspension," *ACS Nano*, vol. 5, no. 3, pp. 2362–2368, Mar. 2011.

[62] Y. Dan, Y. Lu, N. J. Kybert, Z. Luo, and A. T. C. Johnson, "Intrinsic Response of Graphene Vapor Sensors," *Nano Lett.*, vol. 9, no. 4, pp. 1472–1475, Apr. 2009.

[63] Z. Cheng, Q. Zhou, C. Wang, Q. Li, C. Wang, and Y. Fang, "Toward Intrinsic Graphene Surfaces: A Systematic Study on Thermal Annealing and Wet-Chemical Treatment of SiO $_2$ -Supported Graphene Devices," *Nano Lett.*, vol. 11, no. 2, pp. 767–771, Feb. 2011.

[64] W. Choi, M. A. Shehzad, S. Park, and Y. Seo, "Influence of removing PMMA residues on surface of CVD graphene using a contact-mode atomic force microscope," *RSC Adv.*, vol. 7, no. 12, pp. 6943–6949, 2017.

[65] *,†,‡ Masa Ishigami, †,‡ J. H. Chen, †,‡ W. G. Cullen, ‡,§ and M. S. Fuhrer, and ‡ E. D. Williams†, "Atomic Structure of Graphene on SiO2," 2007.

[66] K. I. Bolotin *et al.*, "Ultrahigh electron mobility in suspended graphene," Feb. 2008.

[67] R. R. Nair *et al.*, "Dual origin of defect magnetism in graphene and its reversible switching by molecular doping," Jan. 2013.

[68] A. M. Goossens, V. E. Calado, A. Barreiro, K. Watanabe, T. Taniguchi, and L. M. K. Vandersypen, "Mechanical cleaning of graphene," *Appl. Phys. Lett.*, vol. 100, no. 7, p. 073110, Feb. 2012.

[69] N. Lindvall, A. Kalabukhov, and A. Yurgens, "Erratum: 'Cleaning graphene using atomic force microscope' [J. Appl. Phys. 111, 064904 (2012)]," *J. Appl. Phys.*, vol. 112, no. 3, p. 039903, Aug. 2012.

[70] Y. Zhao *et al.*, "Investigations on the wettability of graphene on a micron-scale hole array substrate," *RSC Adv.*, vol. 6, pp. 1999–2003, 2015.

[71] "Water and its structure." [Online]. Available: http://www.chem1.com/acad/sci/aboutwater.html. [Accessed: 08-May-2017].

[72] L. G. P. Martins, Y. Song, T. Zeng, M. S. Dresselhaus, J. Kong, and P. T. Araujo, "Direct transfer of graphene onto flexible substrates," *Proc. Natl. Acad. Sci. U. S. A.*, vol. 20, no. 20, pp. 1–5, 2013.

[73] Q. H. Wang *et al.*, "Understanding and controlling the substrate effect on graphene electron-transfer chemistry via reactivity imprint lithography," *Nat. Chem.*, vol. 4, no. 9, pp. 724–732, 2012.

[74] K. Nagashio, T. Yamashita, J. Fujita, T. Nishimura, K. Kita, and A. Toriumi, "Impacts of graphene / SiO 2 interaction on FET mobility and Raman spectra in mechanically exfoliated graphene films," pp. 564–567, 2010.

[75] Z. Wang *et al.*, "Comparative studies on single-layer reduced graphene oxide films obtained by electrochemical reduction and hydrazine vapor reduction.," *Nanoscale*

Res. Lett., vol. 7, no. 1, p. 161, Feb. 2012.

[76] S. C. Xu *et al.*, "Flexible and transparent graphene-based loudspeakers," *Appl. Phys. Lett.*, vol. 102, no. 15, p. 151902, Apr. 2013.

[77] S. Wu, Z. Yin, Q. He, X. Huang, X. Zhou, and H. Zhang, "Electrochemical Deposition of Semiconductor Oxides on Reduced Graphene Oxide-Based Flexible, Transparent, and Conductive Electrodes," *J. Phys. Chem. C*, vol. 114, no. 27, pp. 11816–11821, Jul. 2010.

[78] H. Bi, F. Huang, J. Liang, X. Xie, and M. Jiang, "Transparent Conductive Graphene Films Synthesized by Ambient Pressure Chemical Vapor Deposition Used as the Front Electrode of CdTe Solar Cells," *Adv. Mater.*, vol. 23, no. 28, pp. 3202–3206, Jul. 2011.

[79] Xuan Wang, * and Linjie Zhi, and K. Müllen*, "Transparent, Conductive Graphene Electrodes for Dye-Sensitized Solar Cells," 2007.

[80] Y. Lin *et al.*, "Graphene/semiconductor heterojunction solar cells with modulated antireflection and graphene work function," *Energy Environ. Sci.*, vol. 6, no. 1, pp. 108–115, 2013.

[81] Z. Yin *et al.*, "Organic Photovoltaic Devices Using Highly Flexible Reduced Graphene Oxide Films as Transparent Electrodes," *ACS Nano*, vol. 4, no. 9, pp. 5263–5268, Sep. 2010.

[82] L. Gomez De Arco, Y. Zhang, C. W. Schlenker, K. Ryu, M. E. Thompson, and C. Zhou, "Continuous, Highly Flexible, and Transparent Graphene Films by Chemical

Vapor Deposition for Organic Photovoltaics," *ACS Nano*, vol. 4, no. 5, pp. 2865–2873, May 2010.

[83] Y. Wang, S. W. Tong, X. F. Xu, B. Özyilmaz, and K. P. Loh, "Interface Engineering of Layer-by-Layer Stacked Graphene Anodes for High-Performance Organic Solar Cells," *Adv. Mater.*, vol. 23, no. 13, pp. 1514–1518, Apr. 2011.

[84] D. Zhang, F. Xie, P. Lin, and W. C. H. Choy, "Al-TiO2 composite-modified single-layer graphene as an efficient transparent cathode for organic solar cells," *ACS Nano*, vol. 7, no. 2, pp. 1740–1747, 2013.

[85] H. Bi, F. Huang, J. Liang, X. Xie, and M. Jiang, "Transparent Conductive Graphene Films Synthesized by Ambient Pressure Chemical Vapor Deposition Used as the Front Electrode of CdTe Solar Cells," *Adv. Mater.*, vol. 23, no. 28, pp. 3202–3206, Jul. 2011.

[86] H. Park, S. Chang, M. Smith, S. Gradečak, and J. Kong, "Interface engineering of graphene for universal applications as both anode and cathode in organic photovoltaics," *Sci. Rep.*, vol. 3, no. 1, p. 1581, Dec. 2013.

[87] J. Bai, X. Zhong, S. Jiang, Y. Huang, and X. Duan, "Graphene nanomesh," *Nat. Nanotechnol.*, vol. 5, no. 3, pp. 190–194, Mar. 2010.

[88] D. H. Wang *et al.*, "Transferable Graphene Oxide by Stamping Nanotechnology: Electron-Transport Layer for Efficient Bulk-Heterojunction Solar Cells," *Angew. Chemie Int. Ed.*, vol. 52, no. 10, pp. 2874–2880, Mar. 2013.

[89] Z. Yin *et al.*, "Full Solution-Processed Synthesis of All Metal Oxide-Based Tree-

like Heterostructures on Fluorine-Doped Tin Oxide for Water Splitting," *Adv. Mater.*, vol. 24, no. 39, pp. 5374–5378, Oct. 2012.

[90] S.-W. Wang *et al.*, "Transport behavior and negative magnetoresistance in chemically reduced graphene oxide nanofilms," *Nanotechnology*, vol. 22, no. 33, p. 335701, Aug. 2011.

[91] Y.-B. Tang *et al.*, "Incorporation of Graphenes in Nanostructured TiO_2 Films *via* Molecular Grafting for Dye-Sensitized Solar Cell Application," *ACS Nano*, vol. 4, no. 6, pp. 3482–3488, Jun. 2010.

[92] D. H. Wang *et al.*, "Transferable Graphene Oxide by Stamping Nanotechnology: Electron-Transport Layer for Efficient Bulk-Heterojunction Solar Cells," *Angew. Chemie Int. Ed.*, vol. 52, no. 10, pp. 2874–2880, Mar. 2013.

[93] S.-S. Li, K.-H. Tu, C.-C. Lin, C.-W. Chen, and M. Chhowalla, "Solution-Processable Graphene Oxide as an Efficient Hole Transport Layer in Polymer Solar Cells," *ACS Nano*, vol. 4, no. 6, pp. 3169–3174, Jun. 2010.

[94] J. Kim, V. C. Tung, and J. Huang, "Water Processable Graphene Oxide:Single Walled Carbon Nanotube Composite as Anode Modifier for Polymer Solar Cells," *Adv. Energy Mater.*, vol. 1, no. 6, pp. 1052–1057, Nov. 2011.

[95] A. K. Geim and K. S. Novoselov, "The rise of graphene," *Nat. Mater.*, vol. 6, no. 3, pp. 183–191, Mar. 2007.

[96] A. C. Ferrari *et al.*, "Raman Spectrum of Graphene and Graphene Layers," *Phys. Rev. Lett.*, vol. 97, no. 18, p. 187401, Oct. 2006.

[97] D. Stojanović, N. Woehrl, and V. Buck, “Synthesis and characterization of graphene films by hot filament chemical vapor deposition,” *Phys. Scr.*, vol. 2012, no. T149, p. 014068, May 2012.

[98] F. Tuinstra, “Raman Spectrum of Graphite,” *J. Chem. Phys.*, vol. 53, no. 3, p. 1126, 1970.

[99] A. Gupta, G. Chen, P. Joshi, S. Tadigadapa, and P. C. Eklund, “Raman scattering from high-frequency phonons in supported n-graphene layer films,” *Nano Lett.*, vol. 6, no. 12, pp. 2667–2673, Dec. 2006.

[100] D. Geng *et al.*, “Uniform hexagonal graphene flakes and films grown on liquid copper surface,” *Proc. Natl. Acad. Sci.*, Apr. 2012.

[101] M. P. Levendorf, C. S. Ruiz-Vargas, S. Garg, and J. Park, “Transfer-Free Batch Fabrication of Single Layer Graphene Transistors,” *Nano Lett.*, vol. 9, no. 12, pp. 4479–4483, Dec. 2009.

[102] H. I. Rasool *et al.*, “Continuity of Graphene on Polycrystalline Copper,” *Nano Lett.*, vol. 11, no. 1, pp. 251–256, Jan. 2011.

[103] Q. Yu *et al.*, “Control and characterization of individual grains and grain boundaries in graphene grown by chemical vapour deposition,” *Nat. Mater.*, vol. 10, no. 6, pp. 443–449, Jun. 2011.

[104] J. Kong, A. M. Cassell, and H. Dai, “Chemical vapor deposition of methane for single-walled carbon nanotubes,” *Chem. Phys. Lett.*, vol. 292, no. 4–6, pp. 567–574, Aug. 1998.

[105] K. Tanaka and S. (Shinji) Iijima, *Carbon nanotubes and graphene*. .

[106] K. Xiao, H. Wu, H. Lv, X. Wu, and H. Qian, "The study of the effects of cooling conditions on high quality graphene growth by the APCVD method," *Nanoscale*, vol. 5, no. 12, p. 5524, May 2013.

[107] H. Wang *et al.*, "Controllable Synthesis of Submillimeter Single-Crystal Monolayer Graphene Domains on Copper Foils by Suppressing Nucleation," *J. Am. Chem. Soc.*, vol. 134, no. 8, pp. 3627–3630, Feb. 2012.

[108] G. H. Han *et al.*, "Influence of Copper Morphology in Forming Nucleation Seeds for Graphene Growth," *Nano Lett.*, vol. 11, no. 10, pp. 4144–4148, Oct. 2011.

[109] "Basic Plasma Cleaner | Harrick Plasma." [Online]. Available: http://harrickplasma.com/products/basic-plasma-cleaner. [Accessed: 31-Mar-2018].

[110] "DXR™ 2 Raman Microscope." [Online]. Available: https://www.thermofisher.com/order/catalog/product/IQLAADGABFFAHCMAPB. [Accessed: 30-Mar-2018].

[111] L. F. Bates, "PHYSICS," *Science Progress in the Twentieth Century (1919-1933)*, vol. 23. Science Reviews 2000 Ltd., pp. 392–395, 1929.

[112] Princeton Instruments, "Raman Spectroscopy Basics - Application Note," *Internet: http://content. piacton. com/Uploads/Princeton/*, pp. 1–5, 2012.

[113] G. Binnig, C. F. Quate, and C. Gerber, "Atomic Force Microscope," *Phys. Rev. Lett.*, vol. 56, no. 9, pp. 930–933, Mar. 1986.

[114] B. M. Trafas, Y.-N. Yang, R. L. Siefert, and J. H. Weaver, “Scanning tunneling microscopy of Ag growth on GaAs(110) at 300 K: From clusters to crystallites,” *Phys. Rev. B*, vol. 43, no. 17, pp. 14107–14114, Jun. 1991.

[115] “How does atomic force microscopy work? - Quora.” [Online]. Available: https://www.quora.com/How-does-atomic-force-microscopy-work#sezyG. [Accessed: 31-Mar-2018].

[116] “Atomic force microscope and method for imaging surfaces with atomic resolution,” 04-Aug-1986.

[117] U. D. ChemWiki, “Section 4 . 3 : Ultraviolet and visible spectroscopy Section 4 . 3 : Ultraviolet and visible spectroscopy,” pp. 1–8, 2007.

[118] J. Hedberg, “Conduction Band Mediated Charge Transfer for Highly Reduced, Catalytically Active State: A Comparison Between Thin Films and Colloidal Solutions.,” p. 7, 2011.

[119] K. R. Sopka, “The Discovery of the Hall Effect: Edwin Hall’s Hitherto Unpublished Account,” in *The Hall Effect and Its Applications*, Boston, MA: Springer US, 1980, pp. 523–545.

[120] “Hall Effect.” [Online]. Available: http://hyperphysics.phy-astr.gsu.edu/hbase/magnetic/Hall.html. [Accessed: 02-Apr-2018].

[121] “8400 Series | Overview | Lake Shore Cryotronics, Inc.” [Online]. Available: https://www.lakeshore.com/products/Hall-Effect-Systems/8400-Series-HMS/Pages/Overview.aspx. [Accessed: 02-Apr-2018].

[122] G. Lupina *et al.*, “Residual metallic contamination of transferred chemical vapor deposited graphene,” *ACS Nano*, vol. 9, no. 5, pp. 4776–4785, 2015.

[123] A. Ambrosi and M. Pumera, “The CVD graphene transfer procedure introduces metallic impurities which alter the graphene electrochemical properties.,” *Nanoscale*, vol. 6, no. 1, pp. 472–6, Jan. 2014.

[124] O. V. Yazyev and S. G. Louie, “Electronic transport in polycrystalline graphene,” *Nat. Mater.*, vol. 9, no. 10, pp. 806–809, Oct. 2010.

[125] P. Y. Huang *et al.*, “Grains and grain boundaries in single-layer graphene atomic patchwork quilts,” *Nature*, vol. 469, no. 7330, pp. 389–392, Jan. 2011.

[126] J.-H. Chen, C. Jang, S. Xiao, M. Ishigami, and M. S. Fuhrer, “Intrinsic and extrinsic performance limits of graphene devices on SiO2,” *Nat. Nanotechnol.*, vol. 3, no. 4, pp. 206–209, Apr. 2008.

[127] Y. Liu *et al.*, “Giant enhancement in vertical conductivity of stacked CVD graphene sheets by self-assembled molecular layers,” *Nat. Commun.*, vol. 5, p. 5461, Nov. 2014.

[128] K. Ganesan, S. Ghosh, N. Gopala Krishna, S. Ilango, M. Kamruddin, and A. K. Tyagi, “A comparative study on defect estimation using XPS and Raman spectroscopy in few layer nanographitic structures,” *Phys. Chem. Chem. Phys.*, vol. 18, no. 32, pp. 22160–22167, 2016.

[129] D. Ferrah *et al.*, “XPS investigations of graphene surface cleaning using H 2 - and Cl 2 -based inductively coupled plasma,” *Surf. Interface Anal.*, vol. 48, no. 7, pp.

451–455, 2016.

[130] L. Scandella *et al.*, “Friction forces on hydrogen passivated (110) silicon and silicon dioxide studied by scanning force microscopy,” *J. Vac. Sci. Technol. B Microelectron. Nanom. Struct.*, vol. 14, no. 2, p. 1255, Mar. 1996.

[131] S. Ryu *et al.*, “Atmospheric Oxygen Binding and Hole Doping in Deformed Graphene on a SiO 2 Substrate,” pp. 4944–4951, 2010.

[132] L. . Zhang, M. Tsutsui, K. Ito, and M. Yamaguchi, “Effects of ZnSb and Zn inclusions on the thermoelectric properties of β-Zn4Sb3,” *J. Alloys Compd.*, vol. 358, no. 1–2, pp. 252–256, Aug. 2003.

[133] D. Maji, S. K. Lahiri, and S. Das, “Study of hydrophilicity and stability of chemically modified PDMS surface using piranha and KOH solution,” *Surf. Interface Anal.*, vol. 44, no. 1, pp. 62–69, Jan. 2012.

[134] J. K. Bal, S. Kundu, and S. Hazra, “Hydrophobic to hydrophilic transition of HF-treated Si surface during Langmuir–Blodgett film deposition,” *Chem. Phys. Lett.*, vol. 500, no. 1–3, pp. 90–95, Nov. 2010.

[135] X. L. P. Zhu, Z. Weng, X. Li, “Biomedical applications of functionalized ZnO nanomaterials: from biosensors to bioimaging.,” *Adv. Mater. Interfaces 3, 1500494-1–1500494-30*.

[136] M. B. A. Tereshchenko, “Optical biosensors based on ZnO nanostructures: advantages and perspectives.,” *A Rev. Sens. Actuators, B 229, 664–677*.

[137] Ü. Ö. H. Morkoç, “Zinc oxide: fundamentals, materials and device technology. Zinc

Oxide Fundam.," *Mater. Device Technol. (2009).*

[138] T. J. A. Kołodziejczak-Radzimska, "Zinc oxide—from synthesis to application," *a Rev. Mater. 7, 2833–2881 (2014).*

[139] Y. Liu, Y. Li, and H. Zeng, "ZnO-Based Transparent Conductive Thin Films: Doping, Performance, and Processing," *J. Nanomater.*, vol. 2013, pp. 1–9, Mar. 2013.

[140] C. T. EL Lim, CC Yap, MHH Jumali, MAM Teridi, "A Mini Review: Can Graphene Be a Novel Material for Perovskite Solar Cell Applications?," *Nano-Micro Lett. 10, 27-39.*

[141] J. R. Potts, D. R. Dreyer, C. W. Bielawski, and R. S. Ruoff, "Graphene-based polymer nanocomposites," *Polymer (Guildf).*, vol. 52, no. 1, pp. 5–25, Jan. 2011.

[142] J. P. SB Yahia, L Znaidi, A Kanaev, "Raman study of oriented ZnO thin films deposited by sol-gel method.," *Spectrochim Acta Part A 71, 1234–4 (2008).*

[143] L. M. Malard, M. A. Pimenta, G. Dresselhaus, and M. S. Dresselhaus, "Raman spectroscopy in graphene," *Phys. Rep.*, vol. 473, no. 5–6, pp. 51–87, Apr. 2009.

[144] S. E. Zhu, S. Yuan, and G. C. A. M. Janssen, "Optical transmittance of multilayer graphene," *Epl*, vol. 108, no. 1, pp. 1–4, 2014.

Vitae

Name : Ahmed Abdelaal

Nationality : Egyptian

Date of Birth : 24-11-1988

Email : ahmed.abdelaal@h-eng.helwan.edu.eg

Address : 1 sherif street, Faculty of Engineering Helwan University, Helwan, Cairo, 11792, Egypt.

Academic Background:

2016-2018 King Fahd University of Petroleum and Minerals, Dhahran, Saudi Arabia.

- **MSc**. in Mechanical Engineering, Major: Manufacturing and Materials.

2006-2011 Helwan University, Faculty of Engineering, Cairo, Egypt.

- **B.S.** In Mechanical Engineering, Major: Production Engineering

Research Interest:

- Engineering Materials.
- Graphene applications.
- photovoltaic materials for solar cells
- Additive layer manufacturing
- Modeling of machining process

List of Publications:

- **Ahmed F. Abdelaal**, Mohammed K. Hossain, Ahmed Ibrahim, Billel Salhi, Tahar Laoui "**Enhanced Electrical and Optical Properties of Zinc Oxide Ultrathin Film Using Graphene Layer for Solar Cell Application"** (Ready for Submission)
- **Ahmed F. Abdelaal**, Ahmed Ibrahim, Billel Salhi, Tahar Laoui "**Enhanced wet graphene transfer by controlling the hydrophilicity of SiO_2/Si substrate**" (Ready for Submission)